Wave-forced dynamics in the nearshore river mouths, and swash zones

Wave-forced dynamics in the nearshore river mouths, and swash zones

Maurizio Brocchini

DICEA, Università Politecnica delle Marche, Ancona, Italy

Abstract

The role of wave forcing on the main hydro-morphological dynamics evolving in the shallow waters of the nearshore and at river mouths is analyzed. Focus is mainly on the cross-shore dynamics that evolve over mildly sloping barred, dissipative sandy beaches from the storm up to the yearly time scale, at most. Local mechanisms, nonlocal mechanisms and connections across three main inter-related subsystems of the nearshore - the region of generation and evolution of nearshore bars, river mouths and the swash zone - are analyzed. The beach slope is a major controlling parameter for all nearshore dynamics. A local mechanism that must be properly described for a suitable representation of wave-forced dynamics of all such three subsystems is the proper correlation between orbital velocity and sediment concentration in the bottom boundary layer; while specific mechanisms are the wave-current interaction and bar generation at river mouths and the sediment presuspension at the swash zone. Fundamental nonlocal mechanisms are both Infragravity (IG) waves and large-scale horizontal vortices (i.e. with vertical axes), both influencing the hydrodynamics, the sediment transport and the seabed morphology across the whole nearshore. Major connections across the three subsystems are the upriver propagation of IG waves generated by breaking sea waves and swash-swash interactions, the interplay between the swash zone and along-river-flank sediment transport and the evolution of nearshore sand bars.

Introduction

Focus, motivation and method

This work focuses on wave-forced nearshore and river mouth dynamics, as opposite to tidally-forced dynamics - i.e. such that $RTR=TR/H_b<3$, where TR is the tidal range and H_b is the height of breaking waves (Masselink and Short, 1993).

In more detail, cross-shore (mostly) dynamics evolving from the yearly down to the storm time scales are investigated. With reference to coastal and river mouth hydro-morphological regimes the present analysis gives attention to the following two regimes.

First, open-coast, mildly sloping, barred ($\Omega=H_b/w_sT_i>2$, where Ω is the Dean parameter), w_s is the sediment fall velocity and T_i is the period of incoming waves - Wright and Short, 1984) and dissipative ($\epsilon=A_b\omega^2/gtan^2\beta>20$, where the surf-scaling parameter ϵ depends on the amplitude of the breaking waves A_b, on the radian wave frequency $\omega=2\pi/T_i$ and on the beach slope β -Wright and Short, 1984) sandy beaches. Second, wave-dominated or river-dominated and wave-modified (which feed sediments to sea) river mouths (Cooper, 2001).

Scopes of the present contribution are the following. First, to provide a fairly complete (obviously not exhaustive) and clear overall view of what we know and what we do not not know of wave-forced nearshore and river mouth dynamics. Second, to give the needed focus to recent progresses made available on specific dynamics. But the main aim is to ***highlight links and relations among such dynamics***, this by properly highlighting nonlocal agents and relations.

Regarding this problem as a puzzle to be solved (see figure 1), this entailing local and nonlocal relations, this paper tries to: put the analysis in the proper context, with no pretention for a systematic description; move from consolidated knowledge to new results; move from observations to modeling; move from the large to the small scales; inspect different types of models, both in terms of their structure and use.

Figure 1. Wave-forced dynamics in the nearshore and estuaries: a puzzle to be solved. This photo, taken at the microtidal Misa River estuary (Senigallia, Italy), illustrates through one single view the three subsystems analyzed in the paper.

The latter issue is analyzed in some detail because of its intrinsic importance and of the guidance that models provide in exploring the mechanisms of the phenomena at hand.

Generalities on Models

The hydro-morphodynamics of the nearshore region, including that evolving at river mouths, is so complex that a number of different methods and models has been proposed and implemented over the years. However, such abundance of models has also brought to some major ambiguities in the definition and use of such models.

Hence, some clarification seems useful, which is based on a detailed classification of the models in terms of their: intrinsic structure and use.

Model structure

Although this classification, as many others, is somewhat arbitrary (e.g. as function of the level of closure implemented), its use may help understand what model is actually applied for a specific analysis. The structure of the models at hand can be classed as either “process based” or “empirically based”.

“Process-based models” rely on equations derived from fundamental physical principles and/or conservation laws. In the following three examples of such models (at different levels of time/space scales and resolution) are described.

First, wave-averaged models: Nonlinear Shallow Water Equation (NSWE)-type (e.g. Delft3D, https://oss.deltares.nl/web/delft3d/home; Lesser et al., 2004; NHWAVE, Ma et al., 2012); Oceanographic (e.g. ROMS, https://www.myroms.org/index.php, Haas and Warner,

2009), etc. Second, wave-resolving models: NSWE-type (e.g. Postacchini et al., 2012); Boussinesq-type (e.g. Brocchini, 2013; Kirby, 2016); etc. Third, models that account for turbulence through proper closures: Reynolds Averaged Navier-Stokes; Large Eddy Simulations (Chang and Scotti, 2004; Torres-Freyermuth, Lara and Losada, 2010; Lubin et al. 2011) etc.

"Empirically-based models" rely on equations constructed from a mixture of conservation laws and observations, with a significant weight of empirical inputs. In fact, though also turbulence models like RANS and LES do require some empirism for the turbulence closure relations (hence the arbitrariness of classing models), their structure heavily relies on conservation laws and less on closures that are based on solid theoretical foundations. Examples of empirically-based models are: Regression-type models, Machine Learning Approaches (e.g. Pourzangbar et al., 2017), etc. and energetics-type, which solve a sediment mass conservation equation (Exner equation) where the mass fluxes come from empirically-based closure laws (e.g. Bailard, 1981).

Model use

The above models can be, each in its own way, used in terms of either a template/forced approach or a stability approach (at times referred to as "self-organization", see, for example, Coco and Murray, 2007). To clarify the above an example is made with reference to the classical Exner 1D sediment transport equation, which can be formulated as (e.g. Plant et al., 2001):

$$\frac{\partial z_b}{\partial t}(x,t) = I + II + III \quad (1)$$

where z_b is the seabed position and

I = is a forcing term due to initial bathymetry and wave field,

II = gives the modification of forcing due to externally-forced changes in wave height,

III = is a feedback term due to the rate of change of the seabed position z_b, which introduces a feedback behavior in (1).

Template/forced models and stability-type models can be distinguished by the presence of I, II and III. Template/forced morphological models are such that I≠0, II≠0 and III=0, while stability approaches must have III≠0. With reference to the specific problem of seabed features generation, while template models may identify compelling mechanisms, i.e. a template, for the initial stages of formation (e.g. at breakpoint, at nodes/antinodes of standing waves, etc.) stability models are such that perturbations evolve simultaneously in the hydrodynamic and bathymetric fields. This is illustrated by the examples given in figures 2 and 3. The initial bathymetry used for the simulations of figure 3 consisted of a longshore-uniform sand bar.

Figure 2. Forced/template mechanism: “synchronous standing edge waves” (left) and flow imprinted on sand giving beach cusps (right). Adapted from Coco and Murray, (2007).

Figure 3. Stability/Self-organization mechanism: crescentic bars emerge from the feedback between flow and bathymetry (initial longshore-uniform bar bathymetry). Top: waves breaking on shoals force onshore flow, which returns to sea in gaps. Bottom: for suspended sediment decreasing from breaker line to shore, the onshore flow favors deposition (shoals grow) and the offshore flow favors erosion (scour holes grow). Hence, the development of crescentic bars. Adapted from Coco and Murray, (2007).

The rest of the paper is structured as follows. The next section provides detailed information specific to 1) the generation and evolution of nearshore bars, 2) river mouth and 3) swash zone dynamics. A short Discussion and then Conclusions close the paper.

Wave forced-dynamics for three fundamental subsystems: sand bars, river mouths and swash zone

Sand bars

The generation and evolution of sand bars in the nearshore is analyzed as a first applicative topic because of its many implications, which help set the scene for all the rest of the paper. Consolidated observations and models are first illustrated, then followed by more recent findings.

Starting from the observations, sand bars that evolve in the nearshore are usually classed in terms of their planview shape, i.e. longshore uniform (2D) and rhythmic (3D). Different evolution mechanisms lead to different evolution time scales (e.g. Wijnberg and Kroon, 2002). We can distinguish between: 2D sand bars (left panel of figure 4), which emerge as the outcome of wave-induced, cross-shore sediment transport and evolve over scales of days to months (e.g. Ruessink and Kroon, 1994); 3D sand bars (right panel of figure 4), which emerge as the outcome of horizontal circulation patterns and, because of this stronger forcing, evolve on shorter time scales, i.e. hours to days (e.g. Caballeria et al., 2002).

Figure 4. Left panel: planview image of two shore-parallel sand bars at Noordwijk beach (The Netherlands, 19th November 2000). Right panel: planview image of surf zone complex topography at Duck (U.S.A. Atlantic coast, 10th January 1994). Adapted from Ribas Prats (2003).

Three main interpretative models exist for the overall generation and evolution mechanisms of nearshore sandbars.

The most known is the Net Offshore Migration (NOffM) model, which suggests that multiple nearshore 2D bars have multi-annual lifetimes and pass through 3 stages (figure 5). Generation occurs close to shore because of the interaction of undertow, wave orbital velocity asymmetry and group-forced IG orbital motion (Roelvink and Stive, 1989). This is followed by a net seaward migration, which is the outcome of an alternation of gradual onshore movements during calms and episodic strong offshore movements during storms (Van Enckevort and Ruessink, 2003, see also the right panel of figure 5). Finally,

degeneration occurs at the outer surf zone when the bar moves offshore of the breaker line where weakly or non-breaking waves induce a net onshore sediment transport. This step governs the entire cycle and only when the offshore bar degenerates at the breaker line the nearshore bar can start its offshore migration (Wijnberg and Terwindt, 1995).

Figure 5. Left panel: seabed cross-shore profiles at Noordwijk, The Netherlands, from 1979 to 1987, showing cyclic bar behavior with a recurrence interval of about 4-5 years. Adapted from van Enckvort, (2001). Right panel: seabed cross-shore profiles at Duck (U.S.A. Atlantic coast, September-October 1994). Thick curves with red dates are the beginning of storms, resulting in offshore bar migration (red arrows). Thin curves are the subsequent daily profiles. The sandbar migrated onshore (blue arrows) during calm periods between the storms. Courtesy of Dr. S. Elgar.

The second model is the Net Onshore Migration (NOnM) model, which suggests that sand bars are generated inshore of the breakpoint and migrate towards the swash zone (Aagard et al., 2004). The observations made on the Danish North Sea coast suggest that a net onshore bar migration occurs and the onshore bar movement in the mid-outer surf zone is due to a dominance of the wave-induced sediment transport during storm condition. The onshore-directed sediment transport is caused by incident wave skewnesses and enhanced phase couplings between orbital velocity and sediment concentration at times of high energy and water levels.

Alternative to both NOffM and NOnM, the Oscillation around a Position of Equilibrium (OPE, Certain and Barusseau, 2005) proposes a cyclic oscillation of the bar position due to seaward (storms) and shoreward (calms) migration. The mechanisms of this model are essentially similar to those of the NOffM, i.e. seaward migration during storms because of the dominance of the undertow and recovery during calms due to the wave-induced onshore sediment transport, but equilibrium is achieved when the local climate cannot not force storm strong or long enough (e.g. Mediterranean vs. North Sea, see also Armaroli and Ciavola, 2011). Very recent observations (Parlagreco et al., 2019) show that Mediterranean storms

197 can indeed induce a NOffM rather than an OPE behavior and that the longshore flow can
198 sensibly contribute to increase the potential of sediment suspension.
199 Both NOffM and NOnM are preferential for longshore-uniform 2D bars, which evolve for
200 $\Omega \approx 5$ (see in the following), and seem to require large waves (Ω is directly proportional to H_b)
201 and longshore flows (likely contributing to longshore uniformity, Shand et al., 1999).
202 Moreover, since both NOffM and NOnM are observed to evolve over beaches with similar
203 slopes (1:200-1:150) and sediment sizes ($d_{50} \approx 150\mu m$), the different behaviours are probably
204 to be searched into the different incident wave field (steepness and storm sequencing) and
205 possible physiographic constraints.
206 The above observations motivate a detailed analysis, using the mentioned classification,
207 of the models currently available to predict the generation and evolution of 2D sand bars.
208 These are typically distinguished between models for single but non-interacting bars and
209 interacting sand bars.
210 Among the models for single and non-interacting multiple bars we find the “empirical
211 models”, the “template/forced” models and the “stability models”.
212 The “empirical models” are based on use of the Dean parameter Ω (Wright and Short,
213 1984) and of the the $B^* = xs/g \tan\beta \, T_i^2$ parameter (Short and Aagard, 1993), where x_s is the
214 nearshore width (offhore distance to the point where $\beta \approx 0$). Single bar formation is possible
215 for $20 < B^* < 50$ and $2 < \Omega < 6$, while $\Omega < 1$ characterizes reflective beaches and $\Omega > 6$ dissipative
216 beachs. For Ω increasing from 2 to 6 the following features emerge in sequence (Wijnberg
217 and Kroon, 2002): shore-attached bars, 3D bars and 2D bars (the latter ones for $\Omega \approx 5$).
218 Formation of multiple bars requires larger values of B* (e.g. 2 bars for $50 < B^* < 100$, 3 bars
219 for $100 < B^* < 300$, etc.);
220 The “template/forced models” not only give synthetic information on conditions, but also
221 clarify some of the mechanisms for bar formation. Most of them propose bar formation via
222 sediment accumulation at specific spatial locations. Such locations can be (see also figure

6): the anti/nodes of standing waves - be they induced by incoming/outgoing free IG waves (Short, 1975) or edge waves from opposite directions (Holman and Bowen, 1982), this is known as the “standing IG wave mechanism”; the breakpoint location, where flow/sediment convergence is due to the seaward-flowing undertow and the shoreward bottom boundary layer (BBL) streaming, this is known as the “breakpoint-bar mechanism”.

Figure 6. Bar formation because of sediment convergence at: anti/nodes of standing IG waves (left panel), breakpoint (right panel).

Another forced model, by O’Hare and Huntley (1994), suggests bar formation is induced by sediment stirring from sea/short waves and transport by free IG, hence we call this “sea-IG waves correlation mechanism”. Erosion/deposition is function of a fixed phase shift between the stirring given by short-wave envelope and IG waves. If IG are Bound Long Waves (BLW, more efficient on dissipative/mild beaches, Longuet-Higgins and Stewart, 1964), bar formation is inhibited, while if IG are generated by BreakPoint (BP, more efficient on reflective/steep beaches, Symonds et al., 1982) oscillation, bar formation is fostered.

Forced models represent a major improvement over empirical models but are affected by some significant weaknesses. The most important is their intrinsic inability to give accont of the morphology-on-flow- feedback (term III of equation 1 is automatically set to zero). Moreover, standing IG waves and breakpoint-bar mechanisms: prescribe the simultaneous emergence of all bars across the surf zone (this is only observed for rythmic 3D bars, but not for 2D bars); require very specific wave conditions (e.g. narrow-banded spectra, mode selection, etc.), which are not frequent in nature.

Finally, “stability models” have been succesfully used to describe the generation of crescentic or lunate 3D bars (Vittori et al., 1999) and the evolution of a double system of crescentic 3D bars (Klein and Schuttelaars, 2006). Crescentic bars emerge because of steady currents caused by the interaction of the incoming sea/short waves with synchronous

edge waves excited by the incoming waves moving over the wavy seabed. Klein and Schuttelaars (2006) studied a similar problem using a numerical, wave-averaged model (NSWE+Exner). Starting from an equilibrium state and numerically added perturbations the fastest-growing perturbation was computed (see also the left panel of figure 7).

Figure 7. Left panel: nonlinear stability solution for a double sand bar system giving asymmetric crescentic patterns on inner and outer bars (adapted from Klein and Schuttelaars, 2006). Right panel: Evolution of longshore uniform sand bar after 30 days of model run with normal wave incidence. Longshore instability in the form of rip channels (adapted from Dronen and Deigaard, 2007).

However, no study seems available on the emergence of 2D sandbars by means of stability models. Using a wave-averaged model Dronen and Deigaard, (2007) have shown that longshore instabilities of an initially 2D bar emerge for both normal and oblique wave incidence (see also the right panel of figure 7). This inadequacy of stability models in reproducing the emergence and evolution of 2D sandbars calls for intensive investigation, which should also take into proper account the role of longshore currents, which are thought to be fundamental to give longshore uniformity.

With reference to models for interacting multiple bars, Castelle et al. (2010) used a numerical, wave-averaged circulation model (with wave action equation for wave driver) plus Exner equation to investigate the evolution of double crescentic sandbar systems.

Figure 8. Computed (top-right and bottom panels) 180° out of-phase coupled patterns with an outer-bar horn facing an inner-bar bay, similar to observations (top-left panel) on a meso-macro-tidal, high-energy, double-barred beach (adapted from Castelle et al., 2010).

Simulations were run by providing a template in the morphology (inner bar longshore uniform and outer-bar with crescentic patterns). The computed feedback between flow, sediment transport and the evolving morphology allowed to reproduce morphologies similar to those of observed double crescentic sandbar systems (see figure 8). The Authors

advanced that a novel mechanism ("morphological coupling") was introduced that "blurs the distinction between self-organization and template mechanisms". However, inspection of equation (1) suggests that such a novel mechanism is a complete model that retains all terms on the right hand side. In other words, a template of crescentic outer bar is forced (term I of equation 1) in a self-interating model (term III of equation 1).

The above consolidated knowledge has opened the way to some recent findings on: sediment transport due to IG waves, sandbar migration and seabed moulding due to large-scale vortices.

Recent results on IG wave-induced sediment transport come from De Bakker et al. (2016) who have used field data collected in the Netherlands at the gently sloping (β≈1:80) Ballum beach and at the moderately sloping (β ≈1:35) SandMotor beach to investigate the role of the beach slope on IG wave-induced cross-shore sediment transport (q_{IG}). Based on the fundamental idea that sediment is put into suspension by sea/short waves and transported by IG waves (see also the "sea-IG waves correlation mechanism" by O'Hare and Huntley, 1994), the study compares the performances of two proxies for sediment transport in the nearshore. The first proxy is the correlation between the group bound IG wave (BLW) and the sea-wave envelope (see also Baldock, 2006):

$$R_{Uu_{IG}}(\tau) = \frac{\langle U(t)u_{IG}(t+\tau)\rangle}{\sigma_U \sigma_{u_{IG}}} \quad (2)$$

where u_{IG} is the IG wave cross-shore velocity, U is the sea-wave envelope cross-shore velocity, σ_s give the related variances and <> denotes time averaging. The second proxy, proposed by De Bakker et al. (2016), is the IG wave height to sea wave height ratio H_{IG}/H_{SW}.

De Bakker et al. (2016) suggest that $R_{Uu_{IG}}$ is a good proxy for the nearshore sediment transport only on moderately-sloping beaches while H_{IG}/H_{SW} well represents the sediment transport on all beaches. In fact, while over moderate slopes $R_{Uu_{IG}} \neq 0$, it is $R_{Uu_{IG}} = 0$ on

mild slopes. On the other hand, H_{IG}/H_{SW} is always positive and increasing for mild slopes, because IG waves receive more energy from sea waves breaking on wide surf zones.

In the shoaling region it is $R_{Uu_{IG}} < 0$ because the setdown (negative BLW) is associated with the peak of the sea wave envelope and the sediment flux is negative, i.e. seaward (see also figure 9). In the inner surf zone of moderately-sloping beaches the correlation becomes positive because breaking-induced wave setup (positive BLW and shoreward sediment flux) gives deeper waters and allows the faster sea waves to ride the crest of the IG wave (see figure 9). However, in the inner-surf zone of mildly-sloping beaches it is $R_{Uu_{IG}} = 0$ because the sea waves have been almost completely dissipated and $q_{IG}<0$ because the peaks of suspended sediment transport (SST) correlate with $u_{IG}<0$ and the undertow $\bar{u}$.

Figure 9. Sketch of IG-sea wave interaction and cross-shore sediment transport in the nearshore. From left to right: shoaling zone, inner-surf zone of moderately-sloping beaches, inner-surf zone of mildly-sloping beaches.

Other recent results are on the mechanisms for onshore bar migration, fundamental for all bar migration models of above. Early energetics-type models could only reproduce offshore migration due to strong offshore currents (undertow) that are maximum at the bar crest (Gallagher et al.,1998). Observations suggest that onshore migration occurs for weak currents and significant waves. Hence, the role of waves is fundamental for the onshore bar migration, and, as a consequence, it is fundamental to understand what are the model representations of the main wave mechanisms for onshore bar migration.

With reference to the models analyzed in the Introduction we first analyze the energetics-type models. They base their ability to reproduce onshore bar migration on use of the wave acceleration skewness (Sk_a, proportional to the third order acceleration moment) in the sediment transport closure, so that the sediment transport rate is written as (Hoefel and Elgar, 2003):

$$Q_A = K_a\left(a_{spike} - \mathrm{sgn}\left(a_{spike}\right)a_{crit}\right), \text{for } \left|a_{spike}\right| \geq a_{crit} \text{ with } a_{spike} = \frac{\langle a^3 \rangle}{\langle a^2 \rangle} = \langle a^2 \rangle^{1/2} Sk_a \qquad (3)$$

This description is such to properly give account of the rapid onshore flow acceleration under steep wave fronts, which, in turn, generates strong horizontal pressure gradients on the seabed sediment.

On the other hand, process based, wave-resolving models (e.g. Henderson et al., 2004; Hsu et al., 2006) can properly predict onshore bar migration if they accurately describe the correlation between the orbital velocity (*u*) and the sediment concentration (*c*) in the BBL (*q*=<*uc*>).

Figure 10. From left to right: vertical profile of mean cross-shore sediment transport due to waves (q_w) and currents (q_c), total cross-shore sediment transport as function of near-bed (middle) and freestream (right) velocity moments, for the Duck94 migration event. Adapted from Henderson et al. (2004).

Figure 10 shows that onshore migration occurs when the total sediment transport (q_t) is essentially due to waves (q_w) and correlates well with the third-order moment of the nearbed velocity $\langle u_b^3 \rangle$.

The apparent distance between the two models can be reconciled, showing that energetics-type models are successful if they reproduce, at the integral level, the proper sediment flux-nearbed velocity moments correlation given by advective BBL models. The proof can be summarized as follows. First, it is shown that onshore bar migration occurs when *q* correlates well with $\langle u_b^3 \rangle$ in BBL, i.e. with the nearbed wave velocity skweness $Sk_{u_b} = \langle u_b^3 \rangle / \langle u_b^2 \rangle^{3/2}$. Then, using a Fourier decomposition of the velocity field, it is shown that $Sk_{u_b} \propto \sin(\phi_b) A_{u_f}$, where A_{u_f} is the wave freestream velocity asymmetry and ϕ_b is the nearbed-over-freestream velocity phase lead (Henderson et al., 2004; Berni et al., 2013). Finally, for sawtooth bores, i.e. setting $\phi = \pi/2$ in the modal solution $u_f \sim \sum_n \frac{1}{2^n} \sin[(n+1)\omega t + n\phi]$

gives $A_{u_f} \sim Sk_{a_f}$, with Sk_{a_f} wave freestream acceleration skewness (Drake and Calantoni, 2001) of energetics-type models.

Very recently Fernandez-Mora et al., (2015) used an energetics-type model to show the ability of such models to predict onshore/offshore bar migration and assess the role of both Sk_{u_b} and Sk_{a_f}. A complex model was built such that:

$$(1-n)\frac{\partial z_b(x,t)}{\partial t} = -\frac{\partial Q(x,t)}{\partial x} \quad (4)$$

$$\text{with} \quad Q = \alpha_c Q_c\left(Sk_{u_c}\right) + \alpha_u Q_u\left(Sk_{u_f}\right) + \alpha_a Q_a\left(Sk_{a_f}\right) + \alpha_D Q_D\left(\frac{dz_b}{dx}\right)$$

and where Sk_{u_c} is the skewness of the currents velocity vector and dz_b/dx is the, stabilizing, seabed slope term. Hence, if α_u is set to zero the SkA model of Hoefel and Elgar (2002) is obtained, if α_a is set to zero the SkV model of Hsu et al. (2006), while the complete model is the MiX model. The model performances are illustrated in figure 11, always referring to the Duck94 onshore migration event.

Figure 11. Modeling (red line) of the morphological evolution of the Duck94 onshore migration event for: (A) the SkV model, (B) the SkA model, and (C) the MiX model. The initial and final measured profiles are shown by dashed and solid lines, respectively. Adapted from Fernandez-Mora et al. (2015).

All models reproduce well the chosen event, the SkV model better in the shoaling zone and the SkA model better in inner surf zone. However, they all perform poorly in the swash zone, this suggesting further investigation is needed for such region.

Among the most recent results on seabed evolution and bar generation are those dedicated to the roles of macrovortices. Breakers of finite longshore width are known to introduce vertical vorticity ζ that rolls up to form large-scale vortices with vertical axes, also called macrovortices (Peregrine, 1999). Important dynamics characterized by finite longshore breakers are those giving rise to rip currents (e.g. Kennedy et al., 2006) and cross-sea induced breakers (e.g. Postacchini et al., 2014).

The latter condition is seen to be a potentially important cause of seabed morphology alteration with the generation of complex 3D sandbars. The example of figure 12 has been obtained by computing, using the NSWE morphodynamic model of Postacchini et al. (2012), the morphological evolution of a planar beach under the combined action of waves and macrovortices generated by finite longshore breakers due to regular waves (Hi=1m, Ti=10s, β=1/30) crossing at an angle of 15º to the coastline.

Figure 12. Seabed evolution forced by sea waves and macrovortices over a planar beach. Red thin lines give contours of the free surface elevation, while black and blue solid lines are contours of clockwise and anticlockwise vorticity, respectively. Yellow gives sand deposition and green seabed erosion.

Sandbars of 3D shape (yellow colours in figure 12) arise due to the interaction of cross-sea waves and the breaking-induced macrovortices.

River mouths

The hydro-morphodynamics evolving at river mouths, significantly related with the evolution of sandbars, is analyzed, as a second applicative topic, with the same approach used for sandbars: consolidated observations and models first, followed by more recent findings.

In view of the main aim of the paper, i.e. to highlight interactions amongst the subsystems of interest, fundamentals of river mouth dynamics are kept at the minimum, with a preference for those of wave-dominated rivers debouching into sandy coasts.

Analysis of the literature on river mouths dynamics is fairly complex because of the different perspectives taken by the various communities that study river mouths, i.e. engineers, geologists, ecologists, etc. Also, the vocabulary is influenced by such different views and much effort is being spent to provide a systematic description of river mouth dynamics.

The most important efforts have been made in the classification of river deltas (Galloway, 1975), where delta is here generically used as "sedimentary deposit due to river-sea interaction and protruding into the sea". The triangular classification of deltaic depositional systems by Galloway (1975) illustrates how the relative importance of sediment input, wave energy flux and tidal energy determines both morphology and stratigraphy of the delta. Indices have also been introduced to classify deltas. Among them we find the discharge index I_q of very consolidated use (Wright et al., 1974) and the more recent fluvial dominance ratio R (Nienhuis et al., 2015):

$$I_q = discharge\ index = \frac{river\ liquid\ discharge\ per\ unit\ width\ of\ mouth}{wave\ power\ per\ unit\ width\ of\ wave\ crest} \quad (5a)$$

$$R = fluvial\ dominance\ ratio = \frac{Q_r}{Q_{s,max}} = \frac{river\ sand\ flux}{max\ longshore\ sediment\ flux\ at\ river\ mouth} \quad (5b)$$

The former is a dimensional index (units of m^3/Watts/s) and such to increase of orders of magnitude from wave-dominated ($I_q \approx 10^{-5}$ m^3/Watts/s) to river-dominated ($I_q \approx 1$ m^3/Watts/s) systems, while the latter is a dimensionless index, also increasing from $R<1$ for wave-dominated to $R>1$ for river dominated systems (see also figure 13).

Figure 13. Classification of river delta morphologies by means of the fluvial dominance ratio. Adapted from Nienhuis (2016).

Reference classifications of river deltas (Galloway, 1975) also clarify use of the word "estuary", this being attributed to tide-dominated deltas, though at times more broadly (improperly?) used for semi-enclosed regions where river fresh water meets the sea. A number of schemes to classify estuaries is available in the literature, a recent one being that of Valle-Levinson (2011), which provides different classifications based on geomorphology, salinity structure and hydrodynamics.

Because of the ambiguities in using “estuary” and of the present focus on river systems weakly influenced by tides, “river mouth” is here used as a clear and unambiguous definition of the region where the river meets the sea. Analyses of wave-dominated river mouths are also available (e.g. Cooper, 2001), and the very comprehensive, recent, work by Anthony (2015) provides a nice overview of the role of waves at river mouths: waves remove fine sediments at the river mouth and flatten the delta by moving the sediment alongshore. Hence, deltas, placed along smooth coasts with shore-parallel ridges (see figure 14), are shaped from arcuate to cuspate. Waves that approach the coast obliquely generate: littoral (i.e. longshore) sediment transport, maximum for 45° wave attack; an important difference between updrift/downdrift flank transport and sediments (updrift flank made by beach sediments, downdrift flank made by river sediments); an asymmetrical delta. A recent quantitative analysis on delta progradation/migration is that of Nienhuis et al. (2016), which can be summarized as follows. The delta undergoes: a symmetric progradation, for small river sand flux and all longshore transported sediment bypassing the mouth*;* a downdrift migration, for small river sand flux and vanishing sediment bypassing at mouth*;* an updrift migration, for large river sand flux, independently of sediment bypassing at mouth.

Figure 14. River delta geomorphic units and schematic shoreline morphology (wave-dominated morphology circled in red). Adapted from Anthony (2015).

Being the main aim of the present work that of clarifying the interactions - through nonlocal agents - between the sandbar, river mouth and swash zone subsystems, most of the attention is here given to local and nonlocal wave-forced dynamics.

Fundamental wave-forced, river mouth dynamics are the interaction of river current with the sea waves and the related sediment transport.

Seaward flowing currents interact with incoming waves (Chawla and Kirby, 2002) to: slow them down and even block them if the depth-uniform current velocity is equal and opposite

481 to the wave group velocity, this is known as “wave blocking”; steepen and even lead to
482 breaking; decrease the high-frequency content by wave breaking and transfer part of the
483 current energy to lower wave frequencies, this leading to frequency downshift of the
484 incoming waves;

485 The bedload accumulation related to the above dynamics typically leads to the formation
486 of a mouth sandbar. The intensity of the wave field significantly influences the bar formation
487 process. With no waves, a triangular mouth bar is generated just seaward of the mouth, at
488 a distance of about twice the mouth width. The generation process is initiated by the river
489 jet expansion in the sea, which, by continuity arguments, leads to a flow reduction and a
490 consequent sediment deposition (e.g. Fagherazzi et al., 2015). On the other hand, small
491 waves promote mouth bar formation by a process similar to the above: they promote the
492 river jet expansion and flow reduction, with a consequent more intense deposition close to
493 the river mouth. Finally, large waves suppress mouth bar formation because of their intense
494 seabed erosion and longshore transport (Fagherazzi et al., 2015).

495 Analysis of the above-mentioned wave-current interactions reveals that a river mouth acts
496 as a low-pass filter by removing (by breaking) sea and swell waves and letting long waves
497 pass. Recent studies have been dedicated to the propagation and evolution of IG waves at
498 inlets. Observations at the Ría de Santiuste (Spain, see Uncles et al., 2014) reveal how IG
499 waves (with periods of 4-5minutes), believed to be the outcome of estuary-amplified edge
500 waves, propagate upriver. This is well illustrated by the top panel of figure 15, which shows
501 a positive correlation between the water level (*WL*) and the flow velocity (*U'* in the figure).

502
503
504 Figure 15. IG wave propagation at river mouths. Top: positive water level-flow velocity
505 correlation at the Ría de Santiuste (Spain). Adapted from Uncles et al. (2014). Bottom: tide-
506 modulated IG wave propagation in the Albufeira Inlet (Portugal). No IG waves propagate
507 landward of the mouth at ebbs. Adapted from Bertin and Olabarrieta (2016).
508
509

The bottom panel of the same figure nicely illustrates the role of tide on the propagation of IG waves at inlets. Observations and wave-averaged modeling of the Albufeira Inlet (Portugal, see Bertin and Olabarrieta, 2016) reveal that upriver-propagation (from transect 0 to transect 18 of images C-Run 3 and D-Run 4) of IG-waves only occurs during tidal flood. Inspection of the same images reveals that: no propagation is possible at ebb (white areas in corrrespondence of the ebbs), IG waves are equally generated by BLW (image C-Run 3) and BP (image D-Run 4) mechanisms.

Other recent field observation support the role of river mouths and the upriver propagation of IG waves. Among these, notable are the EsCoSed and MORSE project studies (Brocchini et al., 2017; Melito et al., 2018a, 2019) performed at the mouth of the Misa River (Italy, see figures 1 and 17), located at a microtidal site (*RTR<3*) with a dissipative-to-intermediate beach (*5< Ω <20*).

Figure 16. The Misa River estuary in Senigallia (Italy) depicting locations of measuring stations within the final river reach (TGdown, QR1, QR2, QR3, TGup) and in the sea (QS1, QS2, QS3). Adapted from Melito et al. (2018a).

On the basis of water elevation measurements collected at various locations both in the sea (QS in figure 17) and in the river (TG and QR in figure 17), the energy flux density dE_f and the energy flux E_f:

$$dE_f = S(f)C_g \qquad dE_f = \int S(f)C_g df \tag{6}$$

have been computed - where *S(f)* is the power spectral density, C_g the wave group velocity and *f* the frequency. The fundamental result is that while in the sea (QS1, QS2) most of the energy content is due to swell and sea waves, the IG band becomes dominant within the river (e.g. QR2 of the left panel of figure 17) with a weak upriver decay (TGup of the right panel of figure 17).

Figure 17. Energy density flux (left) and energy flux (right) at the Misa River during storm conditions. Adapted from Melito et al. (2018a).

The EsCoSed field campaign has also provided useful information on the seabed morphology at the river mouth, highlighting the formation of large deposits/bars (blue in the right panel of figure 18) and scours holes (red in the right panel of figure 18). The sand deposits are found to be at a typical location, i.e. about twice the mouth width seaward of the mouth itself (Fagherazzi et al., 2015), but characterized by a very complex planview pattern.

Figure 18. Seabed variation between May-September 2013 (left) and between September 2013-February 2014 (right) at the Misa River. Adapted from Brocchini et al. (2017).

The above observations have motivated important efforts in the modeling of the dynamics evolving at a river mouth characterized by a complex morphology, with a specific focus on the role of waves.

Figure 19. Velocity maps for a strong river outflow opposed to three different wave regimes (from top to bottom: H_s = 0.0m, 0.5 m, 1.5 m). Left column: results from Olabarrieta et al. (2014). Right column: results from the wave-resolving solver of Brocchini et al. (2001), averaged over 10 wave periods. Adapted from Melito et al. (2018b).

Olabarrieta et al. (2014) used the wave-averaged 3D Regional Ocean Modeling System (ROMS) and an idealized river mouth shoal bathymetry to explore the wave-river current interactions. The increased, with respect to a planar beach, steepening and breaking of waves over the shoal leads to stronger seaward-flowing currents (undertow). Moreover, waves are seen to increase both the lateral spreading of the river current and the longshore transport.

574 In the attempt to better describe the dynamics forced by the sea waves, Melito et al.
575 (2018b) run the same cases studied by Olabarrieta et al. (2014) using the intra-wave NSWE
576 model of Brocchini et al. (2001), this neglecting vertical flow gradients, but improving the
577 time resolution of the wave forcing. The comparison between the two different numerical
578 solutions, illustrated in figure 19 for the case of a strong river outflow (1.1 m/s river current),
579 suggests that the main features of the wave-current interactions are captured, i.e. the river
580 current intensity and instability (e.g. Canestrelli et al., 2014). However, some significant
581 differences are also evident, among which: a weaker longshore spreading of the river jet,
582 the appearence of a number of large-scale eddies. Both differences seem to be caused by
583 the stronger wave breaking predicted by the NSWE, which removes significant amounts of
584 momentum and energy from the wave field, thus the reduced capacity of pushing shoreward
585 the river jet, in favour of the generation by differential wave breaking of large-scale eddies
586 or macrovortices (see previous subsection and Kennedy et al., 2006).
587 Such macrovortices not only contribute to the near-mouth flow mixing (right panels of
588 figure 19), but, as seen at the end of the previous subsection, also induce significant seabed
589 morphological changes. Falcini et al. (2014) recently sought for a mechanistic relationship
590 between potential vorticity Π (Π=ζ/d in a shallow-water framework) and sediment transport
591 at a river mouth. Lateral advection and diffusion of suspended sediment were found to be
592 directly proportional to the river jet vorticity, so that leeves building is observed in
593 correspondence of regions of large vorticity and mouth bar deposition in regions of low
594 vorticity.
595 In view of the large similarities between the analyses of vorticity-induced dynamics within
596 the nearshore by Kennedy et al. (2006) and Brocchini (2013) and at river mouths by Falcini
597 et al. (2014), an integration of the two analytical approaches seems useful to clarify the role
598 of breaking-wave-induced vorticity on the river mouth morphodynamics.

In the meantime, some numerical experiments are being carried out, by means of the hydro-morphodynamic NSWE solver of Postacchini et al. (2012), to describe the main morphological features that evolve at a simplified (e.g. shoal of Olabarrieta et al., 2014) and natural (e.g. Misa River) river mouth bathymetry. Preliminary numerical results are illustrated in figure 20, describing both a significant sediment deposition at the seaward edge of the idealized shoal and a weaker deposition at the typical location of a mouth bar (left panel) and a complex erosion deposition pattern at the mouth of the Misa River (right panel).

Figure 20. Estimated morphological evolution at the simplified river mouth bathymetry of Olabarieta et al. (2014), left panel and at the Misa River, right panel.

Comparison of the right panels of figures 18 and 20 reveals that these preliminary numerical solution can qualitatively capture the main characteristics of the complex erosion/deposition pattern that evolves just seaward of the river mouth.

Swash zone

The swash zone is that region of the beach that is alternatively covered and uncovered by water because of the action of sea waves (Brocchini and Baldock, 2008). Because of such process, fundamental characteristics of the swash zone are: the flow intermittency; the infiltration/exfiltration of water at the seabed; the very large sediment transport within the swash, which can be quantified, for example, in terms of the cross-shore sediment mass per beach longshore length transported by each swash event (Blenkisopp et al., 2011)

$$-40\,Kg/m < \hat{q}_x < 40\,Kg/m\,, \quad \hat{q}_x \equiv \int_{Tswash} q dt \tag{7}$$

or in terms of the longshore mass flux (Ribeiro et al., 2012).

$$Q_y \sim (1-10)\,Kg/s \tag{8}$$

The swash zone is also a locus for the generation of IG waves by two main mechanisms.

The first is the seaward reflection of BLW released by breaking (e.g., Schäffer, 1993). This is well illustrated in the left panel of figure 21, where a group of sea waves releases through breaking its BLW that propagates to the shoreline and it is there reflected to propagate out to sea as a Free Long Wave (FLW). The process of faster sea waves climbing the crest of the BLW is evident, as also illustrated in figure 9.

The second mechanism is the frequency downshifting of the sea waves that interact in the swash. This interaction occurs because waves in shallow water propagate with a velocity that is proportional to their height. Therefore, large waves travel faster than small waves and catch them up near or inside the swash zone (Mase, 1995). The assimilation of small waves by large waves leads to a reduced number of waves emerging from the swash zone, i.e. to a frequency downshifting, as illustrated in the right panel of figure 21.

Figure 21. Left: example of BLW release on a beach because of sea wave breaking. The shoreward-propagating (from bottom to top) wave group releases its BLW that is reflected at the shoreline and propagated (from top to bottom) out to sea as a FLW (adapted from Watson, Barnes and Peregrine, 1995). Right: example of frequency downshifting within the swash zone. Bichromatic waves propagate from seaward to the shoreline (from top to bottom) over a steep beach and interact in the swash zone giving wave of doubled period (adapted from Mase, 1995).

Most of the modelling of swash zone hydrodynamics, essentially forced by sea waves, has been done by using the NSWE. For an horizontally-1D flow evolving in the crosshore direction *x*, these read (e.g. Brocchini et al., 2001):

$$\begin{cases} d_{,t} + (ud)_{,x} = 0 \\ \vdots \\ u_{,t} + uu_{,x} + gd_{,x} = gh_{,x} + c_f \frac{u|u|}{d} \end{cases} \tag{9}$$

where commas gives partial differentiation, *d* and *h* are the total and still-water depths, respectively, *u* is the depth-averaged flow velocity, *g* is gravity acceleration and c_f a dimensionless coefficient for seabed friction.

Solution of such equations not only provides a quantitative means for studying the nearshore hydrodynamics, but can also be of help to illustrate some of the phenomena above described, like, for example, the interaction of sea waves within the swash zone. An example is provided by figure 22 for the case of a group of 5 sea waves.

Figure 22. Waves interacting at a wall (left) and at a swash zone (right). Top: incoming and outgoing characteristic curves at the shoreline. Bottom: a group of 5 sea waves (thin line) incoming to shore and outgoing IG waves (S-, thick line) resulting from the interaction of sea waves (adapted from Brocchini, 2006).

On the basis of the NSWE a number of analytical solutions has been made available over the years for both non-breaking and breaking waves. The pioneering work of Carrier and Greenspan (1958), who used the method of hodograph transformation, opened the way to some solutions that are currently used as reference for both analytical and numerical studies for the evolution of non-breaking sea waves on a beach. In particular, Brocchini and Peregrine (1996) extended the solution by Carrier and Greenspan (1958) to compute for the longshore flow due to waves propagating almost orthogonally to the beach (see figure 23). This solution can be used to provide estimates of the longshore mass flux to be compared with field measurements, like that of equation (8). More recent studies, e.g. Antuono and Brocchini (2010), suggest that analytical solutions for both non-breaking and breaking waves can be achieved also in the physical space, i.e. avoiding use of the hodograph transformation.

Figure 23. Left: maps, in the (x,t) plane of hodograph coordinates, free surface elevation η crosshore (u) and longshore (v) velocities for two sea waves interacting onto a beach. Right: mean longshore mass flux near and inside the swash zone for waves of different amplitude (adapted from Brocchini and Peregrine, 1996).

688 Cornerstone of analytical solutions for breaking sea waves, i.e. bores, on a beach is that of
689 Shen and Meyer (1963), in the following SM63. A bore of velocity u_0 collapsing onto a beach
690 of slope β forces a swash that is shoreward bounded by a parabolic shoreline x_s:

691 $$x_s = u_0 t - \frac{1}{2} g \, tan\beta \, t^2 \quad (10)$$

692 i.e. similar to the trajectory of a massive point under the action of gravity. This very neat
693 solution, which has been used for long times, has, however, the fundamental weakness of
694 predicting runup lenses much thinner than those observed on a natural beach.

695 Very recently Guard and Baldock (2007), in the following GB07, analyzed this issue and
696 suggested that the problem is caused by the assumption of regarding the collapsing bore
697 as a dam-break flow, where part of the fluid accelerates seaward. This is illustrated in the
698 sketch of the top panel of figure 24, whose left part illustrates the evolution of the SM63
699 solution in similarity with a dam-break flow (dashed line) that leads to both shoreward- and
700 seaward-accelerating fluid. The right image of the same panel illustrates how the GB07
701 solution, achieved by means of a linearly-time-varying (rather than constant) flow forcing at
702 collapse, predicts only shoreward-accelerating fluid after bore collapse. The bottom panel
703 of the same figure shows the fundamental differences in the water depths predicted by the
704 two solutions over a swash period. The SM63 solutions (thick lines) predicts more
705 asymmetric (downrush much longer than uprush) and much thinner (about a half) swash
706 lenses than those predicted by the GB07 solution (thin lines) that well compares with the
707 experimental data given by the symbols.

708 Recent remote sensing data, collected at 6 different beaches in USA and Australia, have
709 been used to assess the value and validity of the assumptions at the basis of the GB07
710 solutions (Power et al., 2011). Such observations confirm that: natural swash lenses are
711 deeper and less asymmetric than those predicted by SM63; a linearly-time-varying forcing
712 of the swash flow is better suited than a time-independent forcing to describe the evolution
713 of natural swashes.

Figure 24. Top: sketches of the flow by bore collapse. The left sketch shows the evolution of the SM63 solution in comparison to a dam-break flow (dashed lines), the right sketch suggests that only shoreward-accelerating fluid motion is predicted by the GB07 solution. Bottom: swash water thickness predicted by the SM63 solution (thick lines) and by the GB07 solution (thin lines) also compared with experimental data (symbols). Bottom panel adapted from GB07.

The fact that natural swash are fairly symmetric (still asymmetric in favour of the downrush) in time and characterized by fairly deep water lenses has important consequences on the understanding and modeling of the swash zone sediment transport and related morphodynamics. Thicker swash lenses lead to increased sediment pickup areas, because the sediment transport rate is directly proportional to the flow depth for a uniform sediment concentration (Pritchard and Hogg, 2005), and increased seaward sediment transport, because of the still existing swash asymmetry in favour of the rundown phase. However, such seaward sediment transport is counter-balanced by two main mechanisms: the presuspension of sediments due to the bore collapse onto the beach (which allows for a significant transport from the surf zone into the swash zone) and the settling lag effects due to the inertia of suspended sediment particles advected into the swash zone (Pritchard and Hogg, 2005). The above competing mechanisms, i.e. reduced swash asymmetry with increased thickness (promoting seaward transport) and sediment presuspension with settling lag effects (promoting shoreward transport) force a very complex swash zone morphology. This has been well described by Kelly and Dodd (2010), who implemented one of the most advanced and physically complete models for the swash zone hydro-moprhodynamics. Some of their results reveal the complexities in beach profile changes due to a swash event (see figure 25).

Figure 25. Left: space-time map of the changes in beach profile due a swash event. The thick dashed lines give the zero contour. Right: snapshots of the swash lens cross-shore sections (adapted from Kelly and Dodd, 2010).

While beach degradation (light tones of grey) occurs virtually over all of the seaward boundary of the swash zone, the most inshore portion of the swash zone undergoes significant, though non-uniform, aggradation (dark tones of grey). Bed discontinuities, typical of the evolution of an erosive bore, are seen to characterize both the uprush and the downrush stages.

The increasing awareness of the fundamental role of the swash zone for the entire nearshore hydro-morphodynamics stimulates always new research focused on links between the surf zone and swash zone dynamics.

From the hydrodynamic viewpoint, one of the most interesting recent studies is that by Moura and Baldock (2017), who focused on the relation between the shoreline (x_s) motion and the IG waves, both BP forced (horizontal BP excursion x_{br}) and BLW (vertical BLW excursion η_{BLW}), generated within the surf zone.

Figure 26. Shoreline relation with BLW and BP forcing. (a) Wave group. The vertical blue line gives the BP between its outer (red), x_o, and inner (green), x_i location. Grey and red lines give the released BLW and incident BP-forced IG wave, respectively. (b) BP excursion (black) and shoreline response to BP-forced (red) and BLW (grey) IG waves. Dashed line gives path for a shallow water wave from the BP to the shoreline. Horizontal colored lines are BP positions as in Figure 2a. (c) Cross-correlation between BP and shoreline excursion, BLW released (grey) and BP-foced IG wave (red). Adapted from Moura and Baldock, (2017).

Such relation can be illustrated with reference to the schematic of figure 26. When a group arrives at breaking (panel a) the first, smaller waves break at x_i (green line) and the subsequent, larger waves, more and more seaward, moving the BP to x_o (red line), the subsequent smaller waves force the BP to move back to x_i. Hence, the BP position $x_{br}(t)$ is – large (x_i), small(x_o), large (x_i) – i.e. in phase with the BLW vertical oscillation $\eta_{BLW}(t)$ (which is large, small, large, i.e. concave upwards). The amplitude of the BP-forced IG wave $\eta_{BP}(t)$ is proportional to the width of the breaking region. Hence, it increases during the passage

779 from small to large waves ($x_{br}(t)$ from zero to max) and decreases from large to small waves
780 ($x_{br}(t)$ from max to zero). Hence, $\eta_{BP}(t)$ is concave downward or in phase opposition to $x_{br}(t)$
781 and $\eta_{BLW}(t)$. The released BLW and the incident BP-forced wave propagate with the same
782 speed ($\sqrt{gh}$) and reach the shoreline at the same time (after traveling through the surf zone),
783 but with opposite phase (panel b). This leads to a positive correlation between $x_{s,BLW}$ *and* x_{br}
784 and a negative correlation between $x_{s,BP}$ *and* x_{br} (panel c).

785 On the basis of the above and using data coming from pressure sensors (water depth,
786 significant wave height and period, etc.) and video observations (shoreline and BP
787 excursion) collected at 3 Australian beaches, correlations between IG waves and shoreline
788 excursion were made. The main findings suggest that: the shoreline excursion is a good
789 proxy for infragravity waves in the inner surf and swash zone, IG wave generation by BLW
790 release is stronger for conditions with relatively narrow surf zones and plunging waves while
791 BP forcing is dominant for wider surf zones and spilling breaker conditions. This seems in
792 contradicition with the established understanding (Battjes et. al, 2004) that the BP forcing is
793 most efficient on steep beaches and the BLW release is most efficient on mildly-sloping
794 beaches, see also the discussion provided in “Template models” of above. Such apparent
795 contradiction can, perhaps, be solved by recalling that the surf zone width is not only function
796 of the beach slope but also of the characteristics of the incoming wave. However, some
797 further research seems needed here.

798 From the morphological point of view, one fundamental link between the surf zone and
799 swash zone dynamics is represented by the feeding of the most inshore sand bar (see also
800 figures 4, 5, 11) by swash zone sediments. This has been recently investigated by Alsina et
801 al. (2012), on the basis of dedicated laboratory experiments. Such experiments have been
802 carried out by using flow conditions (surf zone characterized by plunging breakers, $\varepsilon \approx 12\text{-}13$)
803 that, during an initial stage of run of about 3500 waves, led to the generation, from an almost-
804 planar beach, of a nearshore bar that slowing migrated off to sea (see blue-solid to green-

dashed lines, and vertical red lines in top panel of figure 27). The run was then stopped and the beach profile manually reshaped to a milder slope only inside the swash zone (pink-solid line). The same flow conditions were subsequently run, but bar migration stopped.

Figure 27. Cross-shore distribution of beach profile (top panel) and of cross-shore sediment transport rate (bottom panel) at various times before and after beah reshaping (adapted from Alsina et al., 2012).

This behavior was attributed to a reduced sediment transport from the swash to the surf zone, because of the beach slope reduction forced in the swash zone. Such a conjecture was also verified by analyzing the sediment transport rate illustrated in the bottom panel of figure 27. This shows that, while before beach reshaping it was $Q_x<0$, i.e. sediment transport rate was seaward, in the surf zone and inner swash zone, the sediment transport rate became vanishing to positive after beach reshaping. This is a clear indication of a major reduction of bar sediment feeding from the swash zone.

The above observations can be interpreted on the basis of a simple mechanistic model: the reduction of the swash zone beach slope (β_{swash} decreasing) forces an increase in the natural swash period T_{swash} defined as (Baldock and Holmes, 1999):

$$T_{swash} = \frac{2C\sqrt{gH_b}}{g\sin\beta}, \qquad C = O(1) \tag{12}$$

and, as a consequence, an increase in the swash-swash interactions, this being measured by the T_{swash}/T_i ratio (Baldock and Holmes, 1999); such increased swash-swash interaction makes the size of intense backwash events to decrease and, therefore, also the SST to sea, i.e. to a reduced sediment input to the nearshore bar (Alsina et al., 2012).

This section is closed with some promising ongoing research aimed at including the swash zone dynamics into wave-averaged solvers for the nearshore circulation (see also “Generalities on Models” in the Introduction). By definition, wave-averaged models cannot describe the swash zone dynamics associated to the sea waves, this leading to problems in

834 correctly predicting IG waves radiating out to sea. This is well illustrated by figure 22, whose
835 left panels describe the interaction of groups of 5 sea waves at a rigid wall used in wave-
836 averaged solvers to represent the shoreline, while the right panels describe the same
837 interaction at a swash zone reproduced by means of a wave-resolving model (in the specific
838 that of Brocchini et al., 2001). Two main features are very clear: the interaction at a wall,
839 being a mere reflection of the incoming wave groups, leads to outgoing groups with the
840 same structure of the incoming ones; the interaction at a swash zone allows for a significant
841 swash-swash interaction, for example because of large waves catching up and engulfing
842 small waves (see Mase, 1995 and figure 21), which contributes to increasing the intensity
843 (S^-) of the IG waves radiated out to sea (in the specific 20% larger for the interaction within
844 the swash zone). In view of the fundamental importance of wave-wave interaction within the
845 swash zone Brocchini and co-workers have designed some Shoreline Boundary Conditions
846 (SBCs) for the motion of the mean shoreline x_l and of the flow at at such boundary ($d(x_l)$,
847 $u(x_l)$) on the basis of an integral swash zone model (Brocchini and Peregrine, 1996;
848 Brocchini and Bellotti, 2002). Such SBCs have been successfully validated by means of
849 large-scale laboratory experiments (Bellotti et al., 2003) and have recently been
850 implemented in the ROMS wave-averaged solver (Haas and Warner, 2009). The main aim
851 of such preliminary implementation was to gauge the capabilities of reproducing swash zone
852 dynamics at a reduced computational cost, the final goal being that of predicting such
853 dynamics by simply running a wave-averaged solution. Figure 28 summarizes the main
854 findings of the mentioned implementation (Memmola, 2017; Memmola et al., 2019). The top
855 six panels give the shoreline motion computed by running ROMS alone at the unreasonably-
856 high resolution of 120 grid nodes (Δx) per offshore wavelength L_0 (black line), i.e. using it as
857 a wave-resolving model (benchmark solution), and ROMS coupled with the proposed SBCs
858 at lower and lower resolutions (red line), down to 2 grid nodes per wavelength. It is clear
859 that coupling ROMS with the SBCs allows one to run very cheap calculations that predict

reasonably well the benchmark solution by only using 3 grid nodes per wavelength (with $\Delta x/L_0 \approx 2$ the solution is too deteriorated). The lower two panels of the same figure show that not only the shoreline motion, but the entire flow field is well predicted by using the SBCs. The left and right panels give, respectively, the swash zone free surface elevation and onshore velocity for the benchmark solution (top panels) and ROMS+SBCs solutions for two very coarse meshes (middle and lower panels).

Figure 28. Top 6 panels: comparison of the ROMS ultra-highly resolved shoreline (black line) and ROMS+SBCs shorelines for lower and lower grid resolution. Bottom 2 panels: free surface elevation (left) and onshore velocity (right) for the benchmark ROMS solution (top panels) and ROMS+SBCs solutions for two very coarse meshes (middle and lower panels). Adapted from Memmola (2017).

These preliminary results demonstrate that the SBCs of Brocchini and co-worker can, at least, allow for cheap solutions that also provide the entire structure of the swash zone flow. Work in currently underway to achieve the more ambitious goal of running the ROMS-SBCs system in a prediciting mode (two-way coupled system), i.e. so that the SBCs are actually used to time-step the swash solution to be returned to ROMS.

Discussion

An important contribution of the present work is the identification of nonlocal forcing/dynamics, i.e. those that influence the entire nearshore as a whole. These are, in a cascading order of mutual control the: beach slope (obvious nonlocal forcing), IG waves and large-scale vortices with vertical axes (macrovortices).

The ***beach slope*** controls the role of IG waves, generation of macrovortices and the related sediment transport. In particular, BLW are regareded to be more efficient on mildly-sloping beaches, while IG waves are more likely generated by the oscillation of the BP on steep beaches (Battjes et al., 2004); although some recent studies by Moura and Baldock

(2017) seem to provide different information. The generation of macrovortices is controlled by the beach slope through the longshore differential breaking of sea waves that leads to generation and reorganization of potential vorticity at the lareral edges of breaking wave fronts (e.g. Kennedy et al. 2006). Although the role of SST at the lower boundary of the swash zone can be regarded as a local effect (see above), changes in the swash zone beach slope can significantly alter the swash-swash interactions and intense backwash events, this either promoting or stopping the sediment transport needed for the formation and migration of nearshore sandbars (Alsina et al., 2012).

IG waves provide a nonlocal forcing because the lengths involved in their generation and evolution are comparable to the surf zone width. IG are thought to have a fundamental role in the generation of sandbars, though various different models have been proposed like the "standing IG wave mechanism" (e.g. Short, 1975) and the "sea-IG waves correlation mechanism" of O'Hare and Huntley (1994) in which IG waves are responsible for the transport of sediments put into suspension by sea waves. Hence, the importance of the correlation between BLW and sea-wave envelope or the IG wave height to sea wave height ratio H_{IG}/H_{SW}, which is a good proxy for the sediment transport on beaches of all slopes (De Bakker et al., 2016). IG waves are also important for the riverine sediment transport because they can propagate upriver (e.g. Uncles et al, 2014), while sea and swell waves are dissipated by breaking at river mouths, which act as "low-pass filters". IG waves are not only generated at the seaward boundary of the surf zone, but also in the very shallow waters of the swash zone. This occurs by the wave-wave interaction due to large waves traveling faster than small waves and catching them up in the swash zone (Mase, 1995).

Macrovortices are a nonlocal forcing of the nearshore dynamics because they can maintain their coherent over large distances after their generation. Macrovortices contribute to sediment transport both by mobilizing the nearbed sands and, like IG waves, by carrying the sediments put into suspension by sea waves. The differential breaking that generates

916 macrovortices is particularly intense at river mouths characterized by seabed shoals. Hence,
917 macrovortices, beyond the river jet expansion, provide a significant contribution to both flow
918 mixing and sediment transport at river mouths (Melito et al., 2018b).

919 The analysis of the three subsystems of interest and of the related wave-induced
920 dynamics suggests some lines for future research, proposed with reference to each of such
921 subsystems.

922 Inspection of the state-of-the-art sandbar modeling reveals that we are still in need of
923 suitable stability models for the generation of 2D sandbars. As recalled in the analysis of
924 sandbars, available numerical solutions for the generation of 2D sandbars are characterized
925 by longshore instabilities in the form of rip channels (Dronen and Deigaard, 2007) and no
926 stable 2D sandbar systems can actually be reproduced for either normal or oblique wave
927 incidence. It seems, therefore, essential to investigate the mechanisms for the emergence
928 of 3D instabilities, also inspecting the role of the longshore currents, which are believed to
929 contribute to the maintenance of the stability of a 2D pattern (Shand et al., 1999).

930 The role of longshore flows is becoming of growing interest, as believed to significantly
931 control not only the generation, but also the migration of sandbars. In particular, longshore
932 currents due to waves obliquely incindent to the shore may have the potential to increase
933 the shear stress acting on the seabed and responsible for the sediment mobility (Parlagreco
934 et al., 2019). In this perspective longshore currents are not directly responsible for the
935 direction of cross-shore migration of sandbars (onshore vs offshore) but provide an indirect
936 important control through increased sediment mobility.

937 Observed opposite migration behaviours on beaches of similar steepness and sediment
938 size (Van Enckevort and Ruessink, 2003; Aagard et al., 2004) suggest that other important
939 mechanisms that may characterize conditions for offshore (NOffM model) vs onshore
940 (NOnM model) migration are the steepness and storm sequencing of the incident wave field.

In brief, future studies on sandbar generation and evolution should pay great attention to ***wave obliquity, steepness and storm sequencing***.

A more detailed inspection of the steepness of the incident wave field and related modalities of breaking is also advisable to try to explain the apparent contradiction between the recent findings of Moura and Baldock, (2017), suggesting that IG wave generation by BLW release is stronger for narrow surf zones and plungers while BP forcing is dominant for wider surf zones and spillers, and the established understanding (Battjes et. al, 2004) that the BP forcing is most efficient on steep beaches and the BLW release is most efficient on mildly-sloping beaches. This investigation should also try to encompass an analysis of the different modes of transport of turbulence associated with the two mentioned breaking types (seaward under spilling breakers and landward under plunging breakers – Ting and Kirby, 1994).

The implementation of ***novel Shoreline Boundary Conditions*** into wave averaging models for the nearshore circulation is certainly an important way forward for the inclusion of swash zone dynamics in long-term numerical simulations of the nearshore dynamics. The recent works of Memmola (2017) and Memmola et al. (2019) have shown the potentials of this approach, which will enable accurate and relatively cheap long-term numerical solutions. Work is currently underway for a predictive implementation of such approach.

In relation to the interactions occurring at a river mouth, studies are needed to clarify the roles of the different wave modes acting there. Recent field observations by Melito et al. (2019) confirm that ***the tide has an important role of modulating the IG waves*** that propagate upstream the river, result already obtained through numerical means by Olabarrieta (2016). This modulating effect, considerable even for microtidal environments (e.g. Misa River), should be better analyzed through field studies carried out in macrotidal environments.

The interactions of a river jet and the incoming sea waves should be better investigated also in relation to the generation of macrovortices. Preliminary evidence shows that they can remove significant amounts of energy from the incident wave field, reducing the opposing action of waves to the river stream (Melito et al., 2018b), and also force 3D seabed morphological features, e.g. mouth bars. Hence, both theoretical studies aimed at integrating the analytical approach of Brocchini (2013) for vorticity and potential vorticity generation with that of Falcini et al. (2014) as well as accurate morphological wave-resolving numerical simulations will likely clarify the role of ***breaking-wave-induced vorticity on the river mouth morphodynamics***.

Conclusions

The role of waves on the nearshore hydro-morphodynamics has been analyzed with specific focus to three subsystems of the nearshore i.e. sandbar region, river mouths and swash zone.

Each of these is characterized by very specific local dynamics. For sandbar generation and evolution fundamental is the role the nearbed sediment transport, with the correlation between the orbital velocity and sediment concentration in the BBL being of paramount importance for suitably predicting onshore bar migration (e.g. Henderson et al., 2004). It has also been shown that energetics-type models can achieve similarly good results if they reproduce such correlation through an integral approach, i.e. by including the effects of the wave freestream acceleration skewness (e.g. Hoefel and Elgar, 2002).

Local dynamics specific to river mouths are: the wave-current interaction by which the river current steepens the incoming waves, if intense enough to the point of breaking and/or blocking them, and forces a frequency downshifting (Chawla and Kirby, 2002); the related formation of a mouth bar (Fagherazzi et al., 2015) or the formation of a shoal that largely

991 influences the local dynamics by forcing stronger wave-breaking-induced return currents
992 (Olabarrieta et al., 2014) and wave breaking/sediment deposit farther from the mouth, i.e. at
993 the seaward edge of the shoal.

994 BBL dynamics largely influence the very shallow flows of the swash zone and, like for
995 sandbars, a proper modeling of the swash zone sediment transport can only be achieved if
996 correlation between the orbital velocity and sediment concentration in the BBL is well
997 described. Fundamental is also the description of the SST transport at the lower boundary
998 of the swash zone, which affects the sediment fluxes both from the surf zone, through
999 sediment presuspension at bore collapse (Pritchard and Hogg, 2005), and to the surf zone,
1000 in association to intense backwash events.

1001 A closure can be reached by recalling the main connections among the three subsystems
1002 of interest. IG waves provide a fundamental connection because generated both at the
1003 seaward edge of the surf zone (by BLW release, BP oscillation and edge wave interaction)
1004 and at the swash zone (because of wave-wave interaction) can propagate almost unaltered
1005 upstream at river mouths. Another important connection is provided by the evolution of
1006 macrovortices, which generated by differential breaking move over long distances in the surf
1007 zone and may reach the shoreline where they can rebound and alter the near-shoreline
1008 morphology. From the morphological viewpoint, obvious links are those between: the swash
1009 zone morphology and the along-river-flank sediment transport that can feed the swash zone
1010 and the swash zone and the nearshore sandbars, which can drive sediments for their
1011 evolution from the swash zone.

1012

1013 Acknowledgements

1014 This paper is essentially a written transposition of the same-titled invited talk given at
1015 RCEM2017. The organizers are thanked for the opportunity given to reflect on and present
1016 this material. The following colleagues and friends are thanked for providing both useful

material and insightful discussions: Tom Baldock (University of Queensland, Australia), Riccardo Briganti (University of Nottingham, England), Joe Calantoni (Naval Research Laboratory, USA), Dan Conley (University of Plymouth, England), Steve Elgar (Woods Hole Oceanographic Institution, USA), Tom Hsu (University of Delaware, USA), Matteo Postacchini (Università Politecnica delle Marche, Italy), Gerben Ruessink (Utrecht University, The Nethelands), Alex Sheremet (University of Florida, USA). Financial support from the ONR Global (UK), through the MORSE Research Grant (N62909-17-1-2148) is gratefully acknowledged.

References

Aagard, T., Davidson-Arnott, R., Greenwood, B., Nielsen, J. (2004). Sediment supply from shoreface to dunes: linking sediment transport measurements and long-term morphological evolution. *Geomorphology* **60**: 205-224.

Alsina, J.M., Caceres, I., Brocchini, M., Baldock, T.E. (2012). An experimental study on sediment transport and bed evolution under different swash zone morphological conditions. *Coastal Engineering* **68**: 31-43.

Anthony, E.J. (2015). Wave influence in the construction, shaping and destruction of river deltas: A review. *Marine Geology* **361**: 53-78.

Antuono, M., Brocchini, M. (2010). Solving the Nonlinear Shallow Water Equations in physical space. *Journal of Fluid Mechanics* **643**: 207-232.

Armaroli, C., Ciavola, P. (2011). Dynamics of a nearshore bar system in the northern Adriatic: A video-based morphological classification. *Geomorphology* **126**: 201-216.

Ashton, A.D., Giosan, L. (2011). Wave-angle control of delta evolution. *Geophysical Research Letters* **38**: L13405.

Bailard, J.A. (1981). An energetics total load sediment transport model for a plane sloping beach. *Journal of Geophysical Research – Oceans* **86(C11)**: 10938-10954.

1043 Baldock, T.E. (2006). Long wave generation by the shoaling and breaking of transient wave
1044 groups on a beach. *Proceedings of the Royal Society of London* **A 462**: 1853-1876.
1045 Baldock, T.E., Holmes, P. (1999). Simulation and prediction of swash oscillations on a steep
1046 beach. *Coastal Engineering* **36 (3)**: 219–242.
1047 Battjes, J.A., Bakkenes, H.J., Janssen, T.T., van Dongeren, A.R. (2004). Shoaling of
1048 subharmonic gravity waves. *Journal of Geophysical Research - Oceans* **109**: C02009.
1049 Bellotti, G., Archetti, R., Brocchini, M. (2003). Experimental validation of mean swash zone
1050 boundary conditions, *Journal of Geophysical Research - Oceans* **108(C8)**: 3250,
1051 doi:10.1029/2002JC001510.
1052 Berni, C., Barthelemy, E., Michallet, H. (2013). Surf zone cross-shore boundary layer
1053 velocity asymmetry and skewness: an experimental study on a mobile bed. *Journal of*
1054 *Geophysical Research - Oceans* **118**: 2188–2200.
1055 Bertin, X., Olabarrieta, M. (2015). Relevance of infragravity waves in a wave-dominated
1056 inlet. *Journal of Geophysical Research - Oceans* **121**: 5418–5435.
1057 Blenkinsopp, C.E., Turner, I.L., Masselink, G., Russell, P.E. (2011). Swash zone sediment
1058 fluxes — field observations. *Coastal Engineering* **58**: 28–44.
1059 Brocchini, M. (2006). Integral swash zone models. *Continental Shelf Research* **26**: 653-660.
1060 Brocchini, M. (2013). A reasoned overview on Boussinesq-type models: the interplay
1061 between physics, mathematics and numerics. *Proceedings of the Royal Society of*
1062 *London* **A 469**: 20130496, doi:10.1098/rspa.2013.0496.
1063 Brocchini, M., Peregrine, D.H. (1996). Integral flow properties of the swash zone and
1064 averaging. *Journal of Fluid Mechanics* **317**: 241-273.
1065 Brocchini, B., Bellotti, G. (2002). Integral flow properties of the swash zone and averaging.
1066 Part 2. The shoreline boundary conditions for wave-averaged models. *Journal of Fluid*
1067 *Mechanics* **458**: 269-281.

1068 Brocchini, M., Baldock, T.E. (2008). Recent advances in modeling swash zone dynamics:
1069 influence of surf-swash interaction on nearshore hydrodynamics and morphodynamics.
1070 *Reviews in Geophysics* **46(3)**: RG3003, doi:10.1029/2006RG000215.
1071 Brocchini, M., Calantoni, J., Postacchini, M., Sheremet, A., Staples, T., Smith, J., Reed,
1072 A.H., Braithwaite III, E.F., Lorenzoni, C., Russo, A., Corvaro, S., Mancinelli, A. and
1073 Soldini, L. (2017). Comparison between the wintertime and summertime dynamics of the
1074 Misa River estuary. *Marine Geology* **385**: 27-40.
1075 Caballeria, M., Coco, G., Falqués, A., Huntley, D.A., 2002. Self-organization mechanisms
1076 for the formation of nearshore crescentic sand bars. *Journal of Fluid Mechanics* **465**: 379–
1077 410.
1078 Canestrelli, A., Nardin, W., Edmonds, D., Fagherazzi, S., Slingerland, R. (2014), Importance
1079 of frictional effects and jet instability on the morphodynamics of river mouth bars and
1080 levees, *Journal of Geophysical Research - Oceans* **119**: 509–522.
1081 Certain, R., Barusseau, J.P. (2005). Conceptual modelling of sand bars morphodynamics
1082 for a microtidal beach (Sète, France). *Bulletin de la Société Géologique de France* **176**:
1083 343–354.
1084 Chang, Y.S., Scotti, A. (2004). Modeling unsteady turbulent flows over ripples: Reynolds-
1085 averaged Navier-Stokes equations (RANS) versus large-eddy simulation (LES). *Journal*
1086 *of Geophysical Research - Oceans* **109**: 1-16.
1087 Chawla, A., Kirby, J.T. (2002). Monochromatic and random wave breaking at blocking
1088 points. *Journal of Geophysical Research - Oceans* **107**: 3067.
1089 Coco G., Murray, A.B. (2007). Patterns in the sand: from forcing templates to self-
1090 organization. *Geomorphology* **91**: 271-290.
1091 Cooper, J.A.G. (2001). Geomorphological variability among microtidal estuaries from the
1092 wave-dominated South African coast. *Geomorphology* **40**: 99-122.

1093 de Bakker, A.T.M., Brinkkemper, J.A., van der Steen, F., Tissier, M.F.S., Ruessink B.G.
1094 (2016). Cross-shore sand transport by infragravity waves as a function of beach
1095 steepness. *Journal of Geophysical Research – Earth Science* **121**: 1786-1799.
1096 Drake, T.G., J. Calantoni (2001). Discrete particle model for sheet flow sediment transport
1097 in the nearshore. *Journal of Geophysical Research - Oceans* **106**: 19,859–19,868.
1098 Dronen, N., Deigaard, R. (2007). Quasi-three-dimensional modelling of the morphology of
1099 longshore bars. *Coastal Engineering* **54**: 197-215.
1100 van Enckevort, I.M.J., Ruessink, B.G. (2003). Video observations of nearshore bar
1101 behaviour. Part 1: alongshore uniform variability. *Continental Shelf Research* **23**: 501-
1102 512.
1103 Fagherazzi, S., Edmonds, D.A., Nardin, W., Leonardi, N., Canestrelli, A., Falcini, F.,
1104 Jerolmack, D.J., Mariotti, G., Rowland, J.C., Slingerland, R.L. (2015). Dynamics of river
1105 mouth deposits. *Reviews in Geophysics* **53**, 31pp., doi:10.1002/2014RG000451.
1106 Falcini, F., Piliouras, A., Garra, R., Guerin, A., Jerolmack, D.J., Rowland, J., Paola, C. (2014)
1107 Hydrodynamic and suspended sediment transport controls on river mouth morphology
1108 *Journal of Geophysical Research – Earth Surface* **119**: 1-11, doi:10.1002/2013JF002831.
1109 Gallagher, E., Elgar, S., Guza, R.T. (1998). Observations of sand bar evolution on a natural
1110 beach. *Journal of Geophysical Research - Oceans* **103(C2)**: 3203-3215.
1111 Galloway, W.E. (1975). Process framework for describing themorphologic and stratigraphic
1112 evolution of delta depositional systems. In: Broussard, M.L (Ed.), Deltas: Models for
1113 Exploration. Houston Geological Society, Houston, pp. 87–98.
1114 Guard, P., Baldock, T. (2007). The influence of seaward boundary conditions on swash zone
1115 hydrodynamics. *Coastal Engineering* **54**: 321–331.
1116 Haas, K.A. and Warner, J.C. (2009). Comparing a quasi-3D to a full 3D nearshore circulation
1117 model: SHORECIRC and ROMS. *Ocean Modelling* **26**: 91-103.

1118 Henderson, S.M., Allen, J.S., Newberger P.A. (2004). Nearshore sandbar migration
1119 predicted by an eddy-diffusive boundary layer model. *Journal of Geophysical Research -*
1120 *Oceans* **109**: C06024, doi:10.1029/2003JC002137.
1121 Hoefel, F., Elgar, S. (2003). Wave-induced sediment transport and sandbar migration.
1122 *Science* **299**: 1885-1887.
1123 Holman, R.A., Bowen, J. (1982). Bars, bumps, and holes: models for the generation of
1124 complex beach topography. *Journal of Geophysical Research - Oceans* **87**: 457-468.
1125 Hsu, T., Elgar, S., Guza, R.T. (2006). Wave-induced sediment transport and onshore
1126 sandbar migration. *Coastal Engineering* **53**: 817–824.
1127 Kennedy, A.B., Brocchini, M., Soldini, L., Gutierrez, E. (2006). Topographically controlled,
1128 breaking-wave-induced macrovortices. Part 2. Rip current topographies. *Journal of Fluid*
1129 *Mechanics* **559**: 57–80.
1130 Kirby, J.T. (2016). Boussinesq models and their application to coastal processes across a
1131 wide range of scales. *Journal of Waterways, Port, Coastal and Ocean Engineering* **142**:
1132 03116005.
1133 Lesser, G.R., Roelvink, J.A., van Kester, J.A.T.M., Stelling, G.S. (2004). Development and
1134 validation of a three-dimensional morphological model. *Coastal Engineering* **51**: 883-915.
1135 Longuet-Higgins, M. S., Stewart, R. W. (1964). Radiation stress in water waves: a physical
1136 discussion with applications. *Deep Sea Research I* **11**: 529-562.
1137 Lubin, P., Glockner, S., Kimmoun, O., Branger, H. (2011). Numerical study of the
1138 hydrodynamics of regular waves breaking over a sloping beach. *European Journal of*
1139 *Mechanics B/Fluids* **30**: 552-564.
1140 Ma, G., Shi, F., Kirby, J.T. (2012). Shock-capturing non-hydrostatic model for fully dispersive
1141 surface wave processes. *Ocean Modelling* **43-44**: 22-35.
1142 Mase, H. (1995). Frequency down-shift of swash oscillations compared to incident waves.
1143 *Journal of Hydraulic Research* **33**: 397-411.

1144 Masselink, G., Short, A.D. (1993). The Effect of Tide Range on Beach Morphodynamics and
1145 Morphology: A Conceptual Beach Model. *Journal of Coastal Research* **9**: 785-800.
1146 Melito, L., Postacchini, M., Sheremet, A., Calantoni, J., Zitti, G, Darvini, G., Brocchini, M.
1147 (2018a). Wave-current interactions and infragravity wave propagation at a microtidal inlet.
1148 *E-proceedings of the 3rd EWAS International Conference:* 477-485.
1149 Melito, L., Postacchini, G, Darvini, G., Brocchini, M. (2018b). Waves and currents at a river
1150 mouth: the role of macrovortices, sub-grid turbulence and seabed friction. *Water* **10**: 550,
1151 doi:10.3390/w10050550 .
1152 Melito, L., Postacchini, M., Sheremet, A., Calantoni, J., Zitti, G., Darvini G., Brocchini M.
1153 (2019l). Hydrodynamics at a microtidal inlet: analysis of propagation of the main wave
1154 components. *Estuarine Coastal and Shelf Science* (under peer review).
1155 Memmola, F. (2017). Analysis and development of oceanographic models: reaching the
1156 swash zone. Università Politecnica delle Marche, PhD Thesis, 92pp.
1157 Memmola, F., Coluccelli, A., Russo, A., Warner J.C., Brocchini M. (2019). Wave-resolving
1158 Shoreline Boundary Conditions for wave-averaged coastal models. *Ocean Modeling*
1159 (under peer review).
1160 Moura, T., Baldock, T.E. (2017). Remote sensing of the correlation between breakpoint
1161 oscillations and infragravity waves in the surf and swash zone. *Journal of Geophysical*
1162 *Research - Oceans* **122**: 3106-3122.
1163 Nienhuis, J.H. (2016). Plan-view evolution of wave-dominated deltas. Massachusetts
1164 Institute of Technology and the Woods Hole Oceanographic Institution, PhD Thesis,
1165 182pp.
1166 Nienhuis, J.H., Ashton, A.D., Giosan, L. (2015). What makes a delta wave-dominated?
1167 *Geology* **43(6)**: 511-514.
1168 Nienhuis, J.H., Ashton, A.D., Giosan, L. (2016). Littoral steering of deltaic channels. *Earth*
1169 *and Planetary Science Letters* **453(1)**: 204-214.

1170 O'Hare, T.J., Huntley, D.A. (1994). Bar formation due to wave groups and associated long
1171 waves. *Marine Geology* **116**: 313-325.
1172 Olabarrieta, M., Geyer, W.R., Kumar, N. (2014). The role of morphology and wave-current
1173 interaction at tidal inlets: An idealized modeling analysis. *Journal of Geophysical*
1174 *Research – Oceans* **119**: 8818-8837.
1175 Parlagreco, L. Melito, L. Devoti, S. Perugini, E. Soldini, L. Zitti G., Brocchini M. (2019).
1176 Monitoring for coastal resilience: preliminary data from five Italian sandy beaches. **19**.
1177 1854; doi:10.3390/s19081854
1178 Peregrine, D.H. (1999). Large-scale vorticity generation by breakers in shallow and deep
1179 water. *European Journal of Mechanics B/Fluids* **18**: 403–408.
1180 Plant, N.G., Freilich, M.H., Holman, R.A. (2001). Role of morphologic feedback in surf zones
1181 and bar response. *Journal of Geophysical Research - Oceans* **106**: 973-989.
1182 Postacchini, M., Brocchini, M., Landon, M., Mancinelli, A. (2012). A multi-purpose, intra-
1183 wave, shallow water hydro-morphodynamic solver. *Advances in Water Resources* **38**: 13-
1184 26.
1185 Postacchini, M., Brocchini, M., Soldini, L. (2014). Vorticity generation due to cross-sea.
1186 *Journal of Fluid Mechanics* **744**: 286-309.
1187 Pourzangbar, A., Losada, M.A., Saber, A., Rasoul Ahari, L., Larroudé, P., Vaezi, M. and
1188 Brocchini, M. (2017). Prediction of non-breaking wave induced scour depth at the trunk
1189 section of breakwaters using Genetic Programming and Artificial Neural Networks.
1190 *Coastal Engineering* **121**: 107-118.
1191 Power, H.E., Holman, R.A., Baldock, T.E. (2011). Swash zone boundary conditions derived
1192 from optical remote sensing of swash zone flow patterns. *Journal of Geophysical*
1193 *Research - Oceans* **116**: C06007, doi:10.1029/2010JC006724.
1194 Pritchard, D., Hogg, A.J. (2005). On the transport of suspended sediment by a swash event
1195 on a plane beach, *Coastal Engineering* **52(1)**: 1–23.

1196 Ribas, F. (2003). On the growth of nearshore sand bars as instability processes of
1197 equilibrium beach states. Universitat Politecnica de Catalunya, PhD Thesis, 242pp.
1198 Ribeiro, M., Barrio, F., Taborda, R., Cascalho, J., Bosnic, I. Rodríguez, I., Sanchez, M.
1199 (2012). Longshore drift: experimental and empirical predictors. The example of the Ebro
1200 Delta. *Proceedings of the 2as Jornadas de Engenharia Hidrográfica*, Lisboa, Portugal,
1201 pp. 271–274.
1202 Roelvink, J. A., Stive, M. J. F. (1989) Bar-generating cross-shore flow mechanisms on a
1203 beach. *Journal of Geophysical Research - Oceans* **94**: 4785-4800.
1204 Ruessink, B.G., Kroon, A. (1994). The behaviour of a multiple bar system in the nearshore
1205 zone of Terschelling, the Netherlands: 1965–1993. *Marine Geology* **121**: 187–197.
1206 Schäffer, H.A. (1993). Infragravity waves induced by short wave groups. *Journal of Fluid*
1207 *Mechanics* **247**: 551–588.
1208 Shand, R.D., Bailey, D.G., Shephard, M.J. (1999). An inter-site comparison of net offshore
1209 bar migration characteristics and environmental conditions. *Journal of Coastal Research*
1210 **15**: 750–765.
1211 Shen, M.C., Meyer, E.R. (1963). Climb of a bore on a beach. Part 3. Run-up. *Journal of*
1212 *Fluid Mechanics* **16**: 113–125.
1213 Short, A.D. (1975). Multiple offshore bars and standing waves. *Journal of Geophysical*
1214 *Research - Oceans* **80**: 3838-3840.
1215 Short, A.D., Aagard, T. (1993). Single and multi-bar beach change models. *Journal of*
1216 *Coastal Research* **15**: 141-157.
1217 Symonds, G., Huntley, D.A., Bowen, A.J. (1982). Two-dimensional surf beat: long wave
1218 generation by a time-varying breakpoint. *Journal of Geophysical Research - Oceans* **87**:
1219 492-498.
1220 Ting, F.C.K., Kirby, J.T. (1994). Observation of undertow and turbulence in a laboratory surf
1221 zone. *Coastal Engineering* **24**: 51-80.

1222 Torres-Freyermuth, A., Lara, J.L. and Losada, I.J. (2010). Numerical modelling of short- and
1223 long-wave transformation on a barred beach. *Coastal Engineering* **57**: 317-330.
1224 Uncles, R.J. Stephens, J.A., Harris C. (2014). Infragravity currents in a small ría: Estuary-
1225 amplified coastal edge waves? *Estuarine Coastal and Shelf Science* **150**: 242-251.
1226 Valle-Levinson A. (2011). Classification of Estuarine Circulation. In: Wolanski E and
1227 McLusky DS (eds.) *Treatise on Estuarine and Coastal Science* **1**, 75–86. Waltham:
1228 Academic Press.
1229 Van Enckevort, I.M.J. (2001). Daily to yearly nearshore bar behaviour. Utrecht University,
1230 PhD Thesis, 174pp.
1231 Van Enckevort, I.M.J., Ruessink, B.G. (2003).Video observations of nearshore bar
1232 behaviour. Part 1: alongshore uniform variability. *Continental Shelf Research* **23**: 501–
1233 512.
1234 Vittori, G., DeSwart, H.E., Blondeaux, P. (1999). Crescentic bedforms in the nearshore
1235 region. *Journal of Fluid Mechanics* **381**: 271-303.
1236 Watson, G., Barnes, T. C. D., Peregrine, D. H. (1995). The generation of low-frequency
1237 waves by a single wave group incident on a beach. *24th International Conference on*
1238 *Coastal Engineering*, 776-790.
1239 Wijnberg, K.M., Terwindt, J.H.J. (1995). Extracting decadal morphological behavior from
1240 high-resolution, long-term bathymetric surveys along the Holland coast using
1241 eigenfunction analysis. *Marine Geology* **126**: 301-330.
1242 Wijnberg, K.M., Kroon, A. (2002). Barred beaches. *Geomorphology* **48**: 103-120.
1243 Wright, L.D., Coleman, J.M., Erickson, M.W., (1974). Analysis of major river systems and
1244 their deltas: morphologic and process comparisons. Technical Report 156, Coastal
1245 Studies Institute. Louisiana State University (125 pp.).
1246 Wright, L.D., Short, A.D. 1984. Morphodynamic variability of surf zones and beaches: A
1247 synthesis. *Marine Geology* **56**: 93-118.

1248

Wave-forced dynamics in the nearshore river mouths, and swash zones

Maurizio Brocchini

DICEA, Università Politecnica delle Marche, Ancona, Italy

Abstract

The role of wave forcing on the main hydro-morphological dynamics evolving in the shallow waters of the nearshore and at river mouths is analyzed. Focus is mainly on the cross-shore dynamics that evolve over mildly sloping barred, dissipative sandy beaches from the storm up to the yearly time scale, at most. Local mechanisms, nonlocal mechanisms and connections across three main inter-related subsystems of the nearshore - the region of generation and evolution of nearshore bars, river mouths and the swash zone - are analyzed. The beach slope is a major controlling parameter for all nearshore dynamics. A local mechanism that must be properly described for a suitable representation of wave-forced dynamics of all such three subsystems is the proper correlation between orbital velocity and sediment concentration in the bottom boundary layer; while specific mechanisms are the wave-current interaction and bar generation at river mouths and the sediment presuspension at the swash zone. Fundamental nonlocal mechanisms are both Infragravity (IG) waves and large-scale horizontal vortices (i.e. with vertical axes), both influencing the hydrodynamics, the sediment transport and the seabed morphology across the whole nearshore. Major connections across the three subsystems are the upriver propagation of IG waves generated by breaking sea waves and swash-swash interactions, the interplay between the swash zone and along-river-flank sediment transport and the evolution of nearshore sand bars.

Introduction

Focus, motivation and method

This work focuses on wave-forced nearshore and river mouth dynamics, as opposite to tidally-forced dynamics - i.e. such that $RTR=TR/H_b<3$, where TR is the tidal range and H_b is the height of breaking waves (Masselink and Short, 1993).

In more detail, cross-shore (mostly) dynamics evolving from the yearly down to the storm time scales are investigated. With reference to coastal and river mouth hydro-morphological regimes the present analysis gives attention to the following two regimes.

First, open-coast, mildly sloping, barred ($\Omega=H_b/w_sT_i>2$, where Ω is the Dean parameter), w_s is the sediment fall velocity and T_i is the period of incoming waves - Wright and Short, 1984) and dissipative ($\epsilon=A_b\omega^2/gtan^2\beta>20$, where the surf-scaling parameter ϵ depends on the amplitude of the breaking waves A_b, on the radian wave frequency $\omega=2\pi/T_i$ and on the beach slope β -Wright and Short, 1984) sandy beaches. Second, wave-dominated or river-dominated and wave-modified (which feed sediments to sea) river mouths (Cooper, 2001).

Scopes of the present contribution are the following. First, to provide a fairly complete (obviously not exhaustive) and clear overall view of what we know and what we do not not know of wave-forced nearshore and river mouth dynamics. Second, to give the needed focus to recent progresses made available on specific dynamics. But the main aim is to ***highlight links and relations among such dynamics***, this by properly highlighting nonlocal agents and relations.

Regarding this problem as a puzzle to be solved (see figure 1), this entailing local and nonlocal relations, this paper tries to: put the analysis in the proper context, with no pretention for a systematic description; move from consolidated knowledge to new results; move from observations to modeling; move from the large to the small scales; inspect different types of models, both in terms of their structure and use.

Figure 1. Wave-forced dynamics in the nearshore and estuaries: a puzzle to be solved. This photo, taken at the microtidal Misa River estuary (Senigallia, Italy), illustrates through one single view the three subsystems analyzed in the paper.

The latter issue is analyzed in some detail because of its intrinsic importance and of the guidance that models provide in exploring the mechanisms of the phenomena at hand.

Generalities on Models

The hydro-morphodynamics of the nearshore region, including that evolving at river mouths, is so complex that a number of different methods and models has been proposed and implemented over the years. However, such abundance of models has also brought to some major ambiguities in the definition and use of such models.

Hence, some clarification seems useful, which is based on a detailed classification of the models in terms of their: intrinsic structure and use.

Model structure

Although this classification, as many others, is somewhat arbitrary (e.g. as function of the level of closure implemented), its use may help understand what model is actually applied for a specific analysis. The structure of the models at hand can be classed as either “process based” or “empirically based”.

“Process-based models” rely on equations derived from fundamental physical principles and/or conservation laws. In the following three examples of such models (at different levels of time/space scales and resolution) are described.

First, wave-averaged models: Nonlinear Shallow Water Equation (NSWE)-type (e.g. Delft3D, https://oss.deltares.nl/web/delft3d/home; Lesser et al., 2004; NHWAVE, Ma et al., 2012); Oceanographic (e.g. ROMS, https://www.myroms.org/index.php, Haas and Warner,

2009), etc. Second, wave-resolving models: NSWE-type (e.g. Postacchini et al., 2012); Boussinesq-type (e.g. Brocchini, 2013; Kirby, 2016); etc. Third, models that account for turbulence through proper closures: Reynolds Averaged Navier-Stokes; Large Eddy Simulations (Chang and Scotti, 2004; Torres-Freyermuth, Lara and Losada, 2010; Lubin et al. 2011) etc.

"Empirically-based models" rely on equations constructed from a mixture of conservation laws and observations, with a significant weight of empirical inputs. In fact, though also turbulence models like RANS and LES do require some empirism for the turbulence closure relations (hence the arbitrariness of classing models), their structure heavily relies on conservation laws and less on closures that are based on solid theoretical foundations. Examples of empirically-based models are: Regression-type models, Machine Learning Approaches (e.g. Pourzangbar et al., 2017), etc. and energetics-type, which solve a sediment mass conservation equation (Exner equation) where the mass fluxes come from empirically-based closure laws (e.g. Bailard, 1981).

Model use

The above models can be, each in its own way, used in terms of either a template/forced approach or a stability approach (at times referred to as "self-organization", see, for example, Coco and Murray, 2007). To clarify the above an example is made with reference to the classical Exner 1D sediment transport equation, which can be formulated as (e.g. Plant et al., 2001):

$$\frac{\partial z_b}{\partial t}(x,t) = I + II + III \quad (1)$$

where z_b is the seabed position and

I = is a forcing term due to initial bathymetry and wave field,

II = gives the modification of forcing due to externally-forced changes in wave height,

III = is a feedback term due to the rate of change of the seabed position z_b, which introduces a feedback behavior in (1).

Template/forced models and stability-type models can be distinguished by the presence of I, II and III. Template/forced morphological models are such that I≠0, II≠0 and III=0, while stability approaches must have III≠0. With reference to the specific problem of seabed features generation, while template models may identify compelling mechanisms, i.e. a template, for the initial stages of formation (e.g. at breakpoint, at nodes/antinodes of standing waves, etc.) stability models are such that perturbations evolve simultaneously in the hydrodynamic and bathymetric fields. This is illustrated by the examples given in figures 2 and 3. The initial bathymetry used for the simulations of figure 3 consisted of a longshore-uniform sand bar.

Figure 2. Forced/template mechanism: “synchronous standing edge waves” (left) and flow imprinted on sand giving beach cusps (right). Adapted from Coco and Murray, (2007).

Figure 3. Stability/Self-organization mechanism: crescentic bars emerge from the feedback between flow and bathymetry (initial longshore-uniform bar bathymetry). Top: waves breaking on shoals force onshore flow, which returns to sea in gaps. Bottom: for suspended sediment decreasing from breaker line to shore, the onshore flow favors deposition (shoals grow) and the offshore flow favors erosion (scour holes grow). Hence, the development of crescentic bars. Adapted from Coco and Murray, (2007).

The rest of the paper is structured as follows. The next section provides detailed information specific to 1) the generation and evolution of nearshore bars, 2) river mouth and 3) swash zone dynamics. A short Discussion and then Conclusions close the paper.

Wave forced-dynamics for three fundamental subsystems: sand bars, river mouths and swash zone

Sand bars

The generation and evolution of sand bars in the nearshore is analyzed as a first applicative topic because of its many implications, which help set the scene for all the rest of the paper. Consolidated observations and models are first illustrated, then followed by more recent findings.

Starting from the observations, sand bars that evolve in the nearshore are usually classed in terms of their planview shape, i.e. longshore uniform (2D) and rhythmic (3D). Different evolution mechanisms lead to different evolution time scales (e.g. Wijnberg and Kroon, 2002). We can distinguish between: 2D sand bars (left panel of figure 4), which emerge as the outcome of wave-induced, cross-shore sediment transport and evolve over scales of days to months (e.g. Ruessink and Kroon, 1994); 3D sand bars (right panel of figure 4), which emerge as the outcome of horizontal circulation patterns and, because of this stronger forcing, evolve on shorter time scales, i.e. hours to days (e.g. Caballeria et al., 2002).

Figure 4. Left panel: planview image of two shore-parallel sand bars at Noordwijk beach (The Netherlands, 19th November 2000). Right panel: planview image of surf zone complex topography at Duck (U.S.A. Atlantic coast, 10th January 1994). Adapted from Ribas Prats (2003).

Three main interpretative models exist for the overall generation and evolution mechanisms of nearshore sandbars.

The most known is the Net Offshore Migration (NOffM) model, which suggests that multiple nearshore 2D bars have multi-annual lifetimes and pass through 3 stages (figure 5). Generation occurs close to shore because of the interaction of undertow, wave orbital velocity asymmetry and group-forced IG orbital motion (Roelvink and Stive, 1989). This is followed by a net seaward migration, which is the outcome of an alternation of gradual onshore movements during calms and episodic strong offshore movements during storms (Van Enckevort and Ruessink, 2003, see also the right panel of figure 5). Finally,

degeneration occurs at the outer surf zone when the bar moves offshore of the breaker line where weakly or non-breaking waves induce a net onshore sediment transport. This step governs the entire cycle and only when the offshore bar degenerates at the breaker line the nearshore bar can start its offshore migration (Wijnberg and Terwindt, 1995).

Figure 5. Left panel: seabed cross-shore profiles at Noordwijk, The Netherlands, from 1979 to 1987, showing cyclic bar behavior with a recurrence interval of about 4-5 years. Adapted from van Enckvort, (2001). Right panel: seabed cross-shore profiles at Duck (U.S.A. Atlantic coast, September-October 1994). Thick curves with red dates are the beginning of storms, resulting in offshore bar migration (red arrows). Thin curves are the subsequent daily profiles. The sandbar migrated onshore (blue arrows) during calm periods between the storms. Courtesy of Dr. S. Elgar.

The second model is the Net Onshore Migration (NOnM) model, which suggests that sand bars are generated inshore of the breakpoint and migrate towards the swash zone (Aagard et al., 2004). The observations made on the Danish North Sea coast suggest that a net onshore bar migration occurs and the onshore bar movement in the mid-outer surf zone is due to a dominance of the wave-induced sediment transport during storm condition. The onshore-directed sediment transport is caused by incident wave skewnesses and enhanced phase couplings between orbital velocity and sediment concentration at times of high energy and water levels.

Alternative to both NOffM and NOnM, the Oscillation around a Position of Equilibrium (OPE, Certain and Barusseau, 2005) proposes a cyclic oscillation of the bar position due to seaward (storms) and shoreward (calms) migration. The mechanisms of this model are essentially similar to those of the NOffM, i.e. seaward migration during storms because of the dominance of the undertow and recovery during calms due to the wave-induced onshore sediment transport, but equilibrium is achieved when the local climate cannot not force storm strong or long enough (e.g. Mediterranean vs. North Sea, see also Armaroli and Ciavola, 2011). Very recent observations (Parlagreco et al., 2019) show that Mediterranean storms

1445 can indeed induce a NOffM rather than an OPE behavior and that the longshore flow can
1446 sensibly contribute to increase the potential of sediment suspension.
1447 Both NOffM and NOnM are preferential for longshore-uniform 2D bars, which evolve for
1448 $\Omega \approx 5$ (see in the following), and seem to require large waves (Ω is directly proportional to H_b)
1449 and longshore flows (likely contributing to longshore uniformity, Shand et al., 1999).
1450 Moreover, since both NOffM and NOnM are observed to evolve over beaches with similar
1451 slopes (1:200-1:150) and sediment sizes ($d_{50} \approx 150\mu m$), the different behaviours are probably
1452 to be searched into the different incident wave field (steepness and storm sequencing) and
1453 possible physiographic constraints.
1454 The above observations motivate a detailed analysis, using the mentioned classification,
1455 of the models currently available to predict the generation and evolution of 2D sand bars.
1456 These are typically distinguished between models for single but non-interacting bars and
1457 interacting sand bars.
1458 Among the models for single and non-interacting multiple bars we find the “empirical
1459 models”, the “template/forced” models and the “stability models”.
1460 The “empirical models” are based on use of the Dean parameter Ω (Wright and Short,
1461 1984) and of the the $B^* = x_s / g \tan\beta \, T_i^2$ parameter (Short and Aagard, 1993), where x_s is the
1462 nearshore width (offhore distance to the point where $\beta \approx 0$). Single bar formation is possible
1463 for $20 < B^* < 50$ and $2 < \Omega < 6$, while $\Omega < 1$ characterizes reflective beaches and $\Omega > 6$ dissipative
1464 beachs. For Ω increasing from 2 to 6 the following features emerge in sequence (Wijnberg
1465 and Kroon, 2002): shore-attached bars, 3D bars and 2D bars (the latter ones for $\Omega \approx 5$).
1466 Formation of multiple bars requires larger values of B* (e.g. 2 bars for $50 < B^* < 100$, 3 bars
1467 for $100 < B^* < 300$, etc.);
1468 The “template/forced models” not only give synthetic information on conditions, but also
1469 clarify some of the mechanisms for bar formation. Most of them propose bar formation via
1470 sediment accumulation at specific spatial locations. Such locations can be (see also figure

6): the anti/nodes of standing waves - be they induced by incoming/outgoing free IG waves (Short, 1975) or edge waves from opposite directions (Holman and Bowen, 1982), this is known as the “standing IG wave mechanism”; the breakpoint location, where flow/sediment convergence is due to the seaward-flowing undertow and the shoreward bottom boundary layer (BBL) streaming, this is known as the “breakpoint-bar mechanism”.

Figure 6. Bar formation because of sediment convergence at: anti/nodes of standing IG waves (left panel), breakpoint (right panel).

Another forced model, by O’Hare and Huntley (1994), suggests bar formation is induced by sediment stirring from sea/short waves and transport by free IG, hence we call this “sea-IG waves correlation mechanism”. Erosion/deposition is function of a fixed phase shift between the stirring given by short-wave envelope and IG waves. If IG are Bound Long Waves (BLW, more efficient on dissipative/mild beaches, Longuet-Higgins and Stewart, 1964), bar formation is inhibited, while if IG are generated by BreakPoint (BP, more efficient on reflective/steep beaches, Symonds et al., 1982) oscillation, bar formation is fostered.

Forced models represent a major improvement over empirical models but are affected by some significant weaknesses. The most important is their intrinsic inability to give accont of the morphology-on-flow- feedback (term III of equation 1 is automatically set to zero). Moreover, standing IG waves and breakpoint-bar mechanisms: prescribe the simultaneous emergence of all bars across the surf zone (this is only observed for rythmic 3D bars, but not for 2D bars); require very specific wave conditions (e.g. narrow-banded spectra, mode selection, etc.), which are not frequent in nature.

Finally, “stability models” have been succesfully used to describe the generation of crescentic or lunate 3D bars (Vittori et al., 1999) and the evolution of a double system of crescentic 3D bars (Klein and Schuttelaars, 2006). Crescentic bars emerge because of steady currents caused by the interaction of the incoming sea/short waves with synchronous

edge waves excited by the incoming waves moving over the wavy seabed. Klein and Schuttelaars (2006) studied a similar problem using a numerical, wave-averaged model (NSWE+Exner). Starting from an equilibrium state and numerically added perturbations the fastest-growing perturbation was computed (see also the left panel of figure 7).

Figure 7. Left panel: nonlinear stability solution for a double sand bar system giving asymmetric crescentic patterns on inner and outer bars (adapted from Klein and Schuttelaars, 2006). Right panel: Evolution of longshore uniform sand bar after 30 days of model run with normal wave incidence. Longshore instability in the form of rip channels (adapted from Dronen and Deigaard, 2007).

However, no study seems available on the emergence of 2D sandbars by means of stability models. Using a wave-averaged model Dronen and Deigaard, (2007) have shown that longshore instabilities of an initially 2D bar emerge for both normal and oblique wave incidence (see also the right panel of figure 7). This inadequacy of stability models in reproducing the emergence and evolution of 2D sandbars calls for intensive investigation, which should also take into proper account the role of longshore currents, which are thought to be fundamental to give longshore uniformity.

With reference to models for interacting multiple bars, Castelle et al. (2010) used a numerical, wave-averaged circulation model (with wave action equation for wave driver) plus Exner equation to investigate the evolution of double crescentic sandbar systems.

Figure 8. Computed (top-right and bottom panels) 180° out of-phase coupled patterns with an outer-bar horn facing an inner-bar bay, similar to observations (top-left panel) on a meso-macro-tidal, high-energy, double-barred beach (adapted from Castelle et al., 2010).

Simulations were run by providing a template in the morphology (inner bar longshore uniform and outer-bar with crescentic patterns). The computed feedback between flow, sediment transport and the evolving morphology allowed to reproduce morphologies similar to those of observed double crescentic sandbar systems (see figure 8). The Authors

advanced that a novel mechanism ("morphological coupling") was introduced that "blurs the distinction between self-organization and template mechanisms". However, inspection of equation (1) suggests that such a novel mechanism is a complete model that retains all terms on the right hand side. In other words, a template of crescentic outer bar is forced (term I of equation 1) in a self-interating model (term III of equation 1).

The above consolidated knowledge has opened the way to some recent findings on: sediment transport due to IG waves, sandbar migration and seabed moulding due to large-scale vortices.

Recent results on IG wave-induced sediment transport come from De Bakker et al. (2016) who have used field data collected in the Netherlands at the gently sloping (β≈1:80) Ballum beach and at the moderately sloping (β ≈1:35) SandMotor beach to investigate the role of the beach slope on IG wave-induced cross-shore sediment transport (q_{IG}). Based on the fundamental idea that sediment is put into suspension by sea/short waves and transported by IG waves (see also the "sea-IG waves correlation mechanism" by O'Hare and Huntley, 1994), the study compares the performances of two proxies for sediment transport in the nearshore. The first proxy is the correlation between the group bound IG wave (BLW) and the sea-wave envelope (see also Baldock, 2006):

$$R_{Uu_{IG}}(\tau) = \frac{\langle U(t)u_{IG}(t+\tau)\rangle}{\sigma_U \sigma_{u_{IG}}} \quad (2)$$

where u_{IG} is the IG wave cross-shore velocity, U is the sea-wave envelope cross-shore velocity, σ_s give the related variances and <> denotes time averaging. The second proxy, proposed by De Bakker et al. (2016), is the IG wave height to sea wave height ratio H_{IG}/H_{SW}.

De Bakker et al. (2016) suggest that $R_{Uu_{IG}}$ is a good proxy for the nearshore sediment transport only on moderately-sloping beaches while H_{IG}/H_{SW} well represents the sediment transport on all beaches. In fact while over moderate slopes $R_{Uu_{IG}} \neq 0$, it is $R_{Uu_{IG}} = 0$ on

mild slopes. On the other hand, H_{IG}/H_{SW} is always positive and increasing for mild slopes, because IG waves receive more energy from sea waves breaking on wide surf zones.

In the shoaling region it is $R_{Uu_{IG}} < 0$ because the setdown (negative BLW) is associated with the peak of the sea wave envelope and the sediment flux is negative, i.e. seaward (see also figure 9). In the inner surf zone of moderately-sloping beaches the correlation becomes positive because breaking-induced wave setup (positive BLW and shoreward sediment flux) gives deeper waters and allows the faster sea waves to ride the crest of the IG wave (see figure 9). However, in the inner-surf zone of mildly-sloping beaches it is $R_{Uu_{IG}} = 0$ because the sea waves have been almost completely dissipated and $q_{IG}<0$ because the peaks of suspended sediment transport (SST) correlate with $u_{IG}<0$ and the undertow $\bar{u}$.

Figure 9. Sketch of IG-sea wave interaction and cross-shore sediment transport in the nearshore. From left to right: shoaling zone, inner-surf zone of moderately-sloping beaches, inner-surf zone of mildly-sloping beaches.

Other recent results are on the mechanisms for onshore bar migration, fundamental for all bar migration models of above. Early energetics-type models could only reproduce offshore migration due to strong offshore currents (undertow) that are maximum at the bar crest (Gallagher et al.,1998). Observations suggest that onshore migration occurs for weak currents and significant waves. Hence, the role of waves is fundamental for the onshore bar migration, and, as a consequence, it is fundamental to understand what are the model representations of the main wave mechanisms for onshore bar migration.

With reference to the models analyzed in the Introduction we first analyze the energetics-type models. They base their ability to reproduce onshore bar migration on use of the wave acceleration skewness (Sk_a, proportional to the third order acceleration moment) in the sediment transport closure, so that the sediment transport rate is written as (Hoefel and Elgar, 2003):

$$Q_A = K_a\left(a_{spike} - \mathrm{sgn}\left(a_{spike}\right)a_{crit}\right), \text{for } \left|a_{spike}\right| \geq a_{crit} \text{ with } a_{spike} = \frac{\langle a^3 \rangle}{\langle a^2 \rangle} = \langle a^2 \rangle^{1/2} Sk_a \qquad (3)$$

This description is such to properly give account of the rapid onshore flow acceleration under steep wave fronts, which, in turn, generates strong horizontal pressure gradients on the seabed sediment.

On the other hand, process based, wave-resolving models (e.g. Henderson et al., 2004; Hsu et al., 2006) can properly predict onshore bar migration if they accurately describe the correlation between the orbital velocity (*u*) and the sediment concentration (*c*) in the BBL (*q*=<*uc*>).

Figure 10. From left to right: vertical profile of mean cross-shore sediment transport due to waves (q_w) and currents (q_c), total cross-shore sediment transport as function of near-bed (middle) and freestream (right) velocity moments, for the Duck94 migration event. Adapted from Henderson et al. (2004).

Figure 10 shows that onshore migration occurs when the total sediment transport (q_t) is essentially due to waves (q_w) and correlates well with the third-order moment of the nearbed velocity $\langle u_b^3 \rangle$.

The apparent distance between the two models can be reconciled, showing that energetics-type models are successful if they reproduce, at the integral level, the proper sediment flux-nearbed velocity moments correlation given by advective BBL models. The proof can be summarized as follows. First, it is shown that onshore bar migration occurs when *q* correlates well with $\langle u_b^3 \rangle$ in BBL, i.e. with the nearbed wave velocity skweness $Sk_{u_b} = \langle u_b^3 \rangle / \langle u_b^2 \rangle^{3/2}$. Then, using a Fourier decomposition of the velocity field, it is shown that $Sk_{u_b} \propto \sin(\phi_b) A_{u_f}$, where A_{u_f} is the wave freestream velocity asymmetry and ϕ_b is the nearbed-over-freestream velocity phase lead (Henderson et al., 2004; Berni et al., 2013). Finally, for sawtooth bores, i.e. setting $\phi = \pi/2$ in the modal solution $u_f \sim \sum_n \frac{1}{2^n} \sin[(n+1)\omega t + n\phi]$

gives $A_{u_f} \sim Sk_{a_f}$, with Sk_{a_f} wave freestream acceleration skewness (Drake and Calantoni, 2001) of energetics-type models.

Very recently Fernandez-Mora et al., (2015) used an energetics-type model to show the ability of such models to predict onshore/offshore bar migration and assess the role of both Sk_{u_b} and Sk_{a_f}. A complex model was built such that:

$$(1-n)\frac{\partial z_b(x,t)}{\partial t} = -\frac{\partial Q(x,t)}{\partial x} \quad (4)$$

$$\text{with} \quad Q = \alpha_c Q_c\left(Sk_{u_c}\right) + \alpha_u Q_u\left(Sk_{u_f}\right) + \alpha_a Q_a\left(Sk_{a_f}\right) + \alpha_D Q_D\left(\frac{dz_b}{dx}\right)$$

and where Sk_{u_c} is the skewness of the currents velocity vector and dz_b/dx is the, stabilizing, seabed slope term. Hence, if α_u is set to zero the SkA model of Hoefel and Elgar (2002) is obtained, if α_a is set to zero the SkV model of Hsu et al. (2006), while the complete model is the MiX model. The model performances are illustrated in figure 11, always referring to the Duck94 onshore migration event.

Figure 11. Modeling (red line) of the morphological evolution of the Duck94 onshore migration event for: (A) the SkV model, (B) the SkA model, and (C) the MiX model. The initial and final measured profiles are shown by dashed and solid lines, respectively. Adapted from Fernandez-Mora et al. (2015).

All models reproduce well the chosen event, the SkV model better in the shoaling zone and the SkA model better in inner surf zone. However, they all perform poorly in the swash zone, this suggesting further investigation is needed for such region.

Among the most recent results on seabed evolution and bar generation are those dedicated to the roles of macrovortices. Breakers of finite longshore width are known to introduce vertical vorticity ζ that rolls up to form large-scale vortices with vertical axes, also called macrovortices (Peregrine, 1999). Important dynamics characterized by finite longshore breakers are those giving rise to rip currents (e.g. Kennedy et al., 2006) and cross-sea induced breakers (e.g. Postacchini et al., 2014).

The latter condition is seen to be a potentially important cause of seabed morphology alteration with the generation of complex 3D sandbars. The example of figure 12 has been obtained by computing, using the NSWE morphodynamic model of Postacchini et al. (2012), the morphological evolution of a planar beach under the combined action of waves and macrovortices generated by finite longshore breakers due to regular waves (Hi=1m, Ti=10s, β=1/30) crossing at an angle of 15º to the coastline.

Figure 12. Seabed evolution forced by sea waves and macrovortices over a planar beach. Red thin lines give contours of the free surface elevation, while black and blue solid lines are contours of clockwise and anticlockwise vorticity, respectively. Yellow gives sand deposition and green seabed erosion.

Sandbars of 3D shape (yellow colours in figure 12) arise due to the interaction of cross-sea waves and the breaking-induced macrovortices.

River mouths

The hydro-morphodynamics evolving at river mouths, significantly related with the evolution of sandbars, is analyzed, as a second applicative topic, with the same approach used for sandbars: consolidated observations and models first, followed by more recent findings.

In view of the main aim of the paper, i.e. to highlight interactions amongst the subsystems of interest, fundamentals of river mouth dynamics are kept at the minimum, with a preference for those of wave-dominated rivers debouching into sandy coasts.

Analysis of the literature on river mouths dynamics is fairly complex because of the different perspectives taken by the various communities that study river mouths, i.e. engineers, geologists, ecologists, etc. Also, the vocabulary is influenced by such different views and much effort is being spent to provide a systematic description of river mouth dynamics.

The most important efforts have been made in the classification of river deltas (Galloway, 1975), where delta is here generically used as “sedimentary deposit due to river-sea interaction and protruding into the sea”. The triangular classification of deltaic depositional systems by Galloway (1975) illustrates how the relative importance of sediment input, wave energy flux and tidal energy determines both morphology and stratigraphy of the delta. Indices have also been introduced to classify deltas. Among them we find the discharge index I_q of very consolidated use (Wright et al., 1974) and the more recent fluvial dominance ratio R (Nienhuis et al., 2015):

$$I_q = discharge\ index = \frac{river\ liquid\ discharge\ per\ unit\ width\ of\ mouth}{wave\ power\ per\ unit\ width\ of\ wave\ crest} \quad (5a)$$

$$R = fluvial\ dominance\ ratio = \frac{Q_r}{Q_{s,max}} = \frac{river\ sand\ flux}{max\ longshore\ sediment\ flux\ at\ river\ mouth} \quad (5b)$$

The former is a dimensional index (units of m^3/Watts/s) and such to increase of orders of magnitude from wave-dominated ($I_q \approx 10^{-5}$ m^3/Watts/s) to river-dominated ($I_q \approx 1$ m^3/Watts/s) systems, while the latter is a dimensionless index, also increasing from $R<1$ for wave-dominated to $R>1$ for river dominated systems (see also figure 13).

Figure 13. Classification of river delta morphologies by means of the fluvial dominance ratio. Adapted from Nienhuis (2016).

Reference classifications of river deltas (Galloway, 1975) also clarify use of the word “estuary”, this being attributed to tide-dominated deltas, though at times more broadly (improperly?) used for semi-enclosed regions where river fresh water meets the sea. A number of schemes to classify estuaries is available in the literature, a recent one being that of Valle-Levinson (2011), which provides different classifications based on geomorphology, salinity structure and hydrodynamics.

Because of the ambiguities in using “estuary” and of the present focus on river systems weakly influenced by tides, “river mouth” is here used as a clear and unambiguous definition of the region where the river meets the sea. Analyses of wave-dominated river mouths are also available (e.g. Cooper, 2001), and the very comprehensive, recent, work by Anthony (2015) provides a nice overview of the role of waves at river mouths: waves remove fine sediments at the river mouth and flatten the delta by moving the sediment alongshore. Hence, deltas, placed along smooth coasts with shore-parallel ridges (see figure 14), are shaped from arcuate to cuspate. Waves that approach the coast obliquely generate: littoral (i.e. longshore) sediment transport, maximum for 45° wave attack; an important difference between updrift/downdrift flank transport and sediments (updrift flank made by beach sediments, downdrift flank made by river sediments); an asymmetrical delta. A recent quantitative analysis on delta progradation/migration is that of Nienhuis et al. (2016), which can be summarized as follows. The delta undergoes: a symmetric progradation, for small river sand flux and all longshore transported sediment bypassing the mouth*;* a downdrift migration, for small river sand flux and vanishing sediment bypassing at mouth*;* an updrift migration, for large river sand flux, independently of sediment bypassing at mouth.

Figure 14. River delta geomorphic units and schematic shoreline morphology (wave-dominated morphology circled in red). Adapted from Anthony (2015).

Being the main aim of the present work that of clarifying the interactions - through nonlocal agents - between the sandbar, river mouth and swash zone subsystems, most of the attention is here given to local and nonlocal wave-forced dynamics.

Fundamental wave-forced, river mouth dynamics are the interaction of river current with the sea waves and the related sediment transport.

Seaward flowing currents interact with incoming waves (Chawla and Kirby, 2002) to: slow them down and even block them if the depth-uniform current velocity is equal and opposite

to the wave group velocity, this is known as “wave blocking”; steepen and even lead to breaking; decrease the high-frequency content by wave breaking and transfer part of the current energy to lower wave frequencies, this leading to frequency downshift of the incoming waves;

The bedload accumulation related to the above dynamics typically leads to the formation of a mouth sandbar. The intensity of the wave field significantly influences the bar formation process. With no waves, a triangular mouth bar is generated just seaward of the mouth, at a distance of about twice the mouth width. The generation process is initiated by the river jet expansion in the sea, which, by continuity arguments, leads to a flow reduction and a consequent sediment deposition (e.g. Fagherazzi et al., 2015). On the other hand, small waves promote mouth bar formation by a process similar to the above: they promote the river jet expansion and flow reduction, with a consequent more intense deposition close to the river mouth. Finally, large waves suppress mouth bar formation because of their intense seabed erosion and longshore transport (Fagherazzi et al., 2015).

Analysis of the above-mentioned wave-current interactions reveals that a river mouth acts as a low-pass filter by removing (by breaking) sea and swell waves and letting long waves pass. Recent studies have been dedicated to the propagation and evolution of IG waves at inlets. Observations at the Ría de Santiuste (Spain, see Uncles et al., 2014) reveal how IG waves (with periods of 4-5minutes), believed to be the outcome of estuary-amplified edge waves, propagate upriver. This is well illustrated by the top panel of figure 15, which shows a positive correlation between the water level (*WL*) and the flow velocity (*U’* in the figure).

Figure 15. IG wave propagation at river mouths. Top: positive water level-flow velocity correlation at the Ría de Santiuste (Spain). Adapted from Uncles et al. (2014). Bottom: tide-modulated IG wave propagation in the Albufeira Inlet (Portugal). No IG waves propagate landward of the mouth at ebbs. Adapted from Bertin and Olabarrieta (2016).

The bottom panel of the same figure nicely illustrates the role of tide on the propagation of IG waves at inlets. Observations and wave-averaged modeling of the Albufeira Inlet (Portugal, see Bertin and Olabarrieta, 2016) reveal that upriver-propagation (from transect 0 to transect 18 of images C-Run 3 and D-Run 4) of IG-waves only occurs during tidal flood. Inspection of the same images reveals that: no propagation is possible at ebb (white areas in corrrespondence of the ebbs), IG waves are equally generated by BLW (image C-Run 3) and BP (image D-Run 4) mechanisms.

Other recent field observation support the role of river mouths and the upriver propagation of IG waves. Among these, notable are the EsCoSed and MORSE project studies (Brocchini et al., 2017; Melito et al., 2018a, 2019) performed at the mouth of the Misa River (Italy, see figures 1 and 17), located at a microtidal site (*RTR<3*) with a dissipative-to-intermediate beach (*5< Ω <20*).

Figure 16. The Misa River estuary in Senigallia (Italy) depicting locations of measuring stations within the final river reach (TGdown, QR1, QR2, QR3, TGup) and in the sea (QS1, QS2, QS3). Adapted from Melito et al. (2018a).

On the basis of water elevation measurements collected at various locations both in the sea (QS in figure 17) and in the river (TG and QR in figure 17), the energy flux density dE_f and the energy flux E_f:

$$dE_f = S(f)C_g \qquad dE_f = \int S(f)C_g df \tag{6}$$

have been computed - where *S(f)* is the power spectral density, C_g the wave group velocity and *f* the frequency. The fundamental result is that while in the sea (QS1, QS2) most of the energy content is due to swell and sea waves, the IG band becomes dominant within the river (e.g. QR2 of the left panel of figure 17) with a weak upriver decay (TGup of the right panel of figure 17).

Figure 17. Energy density flux (left) and energy flux (right) at the Misa River during storm conditions. Adapted from Melito et al. (2018a).

The EsCoSed field campaign has also provided useful information on the seabed morphology at the river mouth, highlighting the formation of large deposits/bars (blue in the right panel of figure 18) and scours holes (red in the right panel of figure 18). The sand deposits are found to be at a typical location, i.e. about twice the mouth width seaward of the mouth itself (Fagherazzi et al., 2015), but characterized by a very complex planview pattern.

Figure 18. Seabed variation between May-September 2013 (left) and between September 2013-February 2014 (right) at the Misa River. Adapted from Brocchini et al. (2017).

The above observations have motivated important efforts in the modeling of the dynamics evolving at a river mouth characterized by a complex morphology, with a specific focus on the role of waves.

Figure 19. Velocity maps for a strong river outflow opposed to three different wave regimes (from top to bottom: H_s = 0.0m, 0.5 m, 1.5 m). Left column: results from Olabarrieta et al. (2014). Right column: results from the wave-resolving solver of Brocchini et al. (2001), averaged over 10 wave periods. Adapted from Melito et al. (2018b).

Olabarrieta et al. (2014) used the wave-averaged 3D Regional Ocean Modeling System (ROMS) and an idealized river mouth shoal bathymetry to explore the wave-river current interactions. The increased, with respect to a planar beach, steepening and breaking of waves over the shoal leads to stronger seaward-flowing currents (undertow). Moreover, waves are seen to increase both the lateral spreading of the river current and the longshore transport.

In the attempt to better describe the dynamics forced by the sea waves, Melito et al. (2018b) run the same cases studied by Olabarrieta et al. (2014) using the intra-wave NSWE model of Brocchini et al. (2001), this neglecting vertical flow gradients, but improving the time resolution of the wave forcing. The comparison between the two different numerical solutions, illustrated in figure 19 for the case of a strong river outflow (1.1 m/s river current), suggests that the main features of the wave-current interactions are captured, i.e. the river current intensity and instability (e.g. Canestrelli et al., 2014). However, some significant differences are also evident, among which: a weaker longshore spreading of the river jet, the appearence of a number of large-scale eddies. Both differences seem to be caused by the stronger wave breaking predicted by the NSWE, which removes significant amounts of momentum and energy from the wave field, thus the reduced capacity of pushing shoreward the river jet, in favour of the generation by differential wave breaking of large-scale eddies or macrovortices (see previous subsection and Kennedy et al., 2006).

Such macrovortices not only contribute to the near-mouth flow mixing (right panels of figure 19), but, as seen at the end of the previous subsection, also induce significant seabed morphological changes. Falcini et al. (2014) recently sought for a mechanistic relationship between potential vorticity Π ($\Pi=\zeta/d$ in a shallow-water framework) and sediment transport at a river mouth. Lateral advection and diffusion of suspended sediment were found to be directly proportional to the river jet vorticity, so that leeves building is observed in correspondence of regions of large vorticity and mouth bar deposition in regions of low vorticity.

In view of the large similarities between the analyses of vorticity-induced dynamics within the nearshore by Kennedy et al. (2006) and Brocchini (2013) and at river mouths by Falcini et al. (2014), an integration of the two analytical approaches seems useful to clarify the role of breaking-wave-induced vorticity on the river mouth morphodynamics.

In the meantime, some numerical experiments are being carried out, by means of the hydro-morphodynamic NSWE solver of Postacchini et al. (2012), to describe the main morphological features that evolve at a simplified (e.g. shoal of Olabarrieta et al., 2014) and natural (e.g. Misa River) river mouth bathymetry. Preliminary numerical results are illustrated in figure 20, describing both a significant sediment deposition at the seaward edge of the idealized shoal and a weaker deposition at the typical location of a mouth bar (left panel) and a complex erosion deposition pattern at the mouth of the Misa River (right panel).

Figure 20. Estimated morphological evolution at the simplified river mouth bathymetry of Olabarieta et al. (2014), left panel and at the Misa River, right panel.

Comparison of the right panels of figures 18 and 20 reveals that these preliminary numerical solution can qualitatively capture the main characteristics of the complex erosion/deposition pattern that evolves just seaward of the river mouth.

Swash zone

The swash zone is that region of the beach that is alternatively covered and uncovered by water because of the action of sea waves (Brocchini and Baldock, 2008). Because of such process, fundamental characteristics of the swash zone are: the flow intermittency; the infiltration/exfiltration of water at the seabed; the very large sediment transport within the swash, which can be quantified, for example, in terms of the cross-shore sediment mass per beach longshore length transported by each swash event (Blenkisopp et al., 2011)

$$-40\,Kg/m < \hat{q}_x < 40\,Kg/m\,, \quad \hat{q}_x \equiv \int_{Tswash} q dt \tag{7}$$

or in terms of the longshore mass flux (Ribeiro et al., 2012).

$$Q_y \sim (1-10)\,Kg/s \tag{8}$$

The swash zone is also a locus for the generation of IG waves by two main mechanisms.

The first is the seaward reflection of BLW released by breaking (e.g., Schäffer, 1993). This is well illustrated in the left panel of figure 21, where a group of sea waves releases through breaking its BLW that propagates to the shoreline and it is there reflected to propagate out to sea as a Free Long Wave (FLW). The process of faster sea waves climbing the crest of the BLW is evident, as also illustrated in figure 9.

The second mechanism is the frequency downshifting of the sea waves that interact in the swash. This interaction occurs because waves in shallow water propagate with a velocity that is proportional to their height. Therefore, large waves travel faster than small waves and catch them up near or inside the swash zone (Mase, 1995). The assimilation of small waves by large waves leads to a reduced number of waves emerging from the swash zone, i.e. to a frequency downshifting, as illustrated in the right panel of figure 21.

Figure 21. Left: example of BLW release on a beach because of sea wave breaking. The shoreward-propagating (from bottom to top) wave group releases its BLW that is reflected at the shoreline and propagated (from top to bottom) out to sea as a FLW (adapted from Watson, Barnes and Peregrine, 1995). Right: example of frequency downshifting within the swash zone. Bichromatic waves propagate from seaward to the shoreline (from top to bottom) over a steep beach and interact in the swash zone giving wave of doubled period (adapted from Mase, 1995).

Most of the modelling of swash zone hydrodynamics, essentially forced by sea waves, has been done by using the NSWE. For an horizontally-1D flow evolving in the crosshore direction *x*, these read (e.g. Brocchini et al., 2001):

$$\begin{cases} d_{,t} + (ud)_{,x} = 0 \\ \vdots \\ u_{,t} + uu_{,x} + gd_{,x} = gh_{,x} + c_f \frac{u|u|}{d} \end{cases} \tag{9}$$

where commas gives partial differentiation, *d* and *h* are the total and still-water depths, respectively, *u* is the depth-averaged flow velocity, *g* is gravity acceleration and c_f a dimensionless coefficient for seabed friction.

Solution of such equations not only provides a quantitative means for studying the nearshore hydrodynamics, but can also be of help to illustrate some of the phenomena above described, like, for example, the interaction of sea waves within the swash zone. An example is provided by figure 22 for the case of a group of 5 sea waves.

Figure 22. Waves interacting at a wall (left) and at a swash zone (right). Top: incoming and outgoing characteristic curves at the shoreline. Bottom: a group of 5 sea waves (thin line) incoming to shore and outgoing IG waves (S-, thick line) resulting from the interaction of sea waves (adapted from Brocchini, 2006).

On the basis of the NSWE a number of analytical solutions has been made available over the years for both non-breaking and breaking waves. The pioneering work of Carrier and Greenspan (1958), who used the method of hodograph transformation, opened the way to some solutions that are currently used as reference for both analytical and numerical studies for the evolution of non-breaking sea waves on a beach. In particular, Brocchini and Peregrine (1996) extended the solution by Carrier and Greenspan (1958) to compute for the longshore flow due to waves propagating almost orthogonally to the beach (see figure 23). This solution can be used to provide estimates of the longshore mass flux to be compared with field measurements, like that of equation (8). More recent studies, e.g. Antuono and Brocchini (2010), suggest that analytical solutions for both non-breaking and breaking waves can be achieved also in the physical space, i.e. avoiding use of the hodograph transformation.

Figure 23. Left: maps, in the (x,t) plane of hodograph coordinates, free surface elevation η crosshore (u) and longshore (v) velocities for two sea waves interacting onto a beach. Right: mean longshore mass flux near and inside the swash zone for waves of different amplitude (adapted from Brocchini and Peregrine, 1996).

Cornerstone of analytical solutions for breaking sea waves, i.e. bores, on a beach is that of Shen and Meyer (1963), in the following SM63. A bore of velocity u_0 collapsing onto a beach of slope β forces a swash that is shoreward bounded by a parabolic shoreline x_s:

$$x_s = u_0 t - \tfrac{1}{2} g \, tan\beta \, t^2 \qquad (10)$$

i.e. similar to the trajectory of a massive point under the action of gravity. This very neat solution, which has been used for long times, has, however, the fundamental weakness of predicting runup lenses much thinner than those observed on a natural beach.

Very recently Guard and Baldock (2007), in the following GB07, analyzed this issue and suggested that the problem is caused by the assumption of regarding the collapsing bore as a dam-break flow, where part of the fluid accelerates seaward. This is illustrated in the sketch of the top panel of figure 24, whose left part illustrates the evolution of the SM63 solution in similarity with a dam-break flow (dashed line) that leads to both shoreward- and seaward-accelerating fluid. The right image of the same panel illustrates how the GB07 solution, achieved by means of a linearly-time-varying (rather than constant) flow forcing at collapse, predicts only shoreward-accelerating fluid after bore collapse. The bottom panel of the same figure shows the fundamental differences in the water depths predicted by the two solutions over a swash period. The SM63 solutions (thick lines) predicts more asymmetric (downrush much longer than uprush) and much thinner (about a half) swash lenses than those predicted by the GB07 solution (thin lines) that well compares with the experimental data given by the symbols.

Recent remote sensing data, collected at 6 different beaches in USA and Australia, have been used to assess the value and validity of the assumptions at the basis of the GB07 solutions (Power et al., 2011). Such observations confirm that: natural swash lenses are deeper and less asymmetric than those predicted by SM63; a linearly-time-varying forcing of the swash flow is better suited than a time-independent forcing to describe the evolution of natural swashes.

Figure 24. Top: sketches of the flow by bore collapse. The left sketch shows the evolution of the SM63 solution in comparison to a dam-break flow (dashed lines), the right sketch suggests that only shoreward-accelerating fluid motion is predicted by the GB07 solution. Bottom: swash water thickness predicted by the SM63 solution (thick lines) and by the GB07 solution (thin lines) also compared with experimental data (symbols). Bottom panel adapted from GB07.

The fact that natural swash are fairly symmetric (still asymmetric in favour of the downrush) in time and characterized by fairly deep water lenses has important consequences on the understanding and modeling of the swash zone sediment transport and related morphodynamics. Thicker swash lenses lead to increased sediment pickup areas, because the sediment transport rate is directly proportional to the flow depth for a uniform sediment concentration (Pritchard and Hogg, 2005), and increased seaward sediment transport, because of the still existing swash asymmetry in favour of the rundown phase. However, such seaward sediment transport is counter-balanced by two main mechanisms: the presuspension of sediments due to the bore collapse onto the beach (which allows for a significant transport from the surf zone into the swash zone) and the settling lag effects due to the inertia of suspended sediment particles advected into the swash zone (Pritchard and Hogg, 2005). The above competing mechanisms, i.e. reduced swash asymmetry with increased thickness (promoting seaward transport) and sediment presuspension with settling lag effects (promoting shoreward transport) force a very complex swash zone morphology. This has been well described by Kelly and Dodd (2010), who implemented one of the most advanced and physically complete models for the swash zone hydro-moprhodynamics. Some of their results reveal the complexities in beach profile changes due to a swash event (see figure 25).

Figure 25. Left: space-time map of the changes in beach profile due a swash event. The thick dashed lines give the zero contour. Right: snapshots of the swash lens cross-shore sections (adapted from Kelly and Dodd, 2010).

While beach degradation (light tones of grey) occurs virtually over all of the seaward boundary of the swash zone, the most inshore portion of the swash zone undergoes significant, though non-uniform, aggradation (dark tones of grey). Bed discontinuities, typical of the evolution of an erosive bore, are seen to characterize both the uprush and the downrush stages.

The increasing awareness of the fundamental role of the swash zone for the entire nearshore hydro-morphodynamics stimulates always new research focused on links between the surf zone and swash zone dynamics.

From the hydrodynamic viewpoint, one of the most interesting recent studies is that by Moura and Baldock (2017), who focused on the relation between the shoreline (x_s) motion and the IG waves, both BP forced (horizontal BP excursion x_{br}) and BLW (vertical BLW excursion η_{BLW}), generated within the surf zone.

Figure 26. Shoreline relation with BLW and BP forcing. (a) Wave group. The vertical blue line gives the BP between its outer (red), x_o, and inner (green), x_i location. Grey and red lines give the released BLW and incident BP-forced IG wave, respectively. (b) BP excursion (black) and shoreline response to BP-forced (red) and BLW (grey) IG waves. Dashed line gives path for a shallow water wave from the BP to the shoreline. Horizontal colored lines are BP positions as in Figure 2a. (c) Cross-correlation between BP and shoreline excursion, BLW released (grey) and BP-foced IG wave (red). Adapted from Moura and Baldock, (2017).

Such relation can be illustrated with reference to the schematic of figure 26. When a group arrives at breaking (panel a) the first, smaller waves break at x_i (green line) and the subsequent, larger waves, more and more seaward, moving the BP to x_o (red line), the subsequent smaller waves force the BP to move back to x_i. Hence, the BP position $x_{br}(t)$ is – large (x_i), small(x_o), large (x_i) – i.e. in phase with the BLW vertical oscillation $\eta_{BLW}(t)$ (which is large, small, large, i.e. concave upwards). The amplitude of the BP-forced IG wave $\eta_{BP}(t)$ is proportional to the width of the breaking region. Hence, it increases during the passage

2027 from small to large waves ($x_{br}(t)$ from zero to max) and decreases from large to small waves
2028 ($x_{br}(t)$ from max to zero). Hence, $\eta_{BP}(t)$ is concave downward or in phase opposition to $x_{br}(t)$
2029 and $\eta_{BLW}(t)$. The released BLW and the incident BP-forced wave propagate with the same
2030 speed ($\sqrt{gh}$) and reach the shoreline at the same time (after traveling through the surf zone),
2031 but with opposite phase (panel b). This leads to a positive correlation between $x_{s,BLW}$ *and* x_{br}
2032 and a negative correlation between $x_{s,BP}$ *and* x_{br} (panel c).

2033 On the basis of the above and using data coming from pressure sensors (water depth,
2034 significant wave height and period, etc.) and video observations (shoreline and BP
2035 excursion) collected at 3 Australian beaches, correlations between IG waves and shoreline
2036 excursion were made. The main findings suggest that: the shoreline excursion is a good
2037 proxy for infragravity waves in the inner surf and swash zone, IG wave generation by BLW
2038 release is stronger for conditions with relatively narrow surf zones and plunging waves while
2039 BP forcing is dominant for wider surf zones and spilling breaker conditions. This seems in
2040 contradicition with the established understanding (Battjes et. al, 2004) that the BP forcing is
2041 most efficient on steep beaches and the BLW release is most efficient on mildly-sloping
2042 beaches, see also the discussion provided in “Template models” of above. Such apparent
2043 contradiction can, perhaps, be solved by recalling that the surf zone width is not only function
2044 of the beach slope but also of the characteristics of the incoming wave. However, some
2045 further research seems needed here.

2046 From the morphological point of view, one fundamental link between the surf zone and
2047 swash zone dynamics is represented by the feeding of the most inshore sand bar (see also
2048 figures 4, 5, 11) by swash zone sediments. This has been recently investigated by Alsina et
2049 al. (2012), on the basis of dedicated laboratory experiments. Such experiments have been
2050 carried out by using flow conditions (surf zone characterized by plunging breakers, $\varepsilon \approx 12\text{-}13$)
2051 that, during an initial stage of run of about 3500 waves, led to the generation, from an almost-
2052 planar beach, of a nearshore bar that slowing migrated off to sea (see blue-solid to green-

dashed lines, and vertical red lines in top panel of figure 27). The run was then stopped and the beach profile manually reshaped to a milder slope only inside the swash zone (pink-solid line). The same flow conditions were subsequently run, but bar migration stopped.

Figure 27. Cross-shore distribution of beach profile (top panel) and of cross-shore sediment transport rate (bottom panel) at various times before and after beah reshaping (adapted from Alsina et al., 2012).

This behavior was attributed to a reduced sediment transport from the swash to the surf zone, because of the beach slope reduction forced in the swash zone. Such a conjecture was also verified by analyzing the sediment transport rate illustrated in the bottom panel of figure 27. This shows that, while before beach reshaping it was $Q_x<0$, i.e. sediment transport rate was seaward, in the surf zone and inner swash zone, the sediment transport rate became vanishing to positive after beach reshaping. This is a clear indication of a major reduction of bar sediment feeding from the swash zone.

The above observations can be interpreted on the basis of a simple mechanistic model: the reduction of the swash zone beach slope (β_{swash} decreasing) forces an increase in the natural swash period T_{swash} defined as (Baldock and Holmes, 1999):

$$T_{swash} = \frac{2C\sqrt{gH_b}}{g\sin\beta}, \qquad C = O(1) \tag{12}$$

and, as a consequence, an increase in the swash-swash interactions, this being measured by the T_{swash}/T_i ratio (Baldock and Holmes, 1999); such increased swash-swash interaction makes the size of intense backwash events to decrease and, therefore, also the SST to sea, i.e. to a reduced sediment input to the nearshore bar (Alsina et al., 2012).

This section is closed with some promising ongoing research aimed at including the swash zone dynamics into wave-averaged solvers for the nearshore circulation (see also “Generalities on Models” in the Introduction). By definition, wave-averaged models cannot describe the swash zone dynamics associated to the sea waves, this leading to problems in

correctly predicting IG waves radiating out to sea. This is well illustrated by figure 22, whose left panels describe the interaction of groups of 5 sea waves at a rigid wall used in wave-averaged solvers to represent the shoreline, while the right panels describe the same interaction at a swash zone reproduced by means of a wave-resolving model (in the specific that of Brocchini et al., 2001). Two main features are very clear: the interaction at a wall, being a mere reflection of the incoming wave groups, leads to outgoing groups with the same structure of the incoming ones; the interaction at a swash zone allows for a significant swash-swash interaction, for example because of large waves catching up and engulfing small waves (see Mase, 1995 and figure 21), which contributes to increasing the intensity (S^-) of the IG waves radiated out to sea (in the specific 20% larger for the interaction within the swash zone). In view of the fundamental importance of wave-wave interaction within the swash zone Brocchini and co-workers have designed some Shoreline Boundary Conditions (SBCs) for the motion of the mean shoreline x_l and of the flow at at such boundary ($d(x_l)$, $u(x_l)$) on the basis of an integral swash zone model (Brocchini and Peregrine, 1996; Brocchini and Bellotti, 2002). Such SBCs have been successfully validated by means of large-scale laboratory experiments (Bellotti et al., 2003) and have recently been implemented in the ROMS wave-averaged solver (Haas and Warner, 2009). The main aim of such preliminary implementation was to gauge the capabilities of reproducing swash zone dynamics at a reduced computational cost, the final goal being that of predicting such dynamics by simply running a wave-averaged solution. Figure 28 summarizes the main findings of the mentioned implementation (Memmola, 2017; Memmola et al., 2019). The top six panels give the shoreline motion computed by running ROMS alone at the unreasonably-high resolution of 120 grid nodes (Δx) per offshore wavelength L_0 (black line), i.e. using it as a wave-resolving model (benchmark solution), and ROMS coupled with the proposed SBCs at lower and lower resolutions (red line), down to 2 grid nodes per wavelength. It is clear that coupling ROMS with the SBCs allows one to run very cheap calculations that predict

reasonably well the benchmark solution by only using 3 grid nodes per wavelength (with $\Delta x/L_0 \approx 2$ the solution is too deteriorated). The lower two panels of the same figure show that not only the shoreline motion, but the entire flow field is well predicted by using the SBCs. The left and right panels give, respectively, the swash zone free surface elevation and onshore velocity for the benchmark solution (top panels) and ROMS+SBCs solutions for two very coarse meshes (middle and lower panels).

Figure 28. Top 6 panels: comparison of the ROMS ultra-highly resolved shoreline (black line) and ROMS+SBCs shorelines for lower and lower grid resolution. Bottom 2 panels: free surface elevation (left) and onshore velocity (right) for the benchmark ROMS solution (top panels) and ROMS+SBCs solutions for two very coarse meshes (middle and lower panels). Adapted from Memmola (2017).

These preliminary results demonstrate that the SBCs of Brocchini and co-worker can, at least, allow for cheap solutions that also provide the entire structure of the swash zone flow. Work in currently underway to achieve the more ambitious goal of running the ROMS-SBCs system in a prediciting mode (two-way coupled system), i.e. so that the SBCs are actually used to time-step the swash solution to be returned to ROMS.

Discussion

An important contribution of the present work is the identification of nonlocal forcing/dynamics, i.e. those that influence the entire nearshore as a whole. These are, in a cascading order of mutual control the: beach slope (obvious nonlocal forcing), IG waves and large-scale vortices with vertical axes (macrovortices).

The ***beach slope*** controls the role of IG waves, generation of macrovortices and the related sediment transport. In particular, BLW are regareded to be more efficient on mildly-sloping beaches, while IG waves are more likely generated by the oscillation of the BP on steep beaches (Battjes et al., 2004); although some recent studies by Moura and Baldock

(2017) seem to provide different information. The generation of macrovortices is controlled by the beach slope through the longshore differential breaking of sea waves that leads to generation and reorganization of potential vorticity at the lareral edges of breaking wave fronts (e.g. Kennedy et al. 2006). Although the role of SST at the lower boundary of the swash zone can be regarded as a local effect (see above), changes in the swash zone beach slope can significantly alter the swash-swash interactions and intense backwash events, this either promoting or stopping the sediment transport needed for the formation and migration of nearshore sandbars (Alsina et al., 2012).

IG waves provide a nonlocal forcing because the lengths involved in their generation and evolution are comparable to the surf zone width. IG are thought to have a fundamental role in the generation of sandbars, though various different models have been proposed like the "standing IG wave mechanism" (e.g. Short, 1975) and the "sea-IG waves correlation mechanism" of O'Hare and Huntley (1994) in which IG waves are responsible for the transport of sediments put into suspension by sea waves. Hence, the importance of the correlation between BLW and sea-wave envelope or the IG wave height to sea wave height ratio H_{IG}/H_{SW}, which is a good proxy for the sediment transport on beaches of all slopes (De Bakker et al., 2016). IG waves are also important for the riverine sediment transport because they can propagate upriver (e.g. Uncles et al, 2014), while sea and swell waves are dissipated by breaking at river mouths, which act as "low-pass filters". IG waves are not only generated at the seaward boundary of the surf zone, but also in the very shallow waters of the swash zone. This occurs by the wave-wave interaction due to large waves traveling faster than small waves and catching them up in the swash zone (Mase, 1995).

Macrovortices are a nonlocal forcing of the nearshore dynamics because they can maintain their coherent over large distances after their generation. Macrovortices contribute to sediment transport both by mobilizing the nearbed sands and, like IG waves, by carrying the sediments put into suspension by sea waves. The differential breaking that generates

macrovortices is particularly intense at river mouths characterized by seabed shoals. Hence, macrovortices, beyond the river jet expansion, provide a significant contribution to both flow mixing and sediment transport at river mouths (Melito et al., 2018b).

The analysis of the three subsystems of interest and of the related wave-induced dynamics suggests some lines for future research, proposed with reference to each of such subsystems.

Inspection of the state-of-the-art sandbar modeling reveals that we are still in need of suitable stability models for the generation of 2D sandbars. As recalled in the analysis of sandbars, available numerical solutions for the generation of 2D sandbars are characterized by longshore instabilities in the form of rip channels (Dronen and Deigaard, 2007) and no stable 2D sandbar systems can actually be reproduced for either normal or oblique wave incidence. It seems, therefore, essential to investigate the mechanisms for the emergence of 3D instabilities, also inspecting the role of the longshore currents, which are believed to contribute to the maintenance of the stability of a 2D pattern (Shand et al., 1999).

The role of longshore flows is becoming of growing interest, as believed to significantly control not only the generation, but also the migration of sandbars. In particular, longshore currents due to waves obliquely incindent to the shore may have the potential to increase the shear stress acting on the seabed and responsible for the sediment mobility (Parlagreco et al., 2019). In this perspective longshore currents are not directly responsible for the direction of cross-shore migration of sandbars (onshore vs offshore) but provide an indirect important control through increased sediment mobility.

Observed opposite migration behaviours on beaches of similar steepness and sediment size (Van Enckevort and Ruessink, 2003; Aagard et al., 2004) suggest that other important mechanisms that may characterize conditions for offshore (NOffM model) vs onshore (NOnM model) migration are the steepness and storm sequencing of the incident wave field.

In brief, future studies on sandbar generation and evolution should pay great attention to ***wave obliquity, steepness and storm sequencing***.

A more detailed inspection of the steepness of the incident wave field and related modalities of breaking is also advisable to try to explain the apparent contradiction between the recent findings of Moura and Baldock, (2017), suggesting that IG wave generation by BLW release is stronger for narrow surf zones and plungers while BP forcing is dominant for wider surf zones and spillers, and the established understanding (Battjes et. al, 2004) that the BP forcing is most efficient on steep beaches and the BLW release is most efficient on mildly-sloping beaches. This investigation should also try to encompass an analysis of the different modes of transport of turbulence associated with the two mentioned breaking types (seaward under spilling breakers and landward under plunging breakers – Ting and Kirby, 1994).

The implementation of ***novel Shoreline Boundary Conditions*** into wave averaging models for the nearshore circulation is certainly an important way forward for the inclusion of swash zone dynamics in long-term numerical simulations of the nearshore dynamics. The recent works of Memmola (2017) and Memmola et al. (2019) have shown the potentials of this approach, which will enable accurate and relatively cheap long-term numerical solutions. Work is currently underway for a predictive implementation of such approach.

In relation to the interactions occurring at a river mouth, studies are needed to clarify the roles of the different wave modes acting there. Recent field observations by Melito et al. (2019) confirm that ***the tide has an important role of modulating the IG waves*** that propagate upstream the river, result already obtained through numerical means by Olabarrieta (2016). This modulating effect, considerable even for microtidal environments (e.g. Misa River), should be better analyzed through field studies carried out in macrotidal environments.

The interactions of a river jet and the incoming sea waves should be better investigated also in relation to the generation of macrovortices. Preliminary evidence shows that they can remove significant amounts of energy from the incident wave field, reducing the opposing action of waves to the river stream (Melito et al., 2018b), and also force 3D seabed morphological features, e.g. mouth bars. Hence, both theoretical studies aimed at integrating the analytical approach of Brocchini (2013) for vorticity and potential vorticity generation with that of Falcini et al. (2014) as well as accurate morphological wave-resolving numerical simulations will likely clarify the role of ***breaking-wave-induced vorticity on the river mouth morphodynamics***.

Conclusions

The role of waves on the nearshore hydro-morphodynamics has been analyzed with specific focus to three subsystems of the nearshore i.e. sandbar region, river mouths and swash zone.

Each of these is characterized by very specific local dynamics. For sandbar generation and evolution fundamental is the role the nearbed sediment transport, with the correlation between the orbital velocity and sediment concentration in the BBL being of paramount importance for suitably predicting onshore bar migration (e.g. Henderson et al., 2004). It has also been shown that energetics-type models can achieve similarly good results if they reproduce such correlation through an integral approach, i.e. by including the effects of the wave freestream acceleration skewness (e.g. Hoefel and Elgar, 2002).

Local dynamics specific to river mouths are: the wave-current interaction by which the river current steepens the incoming waves, if intense enough to the point of breaking and/or blocking them, and forces a frequency downshifting (Chawla and Kirby, 2002); the related formation of a mouth bar (Fagherazzi et al., 2015) or the formation of a shoal that largely

influences the local dynamics by forcing stronger wave-breaking-induced return currents (Olabarrieta et al., 2014) and wave breaking/sediment deposit farther from the mouth, i.e. at the seaward edge of the shoal.

BBL dynamics largely influence the very shallow flows of the swash zone and, like for sandbars, a proper modeling of the swash zone sediment transport can only be achieved if correlation between the orbital velocity and sediment concentration in the BBL is well described. Fundamental is also the description of the SST transport at the lower boundary of the swash zone, which affects the sediment fluxes both from the surf zone, through sediment presuspension at bore collapse (Pritchard and Hogg, 2005), and to the surf zone, in association to intense backwash events.

A closure can be reached by recalling the main connections among the three subsystems of interest. IG waves provide a fundamental connection because generated both at the seaward edge of the surf zone (by BLW release, BP oscillation and edge wave interaction) and at the swash zone (because of wave-wave interaction) can propagate almost unaltered upstream at river mouths. Another important connection is provided by the evolution of macrovortices, which generated by differential breaking move over long distances in the surf zone and may reach the shoreline where they can rebound and alter the near-shoreline morphology. From the morphological viewpoint, obvious links are those between: the swash zone morphology and the along-river-flank sediment transport that can feed the swash zone and the swash zone and the nearshore sandbars, which can drive sediments for their evolution from the swash zone.

Acknowledgements

This paper is essentially a written transposition of the same-titled invited talk given at RCEM2017. The organizers are thanked for the opportunity given to reflect on and present this material. The following colleagues and friends are thanked for providing both useful

material and insightful discussions: Tom Baldock (University of Queensland, Australia), Riccardo Briganti (University of Nottingham, England), Joe Calantoni (Naval Research Laboratory, USA), Dan Conley (University of Plymouth, England), Steve Elgar (Woods Hole Oceanographic Institution, USA), Tom Hsu (University of Delaware, USA), Matteo Postacchini (Università Politecnica delle Marche, Italy), Gerben Ruessink (Utrecht University, The Nethelands), Alex Sheremet (University of Florida, USA). Financial support from the ONR Global (UK), through the MORSE Research Grant (N62909-17-1-2148) is gratefully acknowledged.

References

Aagard, T., Davidson-Arnott, R., Greenwood, B., Nielsen, J. (2004). Sediment supply from shoreface to dunes: linking sediment transport measurements and long-term morphological evolution. *Geomorphology* **60**: 205-224.

Alsina, J.M., Caceres, I., Brocchini, M., Baldock, T.E. (2012). An experimental study on sediment transport and bed evolution under different swash zone morphological conditions. *Coastal Engineering* **68**: 31-43.

Anthony, E.J. (2015). Wave influence in the construction, shaping and destruction of river deltas: A review. *Marine Geology* **361**: 53-78.

Antuono, M., Brocchini, M. (2010). Solving the Nonlinear Shallow Water Equations in physical space. *Journal of Fluid Mechanics* **643**: 207-232.

Armaroli, C., Ciavola, P. (2011). Dynamics of a nearshore bar system in the northern Adriatic: A video-based morphological classification. *Geomorphology* **126**: 201-216.

Ashton, A.D., Giosan, L. (2011). Wave-angle control of delta evolution. *Geophysical Research Letters* **38**: L13405.

Bailard, J.A. (1981). An energetics total load sediment transport model for a plane sloping beach. *Journal of Geophysical Research – Oceans* **86(C11)**: 10938-10954.

2291 Baldock, T.E. (2006). Long wave generation by the shoaling and breaking of transient wave
2292 groups on a beach. *Proceedings of the Royal Society of London* **A 462**: 1853-1876.
2293 Baldock, T.E., Holmes, P. (1999). Simulation and prediction of swash oscillations on a steep
2294 beach. *Coastal Engineering* **36 (3)**: 219–242.
2295 Battjes, J.A., Bakkenes, H.J., Janssen, T.T., van Dongeren, A.R. (2004). Shoaling of
2296 subharmonic gravity waves. *Journal of Geophysical Research - Oceans* **109**: C02009.
2297 Bellotti, G., Archetti, R., Brocchini, M. (2003). Experimental validation of mean swash zone
2298 boundary conditions, *Journal of Geophysical Research - Oceans* **108(C8)**: 3250,
2299 doi:10.1029/2002JC001510.
2300 Berni, C., Barthelemy, E., Michallet, H. (2013). Surf zone cross-shore boundary layer
2301 velocity asymmetry and skewness: an experimental study on a mobile bed. *Journal of*
2302 *Geophysical Research - Oceans* **118**: 2188–2200.
2303 Bertin, X., Olabarrieta, M. (2015). Relevance of infragravity waves in a wave-dominated
2304 inlet. *Journal of Geophysical Research - Oceans* **121**: 5418–5435.
2305 Blenkinsopp, C.E., Turner, I.L., Masselink, G., Russell, P.E. (2011). Swash zone sediment
2306 fluxes — field observations. *Coastal Engineering* **58**: 28–44.
2307 Brocchini, M. (2006). Integral swash zone models. *Continental Shelf Research* **26**: 653-660.
2308 Brocchini, M. (2013). A reasoned overview on Boussinesq-type models: the interplay
2309 between physics, mathematics and numerics. *Proceedings of the Royal Society of*
2310 *London* **A 469**: 20130496, doi:10.1098/rspa.2013.0496.
2311 Brocchini, M., Peregrine, D.H. (1996). Integral flow properties of the swash zone and
2312 averaging. *Journal of Fluid Mechanics* **317**: 241-273.
2313 Brocchini, B., Bellotti, G. (2002). Integral flow properties of the swash zone and averaging.
2314 Part 2. The shoreline boundary conditions for wave-averaged models. *Journal of Fluid*
2315 *Mechanics* **458**: 269-281.

2316 Brocchini, M., Baldock, T.E. (2008). Recent advances in modeling swash zone dynamics:
2317 influence of surf-swash interaction on nearshore hydrodynamics and morphodynamics.
2318 *Reviews in Geophysics* **46(3)**: RG3003, doi:10.1029/2006RG000215.
2319 Brocchini, M., Calantoni, J., Postacchini, M., Sheremet, A., Staples, T., Smith, J., Reed,
2320 A.H., Braithwaite III, E.F., Lorenzoni, C., Russo, A., Corvaro, S., Mancinelli, A. and
2321 Soldini, L. (2017). Comparison between the wintertime and summertime dynamics of the
2322 Misa River estuary. *Marine Geology* **385**: 27-40.
2323 Caballeria, M., Coco, G., Falqués, A., Huntley, D.A., 2002. Self-organization mechanisms
2324 for the formation of nearshore crescentic sand bars. *Journal of Fluid Mechanics* **465**: 379–
2325 410.
2326 Canestrelli, A., Nardin, W., Edmonds, D., Fagherazzi, S., Slingerland, R. (2014), Importance
2327 of frictional effects and jet instability on the morphodynamics of river mouth bars and
2328 levees, *Journal of Geophysical Research - Oceans* **119**: 509–522.
2329 Certain, R., Barusseau, J.P. (2005). Conceptual modelling of sand bars morphodynamics
2330 for a microtidal beach (Sète, France). *Bulletin de la Société Géologique de France* **176**:
2331 343–354.
2332 Chang, Y.S., Scotti, A. (2004). Modeling unsteady turbulent flows over ripples: Reynolds-
2333 averaged Navier-Stokes equations (RANS) versus large-eddy simulation (LES). *Journal*
2334 *of Geophysical Research - Oceans* **109**: 1-16.
2335 Chawla, A., Kirby, J.T. (2002). Monochromatic and random wave breaking at blocking
2336 points. *Journal of Geophysical Research - Oceans* **107**: 3067.
2337 Coco G., Murray, A.B. (2007). Patterns in the sand: from forcing templates to self-
2338 organization. *Geomorphology* **91**: 271-290.
2339 Cooper, J.A.G. (2001). Geomorphological variability among microtidal estuaries from the
2340 wave-dominated South African coast. *Geomorphology* **40**: 99-122.

2341 de Bakker, A.T.M., Brinkkemper, J.A., van der Steen, F., Tissier, M.F.S., Ruessink B.G.
2342 (2016). Cross-shore sand transport by infragravity waves as a function of beach
2343 steepness. *Journal of Geophysical Research – Earth Science* **121**: 1786-1799.
2344 Drake, T.G., J. Calantoni (2001). Discrete particle model for sheet flow sediment transport
2345 in the nearshore. *Journal of Geophysical Research - Oceans* **106**: 19,859–19,868.
2346 Dronen, N., Deigaard, R. (2007). Quasi-three-dimensional modelling of the morphology of
2347 longshore bars. *Coastal Engineering* **54**: 197-215.
2348 van Enckevort, I.M.J., Ruessink, B.G. (2003). Video observations of nearshore bar
2349 behaviour. Part 1: alongshore uniform variability. *Continental Shelf Research* **23**: 501-
2350 512.
2351 Fagherazzi, S., Edmonds, D.A., Nardin, W., Leonardi, N., Canestrelli, A., Falcini, F.,
2352 Jerolmack, D.J., Mariotti, G., Rowland, J.C., Slingerland, R.L. (2015). Dynamics of river
2353 mouth deposits. *Reviews in Geophysics* **53**, 31pp., doi:10.1002/2014RG000451.
2354 Falcini, F., Piliouras, A., Garra, R., Guerin, A., Jerolmack, D.J., Rowland, J., Paola, C. (2014)
2355 Hydrodynamic and suspended sediment transport controls on river mouth morphology
2356 *Journal of Geophysical Research – Earth Surface* **119**: 1-11, doi:10.1002/2013JF002831.
2357 Gallagher, E., Elgar, S., Guza, R.T. (1998). Observations of sand bar evolution on a natural
2358 beach. *Journal of Geophysical Research - Oceans* **103(C2)**: 3203-3215.
2359 Galloway, W.E. (1975). Process framework for describing themorphologic and stratigraphic
2360 evolution of delta depositional systems. In: Broussard, M.L (Ed.), Deltas: Models for
2361 Exploration. Houston Geological Society, Houston, pp. 87–98.
2362 Guard, P., Baldock, T. (2007). The influence of seaward boundary conditions on swash zone
2363 hydrodynamics. *Coastal Engineering* **54**: 321–331.
2364 Haas, K.A. and Warner, J.C. (2009). Comparing a quasi-3D to a full 3D nearshore circulation
2365 model: SHORECIRC and ROMS. *Ocean Modelling* **26**: 91-103.

Henderson, S.M., Allen, J.S., Newberger P.A. (2004). Nearshore sandbar migration predicted by an eddy-diffusive boundary layer model. *Journal of Geophysical Research - Oceans* **109**: C06024, doi:10.1029/2003JC002137.

Hoefel, F., Elgar, S. (2003). Wave-induced sediment transport and sandbar migration. *Science* **299**: 1885-1887.

Holman, R.A., Bowen, J. (1982). Bars, bumps, and holes: models for the generation of complex beach topography. *Journal of Geophysical Research - Oceans* **87**: 457-468.

Hsu, T., Elgar, S., Guza, R.T. (2006). Wave-induced sediment transport and onshore sandbar migration. *Coastal Engineering* **53**: 817–824.

Kennedy, A.B., Brocchini, M., Soldini, L., Gutierrez, E. (2006). Topographically controlled, breaking-wave-induced macrovortices. Part 2. Rip current topographies. *Journal of Fluid Mechanics* **559**: 57–80.

Kirby, J.T. (2016). Boussinesq models and their application to coastal processes across a wide range of scales. *Journal of Waterways, Port, Coastal and Ocean Engineering* **142**: 03116005.

Lesser, G.R., Roelvink, J.A., van Kester, J.A.T.M., Stelling, G.S. (2004). Development and validation of a three-dimensional morphological model. *Coastal Engineering* **51**: 883-915.

Longuet-Higgins, M. S., Stewart, R. W. (1964). Radiation stress in water waves: a physical discussion with applications. *Deep Sea Research I* **11**: 529-562.

Lubin, P., Glockner, S., Kimmoun, O., Branger, H. (2011). Numerical study of the hydrodynamics of regular waves breaking over a sloping beach. *European Journal of Mechanics B/Fluids* **30**: 552-564.

Ma, G., Shi, F., Kirby, J.T. (2012). Shock-capturing non-hydrostatic model for fully dispersive surface wave processes. *Ocean Modelling* **43-44**: 22-35.

Mase, H. (1995). Frequency down-shift of swash oscillations compared to incident waves. *Journal of Hydraulic Research* **33**: 397-411.

2392 Masselink, G., Short, A.D. (1993). The Effect of Tide Range on Beach Morphodynamics and
2393 Morphology: A Conceptual Beach Model. *Journal of Coastal Research* **9**: 785-800.
2394 Melito, L., Postacchini, M., Sheremet, A., Calantoni, J., Zitti, G, Darvini, G., Brocchini, M.
2395 (2018a). Wave-current interactions and infragravity wave propagation at a microtidal inlet.
2396 *E-proceedings of the 3rd EWAS International Conference:* 477-485.
2397 Melito, L., Postacchini, G, Darvini, G., Brocchini, M. (2018b). Waves and currents at a river
2398 mouth: the role of macrovortices, sub-grid turbulence and seabed friction. *Water* **10**: 550,
2399 doi:10.3390/w10050550 .
2400 Melito, L., Postacchini, M., Sheremet, A., Calantoni, J., Zitti, G., Darvini G., Brocchini M.
2401 (2019l). Hydrodynamics at a microtidal inlet: analysis of propagation of the main wave
2402 components. *Estuarine Coastal and Shelf Science* (under peer review).
2403 Memmola, F. (2017). Analysis and development of oceanographic models: reaching the
2404 swash zone. Università Politecnica delle Marche, PhD Thesis, 92pp.
2405 Memmola, F., Coluccelli, A., Russo, A., Warner J.C., Brocchini M. (2019). Wave-resolving
2406 Shoreline Boundary Conditions for wave-averaged coastal models. *Ocean Modeling*
2407 (under peer review).
2408 Moura, T., Baldock, T.E. (2017). Remote sensing of the correlation between breakpoint
2409 oscillations and infragravity waves in the surf and swash zone. *Journal of Geophysical*
2410 *Research - Oceans* **122**: 3106-3122.
2411 Nienhuis, J.H. (2016). Plan-view evolution of wave-dominated deltas. Massachusetts
2412 Institute of Technology and the Woods Hole Oceanographic Institution, PhD Thesis,
2413 182pp.
2414 Nienhuis, J.H., Ashton, A.D., Giosan, L. (2015). What makes a delta wave-dominated?
2415 *Geology* **43(6)**: 511-514.
2416 Nienhuis, J.H., Ashton, A.D., Giosan, L. (2016). Littoral steering of deltaic channels. *Earth*
2417 *and Planetary Science Letters* **453(1)**: 204-214.

2418 O'Hare, T.J., Huntley, D.A. (1994). Bar formation due to wave groups and associated long
2419 waves. *Marine Geology* **116**: 313-325.
2420 Olabarrieta, M., Geyer, W.R., Kumar, N. (2014). The role of morphology and wave-current
2421 interaction at tidal inlets: An idealized modeling analysis. *Journal of Geophysical*
2422 *Research – Oceans* **119**: 8818-8837.
2423 Parlagreco, L. Melito, L. Devoti, S. Perugini, E. Soldini, L. Zitti G., Brocchini M. (2019).
2424 Monitoring for coastal resilience: preliminary data from five Italian sandy beaches. **19**.
2425 1854; doi:10.3390/s19081854
2426 Peregrine, D.H. (1999). Large-scale vorticity generation by breakers in shallow and deep
2427 water. *European Journal of Mechanics B/Fluids* **18**: 403–408.
2428 Plant, N.G., Freilich, M.H., Holman, R.A. (2001). Role of morphologic feedback in surf zones
2429 and bar response. *Journal of Geophysical Research - Oceans* **106**: 973-989.
2430 Postacchini, M., Brocchini, M., Landon, M., Mancinelli, A. (2012). A multi-purpose, intra-
2431 wave, shallow water hydro-morphodynamic solver. *Advances in Water Resources* **38**: 13-
2432 26.
2433 Postacchini, M., Brocchini, M., Soldini, L. (2014). Vorticity generation due to cross-sea.
2434 *Journal of Fluid Mechanics* **744**: 286-309.
2435 Pourzangbar, A., Losada, M.A., Saber, A., Rasoul Ahari, L., Larroudé, P., Vaezi, M. and
2436 Brocchini, M. (2017). Prediction of non-breaking wave induced scour depth at the trunk
2437 section of breakwaters using Genetic Programming and Artificial Neural Networks.
2438 *Coastal Engineering* **121**: 107-118.
2439 Power, H.E., Holman, R.A., Baldock, T.E. (2011). Swash zone boundary conditions derived
2440 from optical remote sensing of swash zone flow patterns. *Journal of Geophysical*
2441 *Research - Oceans* **116**: C06007, doi:10.1029/2010JC006724.
2442 Pritchard, D., Hogg, A.J. (2005). On the transport of suspended sediment by a swash event
2443 on a plane beach, *Coastal Engineering* **52(1)**: 1–23.

2444 Ribas, F. (2003). On the growth of nearshore sand bars as instability processes of
2445 equilibrium beach states. Universitat Politecnica de Catalunya, PhD Thesis, 242pp.
2446 Ribeiro, M., Barrio, F., Taborda, R., Cascalho, J., Bosnic, I. Rodríguez, I., Sanchez, M.
2447 (2012). Longshore drift: experimental and empirical predictors. The example of the Ebro
2448 Delta. *Proceedings of the 2as Jornadas de Engenharia Hidrográfica*, Lisboa, Portugal,
2449 pp. 271–274.
2450 Roelvink, J. A., Stive, M. J. F. (1989) Bar-generating cross-shore flow mechanisms on a
2451 beach. *Journal of Geophysical Research - Oceans* **94**: 4785-4800.
2452 Ruessink, B.G., Kroon, A. (1994). The behaviour of a multiple bar system in the nearshore
2453 zone of Terschelling, the Netherlands: 1965–1993. *Marine Geology* **121**: 187–197.
2454 Schäffer, H.A. (1993). Infragravity waves induced by short wave groups. *Journal of Fluid*
2455 *Mechanics* **247**: 551–588.
2456 Shand, R.D., Bailey, D.G., Shephard, M.J. (1999). An inter-site comparison of net offshore
2457 bar migration characteristics and environmental conditions. *Journal of Coastal Research*
2458 **15**: 750–765.
2459 Shen, M.C., Meyer, E.R. (1963). Climb of a bore on a beach. Part 3. Run-up. *Journal of*
2460 *Fluid Mechanics* **16**: 113–125.
2461 Short, A.D. (1975). Multiple offshore bars and standing waves. *Journal of Geophysical*
2462 *Research - Oceans* **80**: 3838-3840.
2463 Short, A.D., Aagard, T. (1993). Single and multi-bar beach change models. *Journal of*
2464 *Coastal Research* **15**: 141-157.
2465 Symonds, G., Huntley, D.A., Bowen, A.J. (1982). Two-dimensional surf beat: long wave
2466 generation by a time-varying breakpoint. *Journal of Geophysical Research - Oceans* **87**:
2467 492-498.
2468 Ting, F.C.K., Kirby, J.T. (1994). Observation of undertow and turbulence in a laboratory surf
2469 zone. *Coastal Engineering* **24**: 51-80.

2470 Torres-Freyermuth, A., Lara, J.L. and Losada, I.J. (2010). Numerical modelling of short- and
2471 long-wave transformation on a barred beach. *Coastal Engineering* **57**: 317-330.
2472 Uncles, R.J. Stephens, J.A., Harris C. (2014). Infragravity currents in a small ría: Estuary-
2473 amplified coastal edge waves? *Estuarine Coastal and Shelf Science* **150**: 242-251.
2474 Valle-Levinson A. (2011). Classification of Estuarine Circulation. In: Wolanski E and
2475 McLusky DS (eds.) *Treatise on Estuarine and Coastal Science* **1**, 75–86. Waltham:
2476 Academic Press.
2477 Van Enckevort, I.M.J. (2001). Daily to yearly nearshore bar behaviour. Utrecht University,
2478 PhD Thesis, 174pp.
2479 Van Enckevort, I.M.J., Ruessink, B.G. (2003).Video observations of nearshore bar
2480 behaviour. Part 1: alongshore uniform variability. *Continental Shelf Research* **23**: 501–
2481 512.
2482 Vittori, G., DeSwart, H.E., Blondeaux, P. (1999). Crescentic bedforms in the nearshore
2483 region. *Journal of Fluid Mechanics* **381**: 271-303.
2484 Watson, G., Barnes, T. C. D., Peregrine, D. H. (1995). The generation of low-frequency
2485 waves by a single wave group incident on a beach. *24th International Conference on*
2486 *Coastal Engineering*, 776-790.
2487 Wijnberg, K.M., Terwindt, J.H.J. (1995). Extracting decadal morphological behavior from
2488 high-resolution, long-term bathymetric surveys along the Holland coast using
2489 eigenfunction analysis. *Marine Geology* **126**: 301-330.
2490 Wijnberg, K.M., Kroon, A. (2002). Barred beaches. *Geomorphology* **48**: 103-120.
2491 Wright, L.D., Coleman, J.M., Erickson, M.W., (1974). Analysis of major river systems and
2492 their deltas: morphologic and process comparisons. Technical Report 156, Coastal
2493 Studies Institute. Louisiana State University (125 pp.).
2494 Wright, L.D., Short, A.D. 1984. Morphodynamic variability of surf zones and beaches: A
2495 synthesis. *Marine Geology* **56**: 93-118.

2496

LIST OF FIGURES

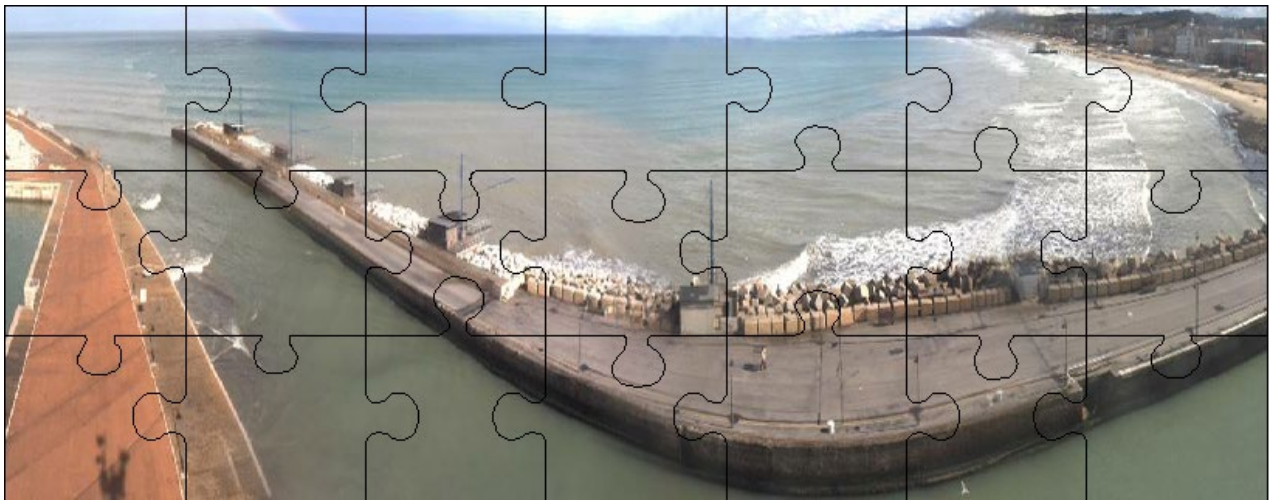

Figure 1. Wave-forced dynamics in the nearshore and estuaries: a puzzle to be solved.

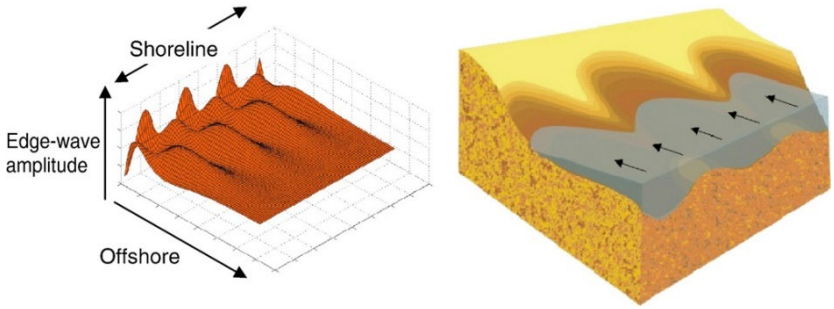

Figure 2. Forced/template mechanism: “synchronous standing edge waves” (left) and flow imprinted on sand giving beach cusps (right). Adapted from Coco and Murray, (2007).

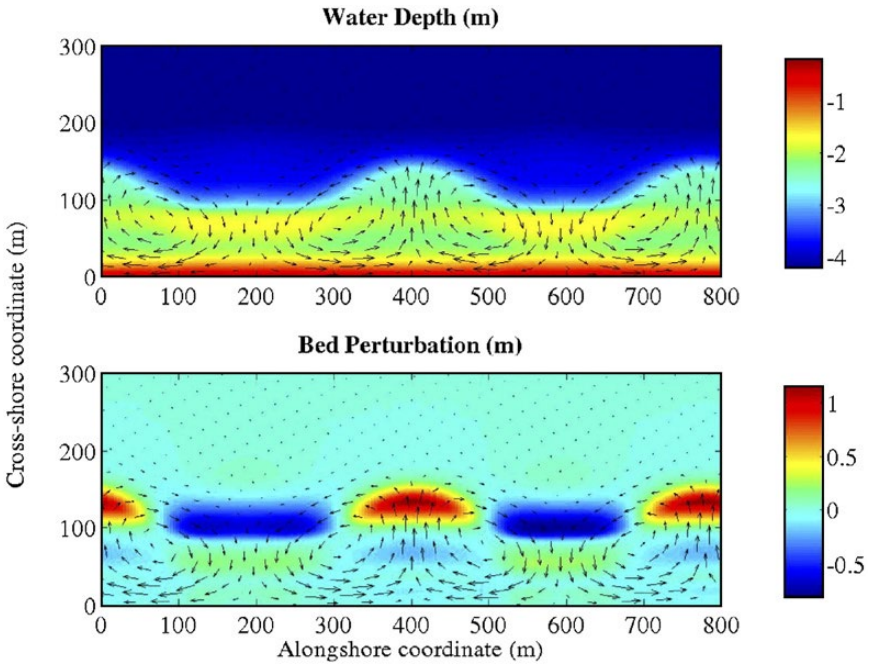

Figure 3. Stability/Self-organization mechanism: crescentic bars emerge from the feedback between flow and bathymetry (initial longshore-uniform bar bathymetry). Top: waves breaking on shoals force onshore flow, which returns to sea in gaps. Bottom: for suspended sediment decreasing from breaker line to shore, the onshore flow favors deposition (shoals grow) and the offshore flow favors erosion (scour holes grow). Hence, the development of crescentic bars. Adapted from Coco and Murray, (2007).

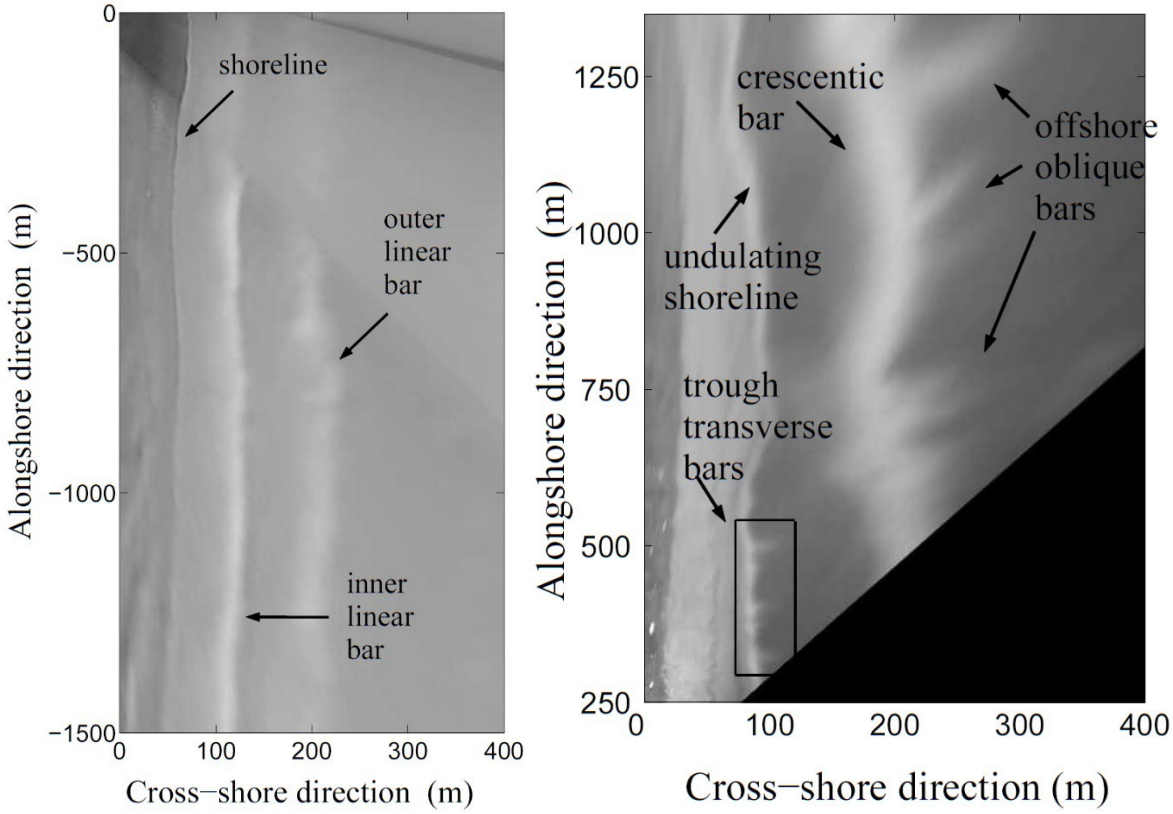

Figure 4. Left panel: planview image of two shore-parallel sand bars at Noordwijk beach (The Netherlands, 19th November 2000). Right panel: Planview image of surf zone complex topography at Duck (U.S.A. Atlantic coast, 10th January 1994). Adapted from Ribas Prats (2003).

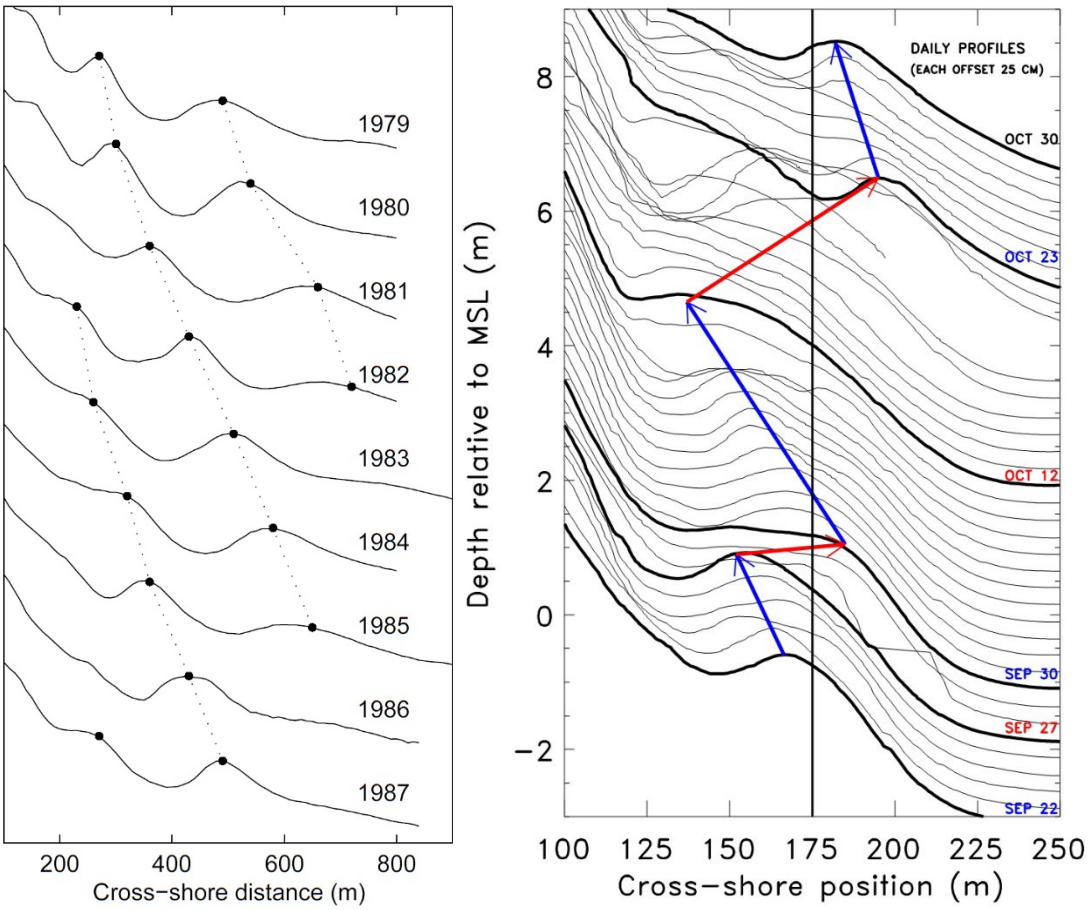

Figure 5. Left panel: seabed cross-shore profiles at Noordwijk, The Netherlands, from 1979 to 1987, showing cyclic bar behavior with a recurrence interval of about 4-5 years. Adapted from van Enckvort, (2001). Right panel: seabed cross-shore profiles at Duck (U.S.A. Atlantic coast, September-October 1994). Thick curves with red dates are the beginning of storms, resulting in offshore bar migration (red arrows). Thin curves are the subsequent daily profiles. The sandbar migrated onshore (blue arrows) during calm periods between the storms. Courtesy of Dr. S. Elgar.

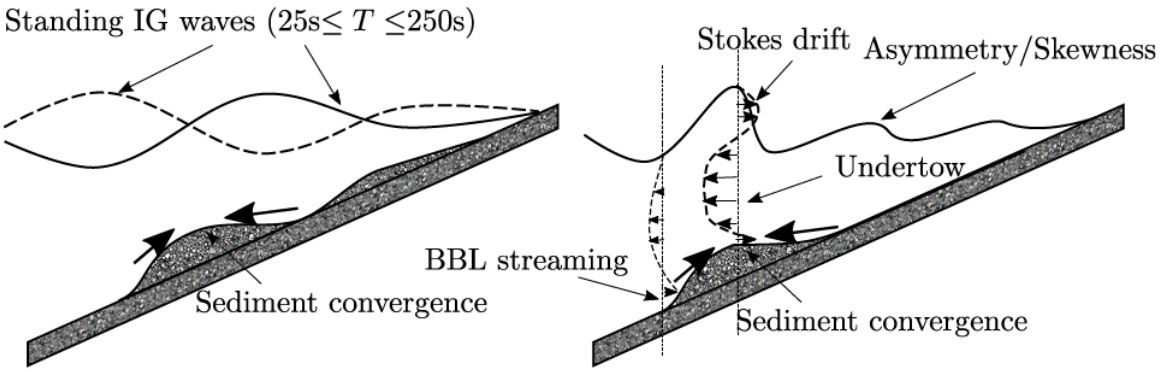

Figure 6. Bar formation because of sediment convergence at: anti/nodes of standing IF waves (left panel), breakpoint (right panel).

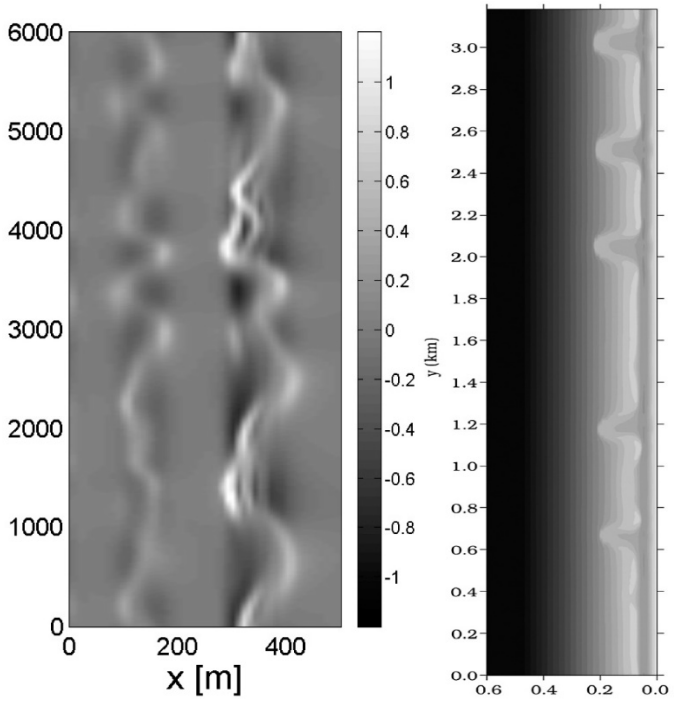

Figure 7. Left panel: non-linear stability solution for a double sand bar system giving asymmetric crescentic patterns on inner and outer bars (adapted from Klein and Schuttelaars, 2006). Right panel: Evolution of longshore uniform sand bar after 30 days of model run with normal wave incidence. Longshore instability in the form of rip channels (adapted from Dronen and Deigaard, 2007).

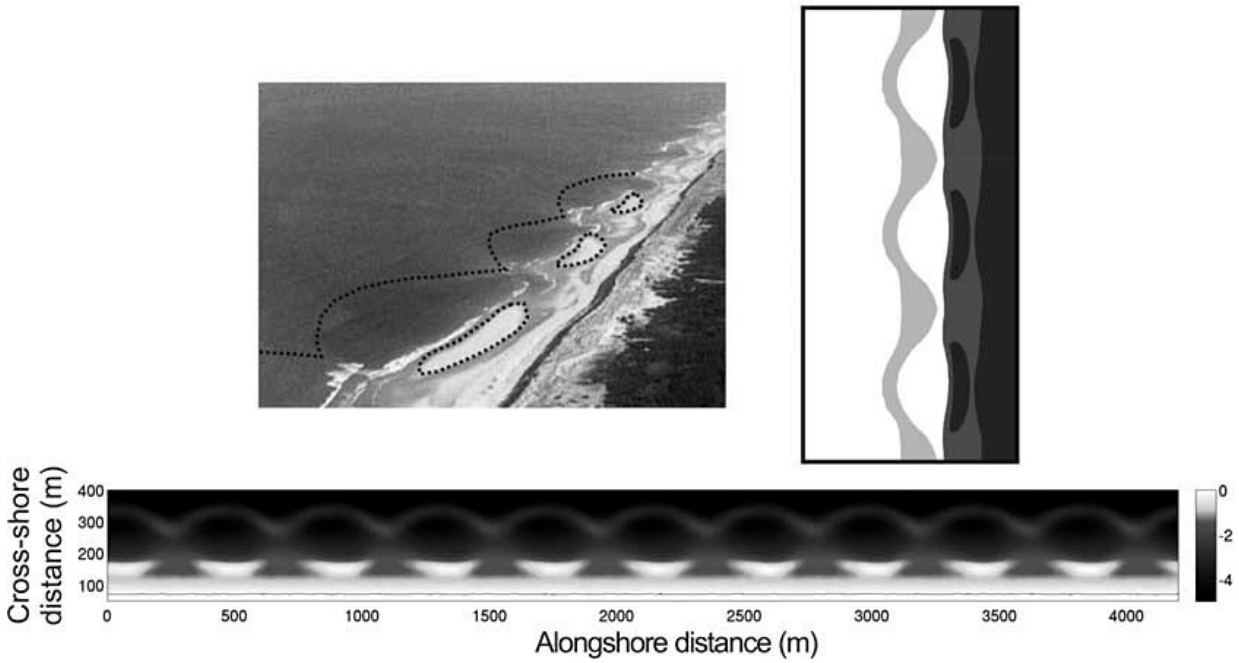

Figure 8. Computed (top-right and bottom panels) 180° out of-phase coupled patterns with an outer-bar horn facing an inner-bar bay, similar to observations (top-left panel) on a meso-macro-tidal, high-energy, double-barred beach (adapted from Castelle et al., 2010).

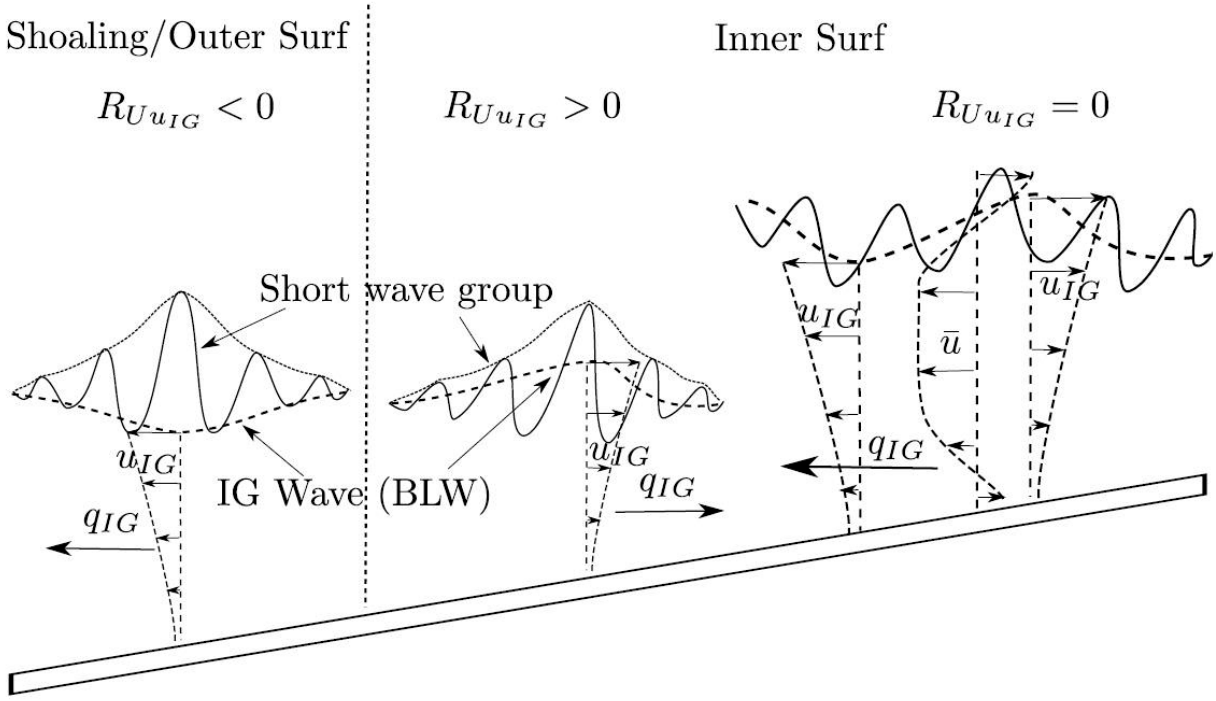

Figure 9. Sketch of IG-sea wave interaction and cross-shore sediment transport in the nearshore. From left to right: shoaling zone, inner-surf zone of moderately-sloping beaches, inner-surf zone of mildly-sloping beaches.

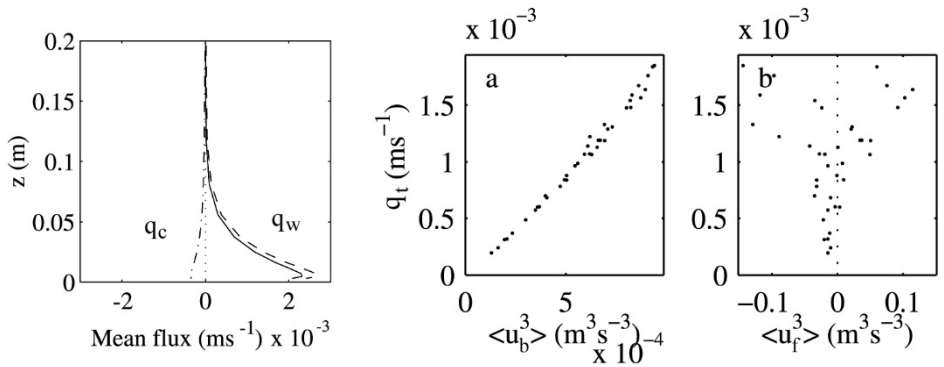

Figure 10. Top: observed (lines) and predicted (symbols) seabed profiles at the beginning (dashed line) and end (solid line and symbols) of the Duck94 onshore bar migration event. Bottom, from left to right: vertical profile of mean cross-shore sediment transport due to waves (q_w) and currents (q_c), total cross-shore sediment transport as function of near-bed (middle) and freestream (right) velocity moments. Adapted from Henderson et al. (2004).

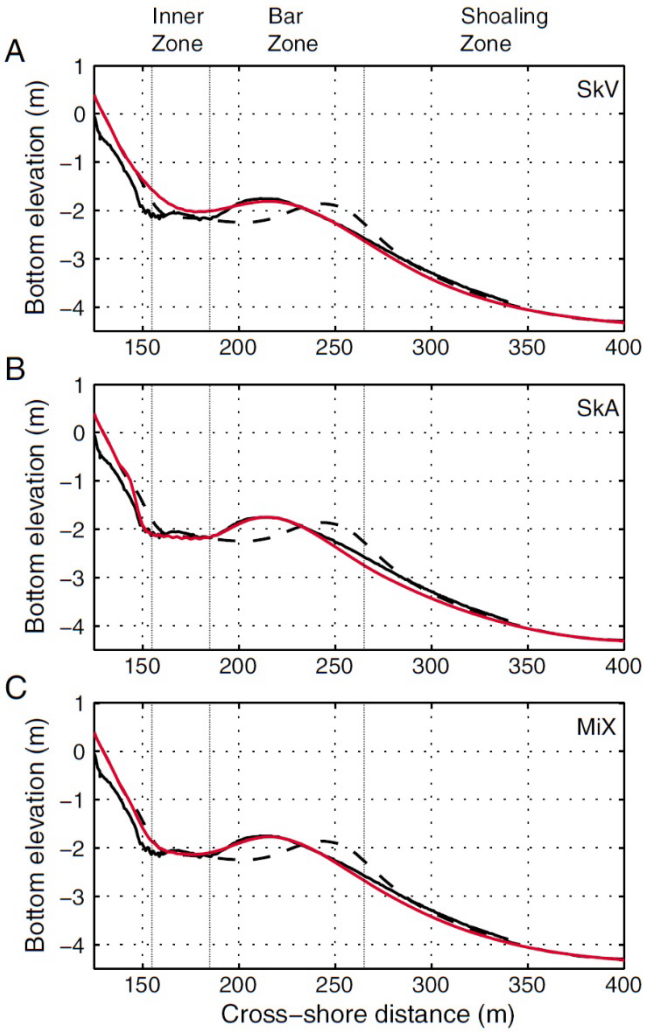

Figure 11. Modeling (red line) of the morphological evolution of the Duck94 onshore migration event for (A) the SkV model, (B) the SkA model, and (C) the MiX model. The initial and final measured profiles are shown by dashed and solid lines, respectively. Adapted from Fernandez-Mora et al. (2015).

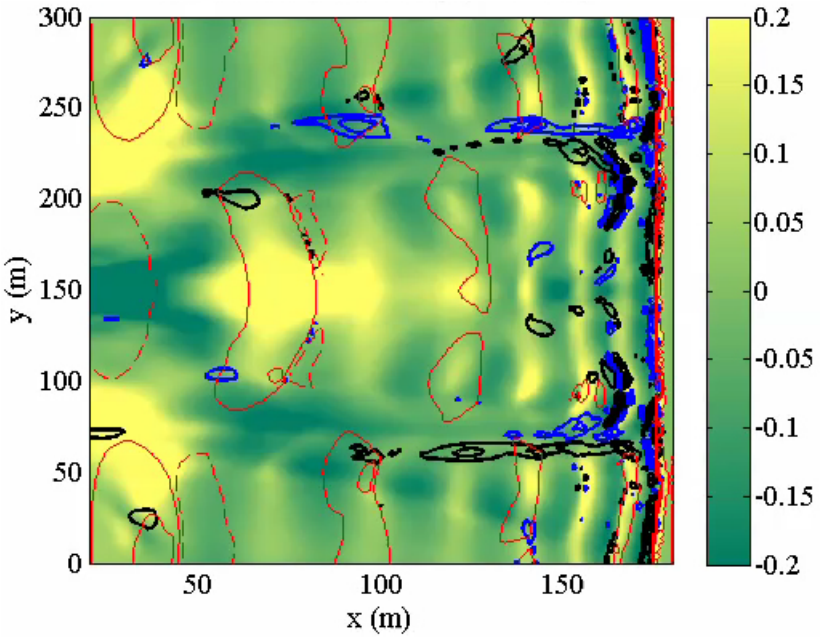

Figure 12. Seabed evolution forced by sea waves and macrovortices over a planar beach. Red thin lines give contours of the free surface elevation, while black and blue solid lines are contours of clockwise and anticlockwise vorticity, respectively. Yellow gives sand deposition and green seabed erosion.

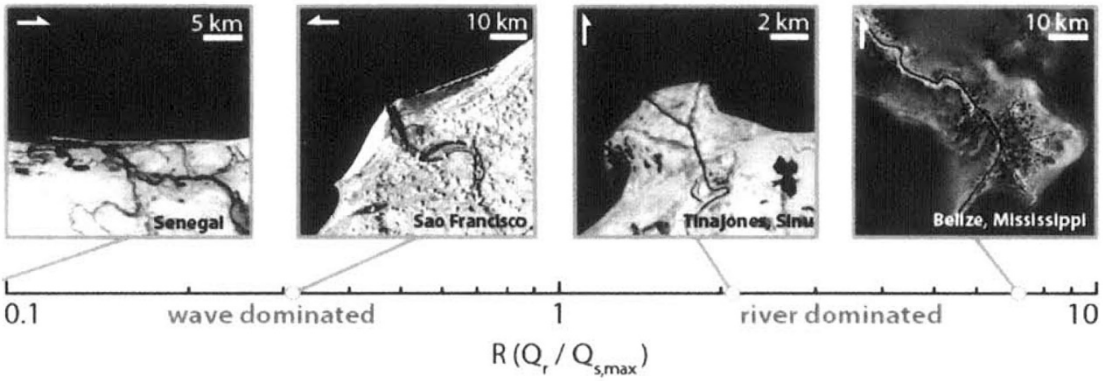

Figure 13. Classification of river delta morphologies by means of the fluvial dominance ratio. Adapted from Nienhuis (2016).

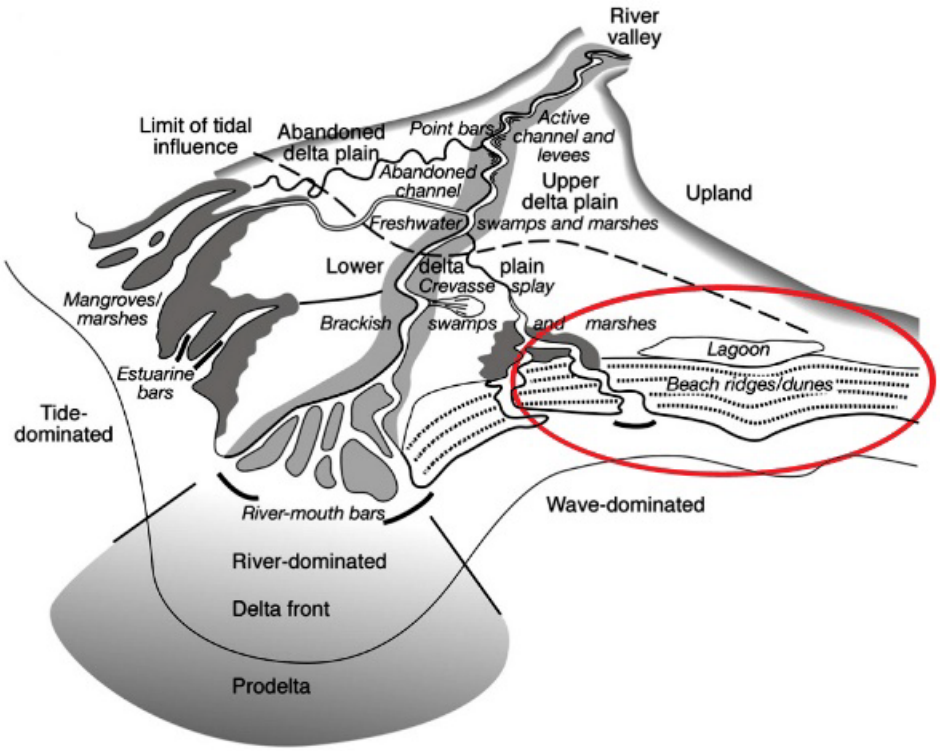

Figure 14. Left: river delta geomorphic units and schematic shoreline morphology (wave-dominated morphology circled in red). Adapted from Anthony (2015).

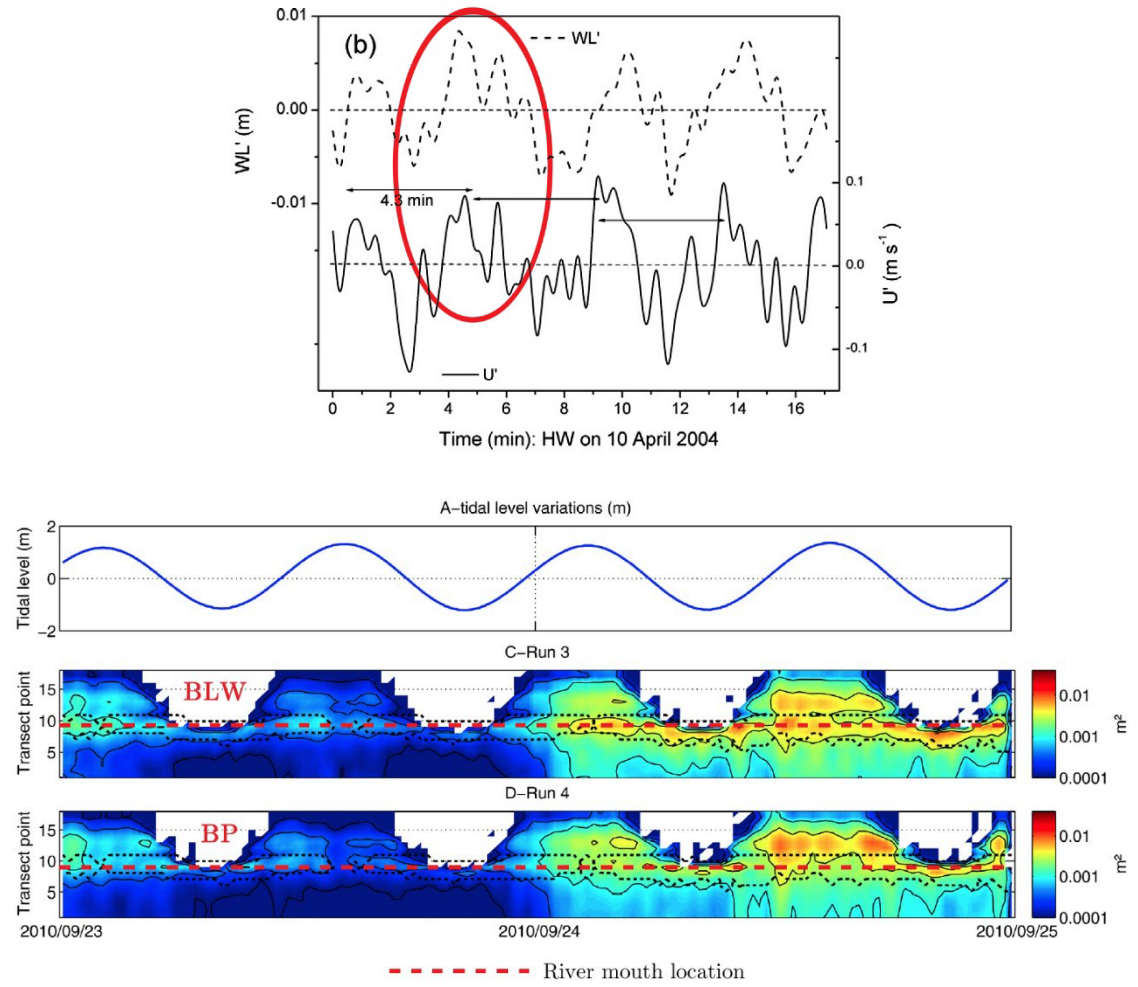

Figure 15. IG wave propagation at river mouths. Top: positive water level-flow velocity correlation at the Ría de Santiuste (Spain). Adapted from Uncles et al. (2014). Bottom: tide-modulated IG wave propagation in the Albufeira Inlet (Portugal). No IG waves propagate landward of the mouth at ebbs. Adapted from Bertin and Olabarrieta (2016).

Figure 16. The Misa River estuary in Senigallia (Italy) depicting locations of measuring stations within the final river reach (TGdown, QR1, QR2, QR3, TGup) and in the sea (QS1, QS2, QS3). Adapted from Melito et al. (2018a).

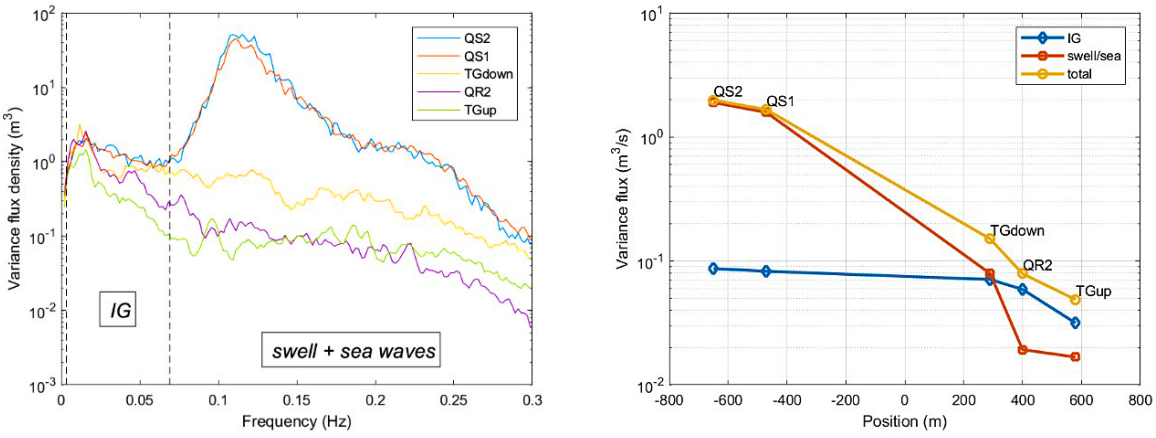

Figure 17. Energy density flux (left) and energy flux (right) at the Misa River during storm conditions. Adapted from Melito et al. (2018a).

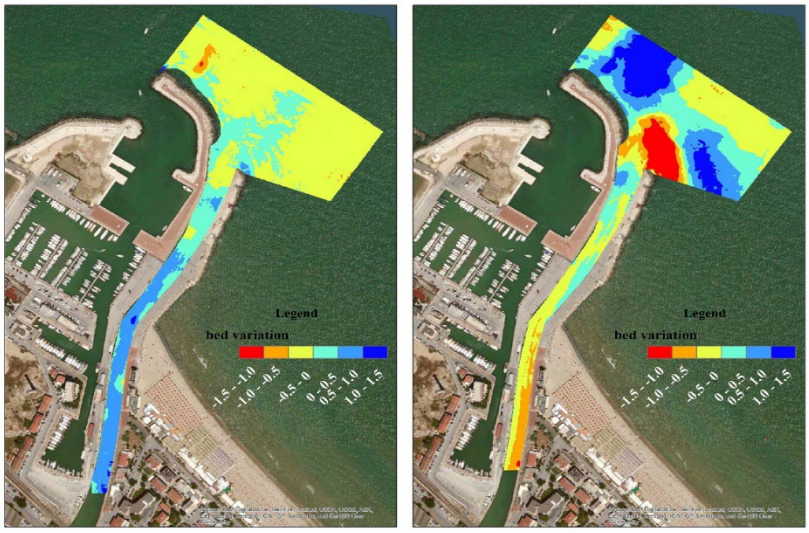

Figure 18. Seabed variation between May-September 2013 (left) and between September 2013-February 2014 (right) at the Misa River. Adapted from Brocchini et al. (2017).

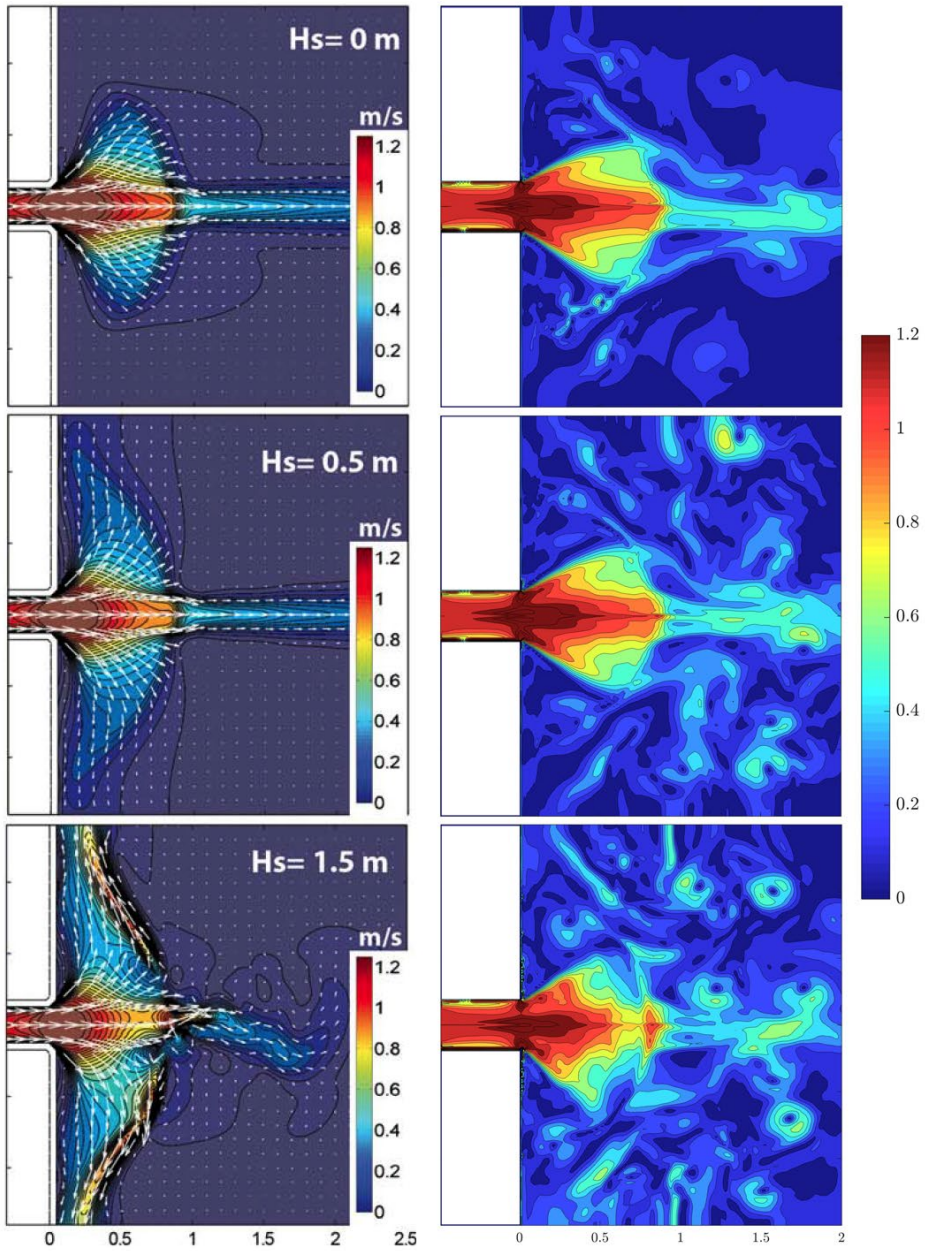

Figure 19. Velocity maps for a strong river outflow opposed to three different wave regimes (from top to bottom: H_s = 0.0m, 0.5 m, 1.5 m). Left column: results from Olabarrieta et al. (2014). Right column: results from the wave-resolving solver of Brocchini et al. (2001), averaged over 10 wave periods. Adapted from Melito et al. (2018b).

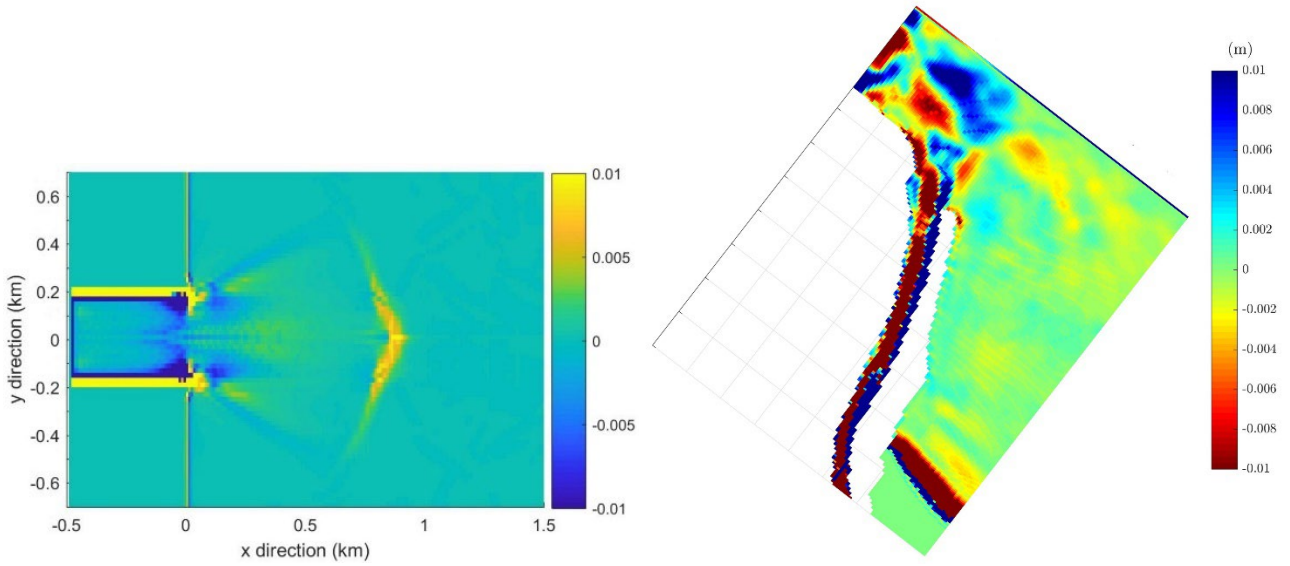

2602

2603 Figure 20. Estimated morphological evolution at the simplified river mouth bathymetry of

2604 Olabarieta et al. (2014), left panel and at the Misa River, right panel.

2605

2606

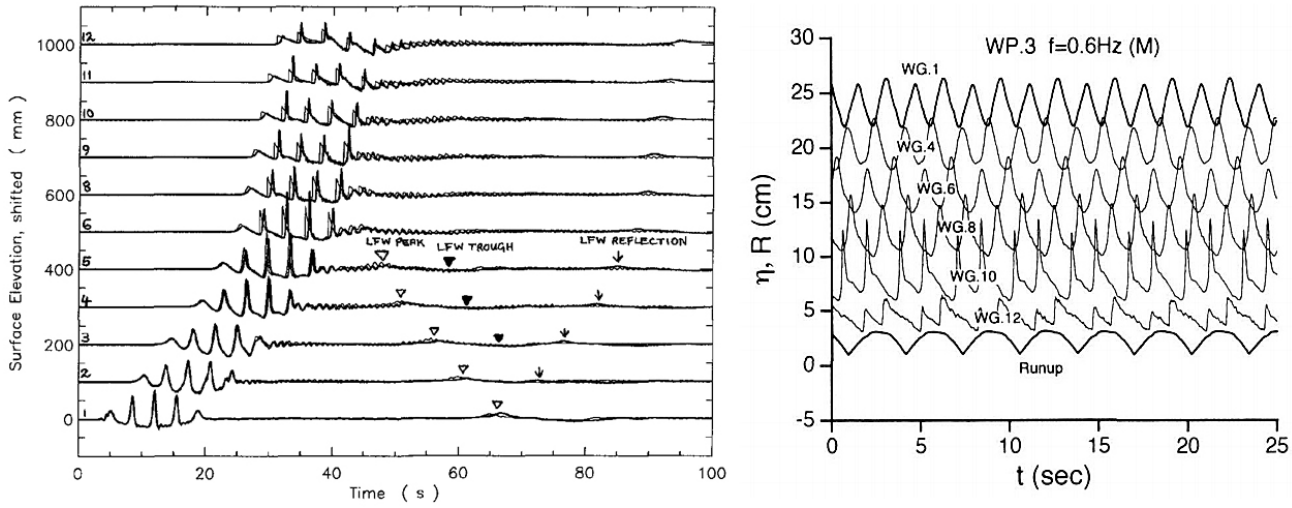

Figure 21. Left: example of BLW release on a beach because of sea wave breaking. The shoreward-propagating (from bottom to top) wave group releases its BLW that is reflected at the shoreline and propagated (from top to bottom) out to sea as a FLW (adapted from Watson, Barnes & Peregrine 1995). Right: example of frequency downshifting within the swash zone. Bichromatic waves propagate from seaward to the shoreline (from top to bottom) over a steep beach and interact in the swash zone giving wave of doubled period (adapted from Mase, 1995).

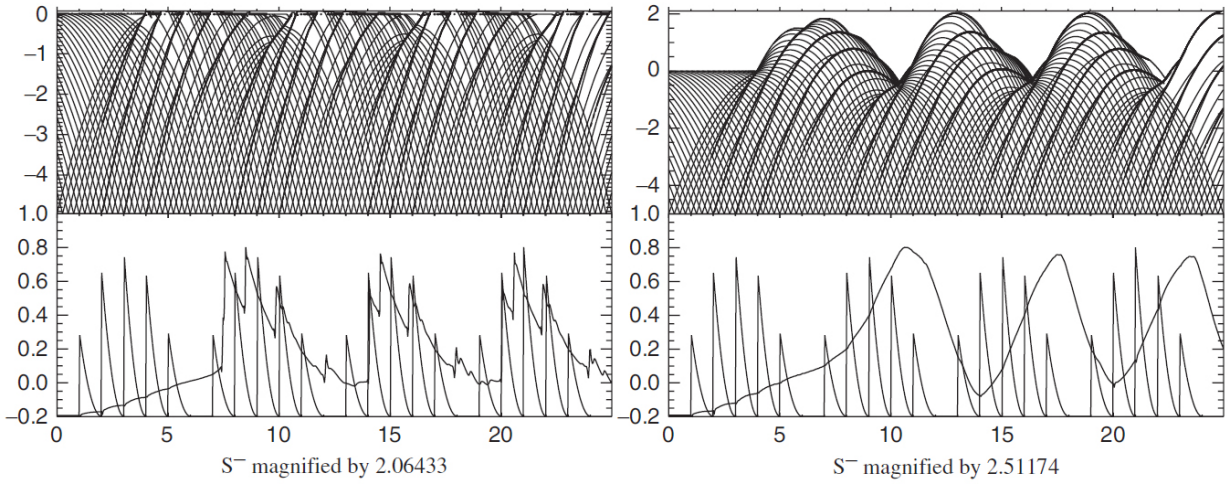

Figure 22. Waves interacting at a wall (left) and at a swash zone (right). Top: incoming and outgoing characteristic curves at the shoreline. Bottom: a group of 5 sea waves (thin line) incoming to shore and outgoing IG waves (S^-, thick line) resulting from the interaction of sea waves (adapted from Brocchini, 2006).

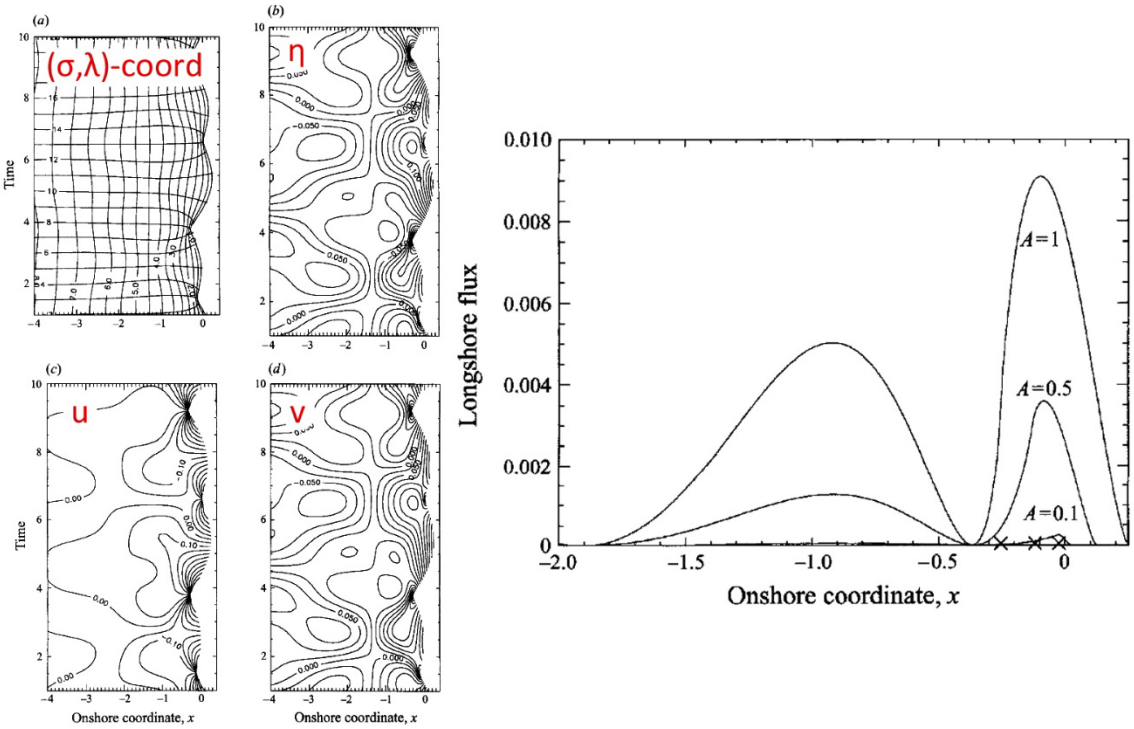

Figure 23. Left: maps, in the *(x,t)* plane of hodograph coordinates, free surface elevation η crosshore (u) and longshore (v) velocities for two sea waves interacting onto a beach. Right: mean longshore mass flux near and inside the swash zone for waves of different amplitude (adapted from Brocchini & Peregrine, 1996).

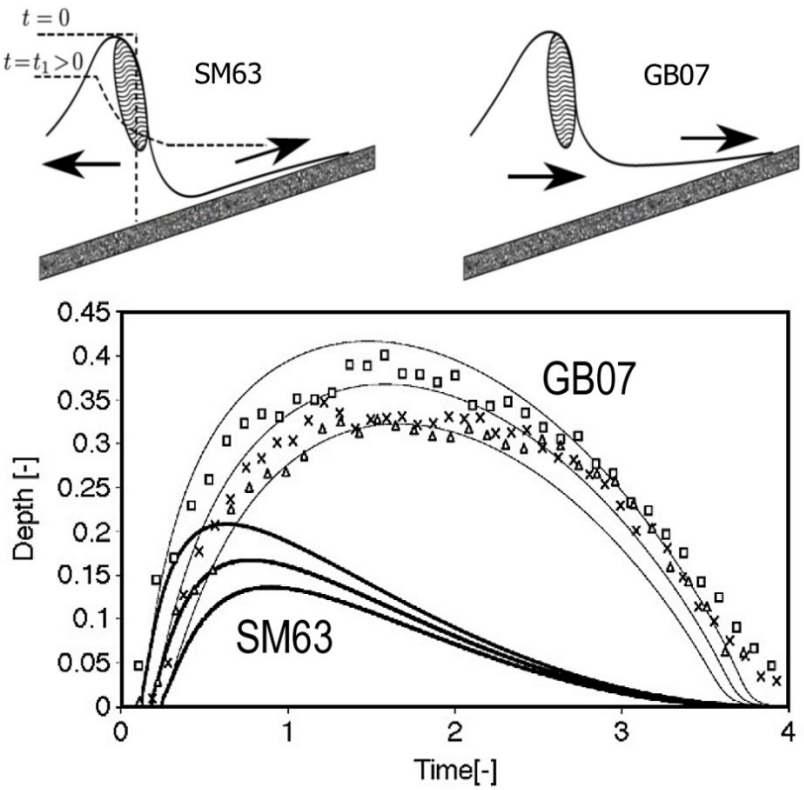

Figure 24. Top: sketches of the flow by bore collapse. The left sketch shows the evolution of the SM63 solution in comparison to a dam-break flow (dashed lines), the right sketch suggests that only shoreward-accelerating fluid motion is predicted by the GB07 solution. Bottom: swash water thickness predicted by the SM63 solution (thick lines) and by the GB07 solution (thin lines) also compared with experimental data (symbols). Bottom panel adapted from GB07.

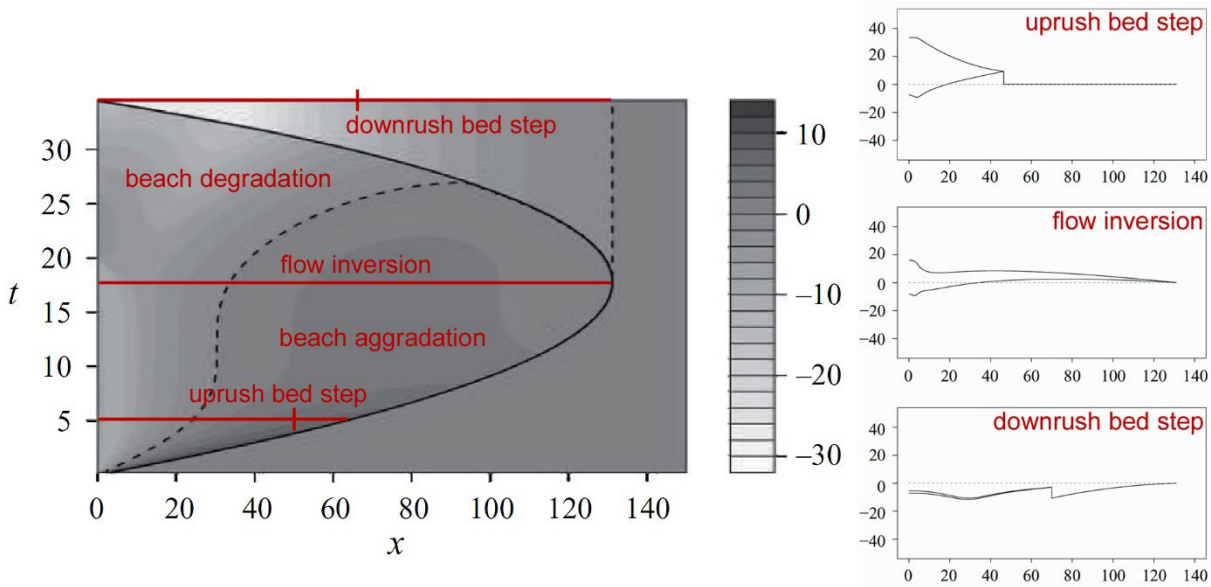

Figure 25. Left: space-time map of the changes in beach profile due a swash event. The thick dashed lines give the zero contour. Right: snapshots of the swash lens cross-shore sections (adapted from Kelly & Dodd, 2010).

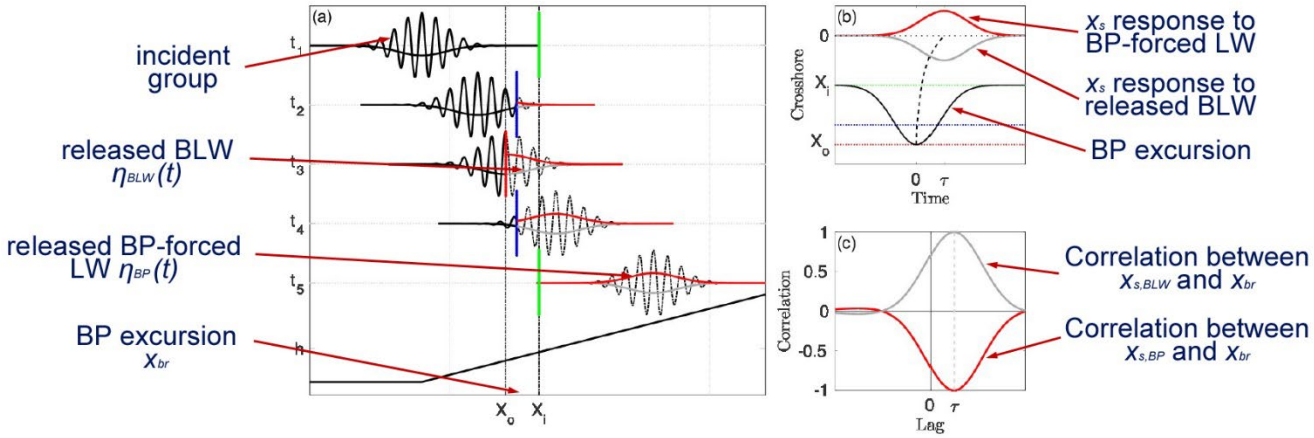

Figure 26. Shoreline relation with BLW and BP forcing. (a) Wave group. The vertical blue line gives the BP between its outer (red), x_o, and inner (green), x_i location. Grey and red lines give the released BLW and incident BP-forced IG wave, respectively. (b) BP excursion (black) and shoreline response to BP-forced (red) and BLW (grey) IG waves. Dashed line gives path for a shallow water wave from the BP to the shoreline. Horizontal colored lines are BP positions as in Figure 2a. (c) Cross-correlation between BP and shoreline excursion, BLW released (grey) and BP-foced IG wave (red). Adapted from Moura & Baldock, (2017).

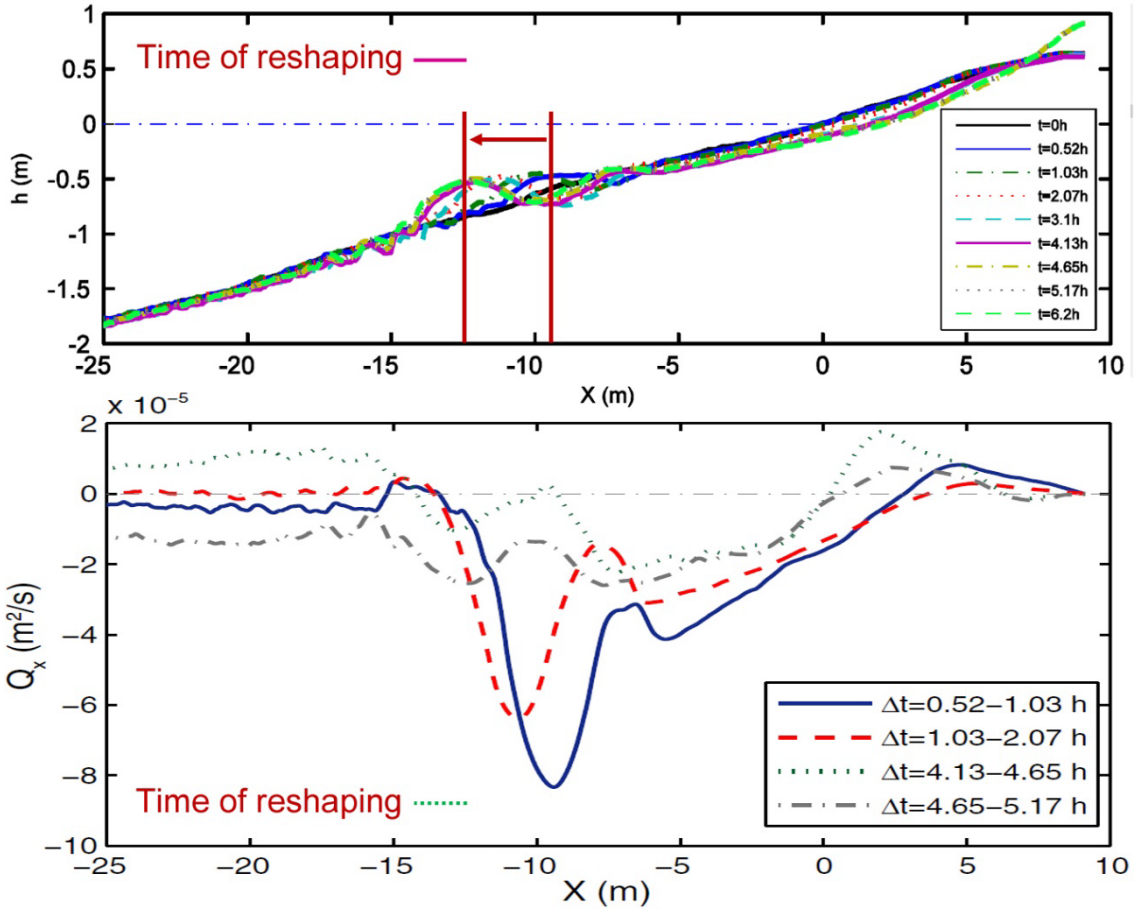

Figure 27. Cross-shore distribution of beach profile (top panel) and of cross-shore sediment transport rate (bottom panel) at various times before and after beah reshaping (adapted from Alsina et al., 2012).

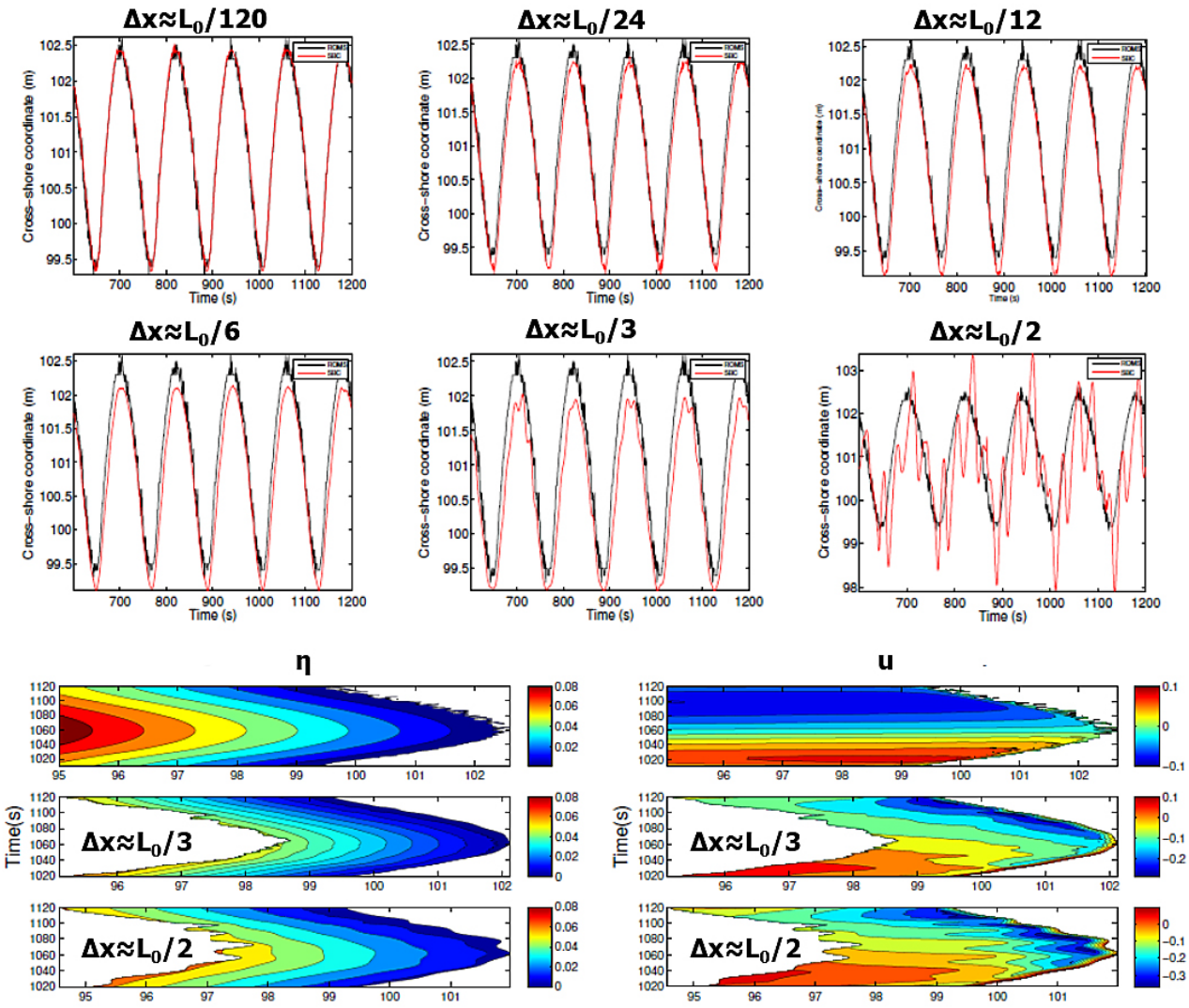

Figure 28. Top 6 panels: comparison of the ROMS ultra-highly resolved shoreline (black line) and ROMS+SBCs shorelines for lower and lower grid resolution. Bottom 2 panels: free surface elevation (left) and onshore velocity (right) for the benchmark ROMS solution (top panels) and ROMS+SBCs solutions for two very coarse meshes (middle and lower panels). Adapted from Memmola (2017).